ELECTRON EMISSION THERMAL ENERGY CONVERSION

A Thesis presented to the

Graduate School Faculty

UNIVERSITY OF MISSOURI – COLUMBIA

In Partial Fulfillment of the

Requirements for a Master of

Science - Mechanical Engineering

By

DOMINICK LOVICOTT

Dr. Gary Solbrekken   Thesis Supervisor

JULY 2010

The undersigned, appointed by the dean of the Graduate School, have examined the

thesis entitled

ELECTRON EMISSION THERMAL ENERGY CONVERSION

presented by Dominick Lovicott,

a candidate for the degree of Master of Science of Mechanical Engineering

and hereby certify that, in their opinion, it is worthy of acceptance.

Assistant Professor Gary Solbrekken

Professor Frank Feng

Assistant Professor Gregory Triplett

ELECTRON EMISSION THERMAL ENERGY CONVERSION

Dominick A. Lovicott

Dr. Gary Solbrekken   Thesis Supervisor

ABSTRACT

Energy consumption is driving both an intellectual and financial investment into the exploration of alternative energy sources and more efficient use of that energy. Efficient energy conversion for electrical power generation is a key component of curbing the world's ever increasing energy demands and waste heat is one of the primary byproducts of inefficient energy consumption. In general, high temperature heat sources are easier to be efficiently harvested and low temperature or low grade waste heat is more challenging to recover because of the small temperature delta. Appreciable adoption of low grade waste heat recovery will require devices that can convert low temperature waste heat efficiently into useful electrical power.

Electron emission from a surface can be achieved via two mechanisms: tunneling and thermionics. Converting thermal energy to electrical power using these mechanisms is achieved by generation of an electron current from the emitter to the collector, and production of a voltage potential between electrodes due to the potential energy difference between the electrodes. Efficient low temperature energy conversion is investigated in this thesis utilizing these two emission mechanisms.

Two device concepts were developed based on thermal field (a form of tunneling) and thermionic emission that incorporate nontraditional design elements and novel implementations of existing technologies. These device concepts were developed with the intent to help mitigate some of the common downfalls of this solid state energy conversion.

In addition to the novel implementation and device concepts, a unique system level modeling approach is taken that combines a more detailed thermal network with the emission modeling. Advantages of this method include a better estimate for boundary conditions and emission temperatures. Typically emission models assume constant temperature boundary conditions which can over estimate device performance.

Modeling of a magnetically enhanced thermionic diode illustrated significant reductions in thermal radiation exchange between emitter and collector. This reduction is attributed to the ability to spatially reorient the electrodes due to the magnetically altered electron trajectories, and was shown to have a substantial effect on the energy conversion efficiency. Efficient low temperature thermionic energy conversion is currently not viable due to the high temperatures required to excite electrons above the material work function. With lower material work functions, low temperature thermionic energy conversion would be achievable.

The second design concept investigated in this thesis utilizes the transition region between field emission and thermionic emission known as thermal-field

emission. This type of emission uses a high electric field produced by a gate electrode to increase the probability of electron tunneling. High electric fields at relatively low gate voltages are achieved by concentrating the field around nanowire tip emission sites. Unlike field emission, the electrode is heated by a heat source which further increases the probability of electron emission. Unlike thermionic devices, which suffer poor emission rates at low temperature, the thermal-field nanowire converter can produce appreciable emission at low temperatures. Modeling showed promising conversion efficiencies for this device at low temperature. However, the model does not account for gate leakage currents which will likely be the primary obstacle of this technology. Initial steps towards fabrication of this device have been taken including the growth of Si nanowires.

TABLE OF CONTENTS

LIST OF TABLES

LIST OF FIGURES

NOMENCLATURE

a	Half the foci distance (m)
A_c	Cross sectional area (m^2)
A_o	Thermionic emission constant (A/cm^{2}K^2)
B	Magnetic field (T)
$c_{p,Solid}$	Specific heat of solid or liquid (kJ/mol K)
$c_{p,vapor}$	Specific heat of vaporization at constant temperature (kJ/mol K)
C	Constant of integration
C_0	Universal constant
d	Electrode gap (m)
D	Tunneling transmission coefficient
e	Charge of an electron (Coulomb)
E	Energy (eV)
E	TFE variable in chapter 3.iii.b
E_O	Permittivity of free space (F/m)
f_F	Fermi distribution
F	Electric field in chapter 3 (V/m)
F	Thermal radiation view factor in chapters 4 and 5
F_B	Force due to a magnetic field (N)
h	Plank constant (eV s)
$\hbar$	Reduced Plank constant (eV s)
$\bar{h}_{fg}$	Molar heat of vaporization of a monatomic gas (kJ/mol)
$\bar{h}_0$	Latent heat of vaporization at constant temperature (kJ/mol)

J	Current density (A/cm^2)
k	TFE variable
k_B	Boltzmann's constant (m^2 kg/s^2 K)
K	TFE variable
L	Plate gap (m)
m	Mass (kg)
M	Molecular weight
n	Number per unit volume in chapter 3 section i
n	Number per unit area in chapter 3 section ii
n	Summation index variable in chapter 3.iii
N	Electron supply function (1/cm^2 s eV)
N_A	Avogadro 's number (mol^{-1})
P	Pressure (Pa)
q	Particle charge (Coulomb)
Q	Heat/thermal energy (W)
r	Emitter tip radius in chapter 3 (m)
r	Electron trajectory radius of curvature in chapter 5 (m)
R	Gate electrode radius (m)
$\bar{R}$	Universal gas constant (kJ/K mol)
t	TFE variable
T	Temperature (K)
v	Electron velocity (m/s)
$\bar{v}$	Initial velocity (m/s)

v_{fg}	Specific volume of a monatomic gas (m^3/mol)
V	Voltage potential (V)
V_{bias}	Applied voltage (V)
$V(x)$	Potential barrier between electrodes (eV)
w	Plate width (m)
W	Electrical work or generated power in chapter 4.i (W)
W	Plate width to gap ratio in chapter 4.ii (m)
x	Coordinate direction
x_1	Root of eV(x)-E$_x$
x_2	Root of eV(x)-E$_x$
y	TFE variable
y	Coordinate direction
z	Coordinate direction

Greek Letters

α	Angle between planes in chapter 4
α	Temperature coefficient in chapter 3.i (eV/K)
α	TFE variable in chapter 3.iii.b
β	Geometrical enhancement factor in chapter 3.iii.a
β	TFE scaling factor in chapter 3.iii.b
ξ	Orthogonal coordinate
θ	Tip half-angle (degrees) in chapter 3.iii.a
θ	Nordheim elliptical function in chapter 3.iii.b

ε	Emissivity
η	Efficiency
ϕ	Work function (eV)
σ	Stefan-Boltzmann constant (W/m^2 K^4)
χ	Chemical potential (eV)
ρ	Space charge density (C/m^3)
ψ	Thermal resistance (C/W)
ω	TFE variable
∞	Ambient

Subscripts

I	1st law of Thermodynamics
II	2nd law of Thermodynamics
c	Cold
C	Collector
$Carnot$	Carnot heat engine
$Cond, EC$	Conduction path between emitter and collector
$Cond, Circuitry$	Heat conduction through electrical circuitry
$Cond, Gate$	Conduction through the gate electrode
$Cond, NW$	Conduction through the nanowires
$Cond, Structural$	Conduction through structural housing
$Cond, Sub, E$	Conduction through emitter substrate

$Cond, Sub, C$	Conduction through collector substrate
$Conv, HS$	Convection from the collector heat sink
$Conv, SHS$	Convection from the shunt heat sink
$C - L$	Child-Langmuir
e	Electron
E	Emitter
$E - C$	Between emitter and collector
$Electrode$	Emission plate
$Emission, C$	Collector emitted electron energy
$Emission, E$	Emitter emitted electron energy
$Enclosure$	Device enclosure
f	Fermi
FE	Field emission
h	Hot
in	Input
$Loss$	Lumped parasitic heat losses
mg	Monatomic gas
$material$	Material property
R	Rejected heat from the collector
Rad, C	Thermal radiation emitted by the collector
Rad, E	Thermal radiation emitted by the emitter

$Rad, Enclosure$	Thermal radiation emitted by the enclosure
$Rad, Gate$	Thermal radiation emitted by the gate electrode
Rad, net	Net thermal radiation
Rad, NW	Thermal radiation emitted by the nanowires
Rad, Sub	Thermal radiation emitted by the substrate
S	Source
TI	Thermionic emission
TFE	Thermal field emission
TFE, C	Collector thermal field emission
TFE, E	Emitter thermal field emission
Superscripts	
$*$	Work function at 0K

1. INTRODUCTION

A United States Department of Energy study reports that energy consumption of

the U.S. has risen over 200% in the last 50 years (Energy Information Administration

2006), as shown in Fig. 1.1. The study also indicates that United States reliance on

foreign energy imports has risen at a higher rate than U.S. production of energy making

the U.S. more dependent on foreign sources.

Overview, 1949-2006
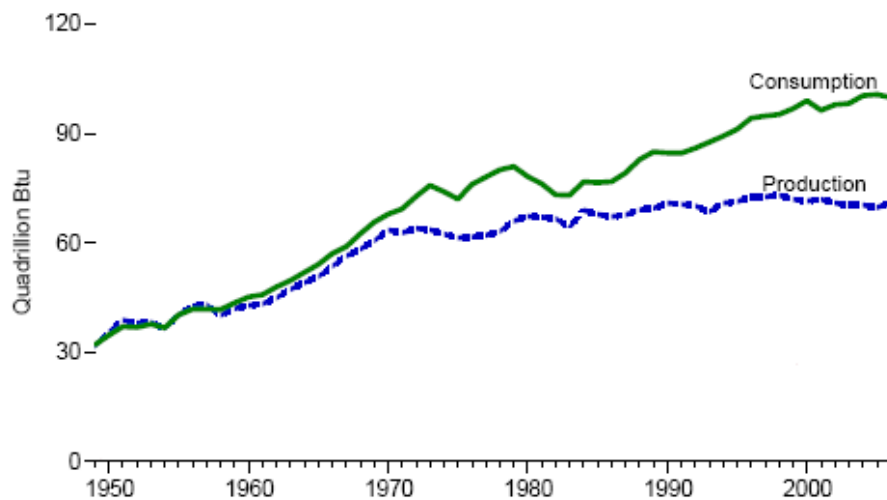
Fig. 1.1   US energy consumption and US energy production (Energy Information
               Administration 2006)

The cost for this energy is also on the rise as the study reports that US energy

expenditures have risen steadily as reflected by the graph in Fig. 1.2. Emerging energy

markets in countries like China and India are having a dramatic effect on the world

energy consumption and are projected to double in the next 30 years, as seen in Fig.

1.3. World energy consumption is projected to increase by 57% as a whole in the same

timeframe (Energy Information Administration 2007).

Energy Expenditures, 1970-2004

Energy Expenditures per Person, 1970-2004

[1]Nominal Dollars are not adjusted for inflation
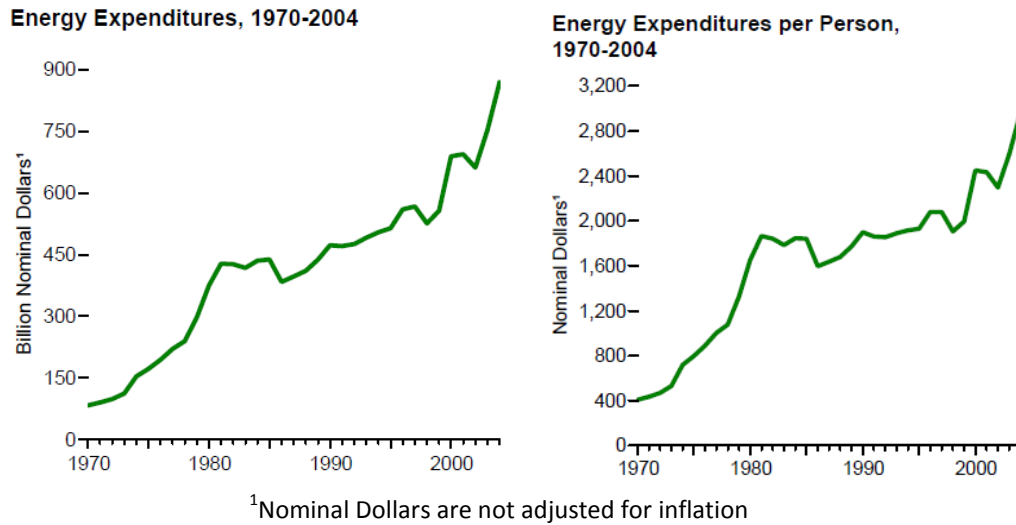
Fig. 1.2   US energy expenditures (Energy Information Administration 2006)

Quadrillion Btu
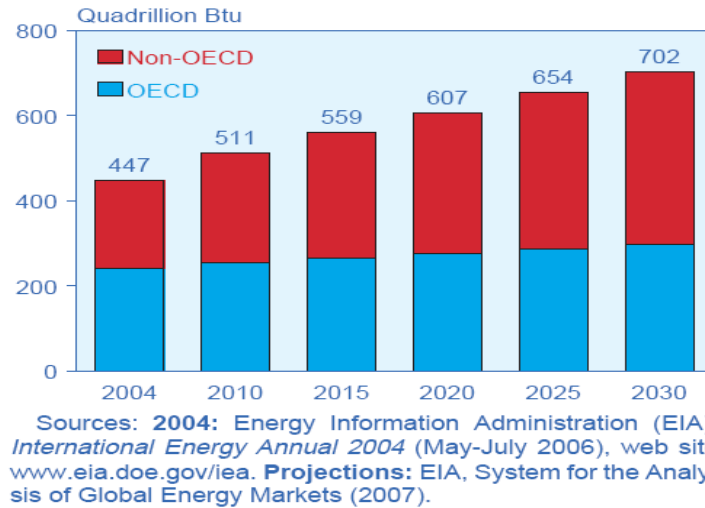
Members of OECD are generally regarded as developed countries, whereas, Non-OECD countries are generally regarded as developing

Fig. 1.3   World marketed energy consumption by region (Energy Information Administration 2007)

A majority of the energy being consumed is from non-renewable sources that are finite

in quantity as illustrated in Fig. 1.4.

Sources: **2004:** Energy Information Administration (EIA), *International Energy Annual 2004* (May-July 2006), web site www.eia.doe.gov/iea. **Projections:** EIA, System for the Analysis of Global Energy Markets (2007).
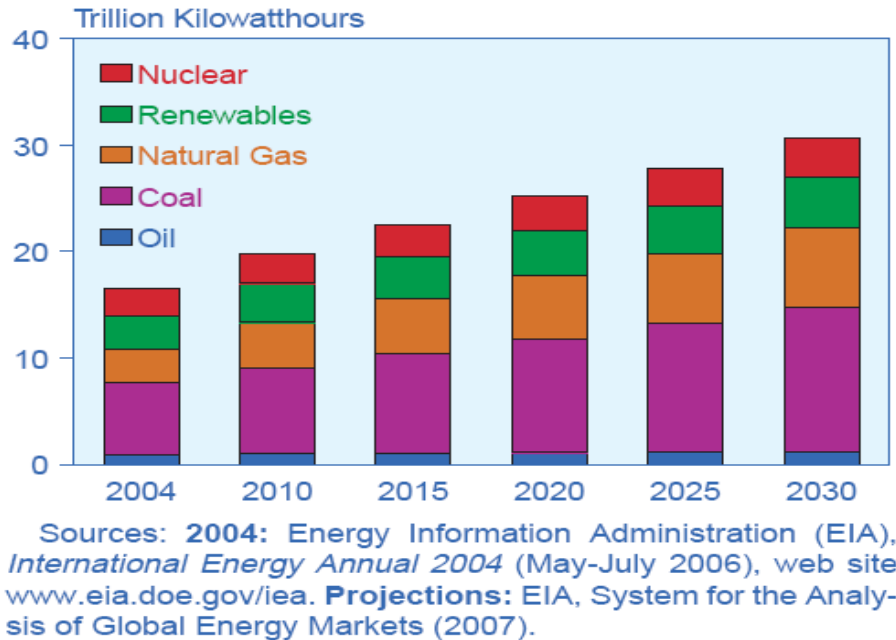
Fig. 1.4   World Electricity generation by fuel source (Energy Information Administration 2007)

The U.S. reliance on foreign energy imports, exploration of domestic alternatives, and consumption have become major U.S. social and political topics. Energy consumption and sourcing issues are not restricted to the U.S., and are a global problem. Initiatives based on environmental, social, and economic factors are attempting to reduce energy consumption and are being motivated among others by an increase in government regulations, energy prices, and environmental awareness. All of these factors are driving private industry and academia to research new energy focused technologies.

Combustion byproducts are believed by many to be harmful to the environment. One of the major contributors to air pollution is carbon dioxide, and the total amount of carbon dioxide byproduct produced by the U.S. has steadily increased in the last 25

years (Energy Information Administration 2006), as shown in Fig. 1.5. These

environmental factors are also contributing to a vigorous look at alternative energy

sources and technologies.

Based on Global Warming Potential, 1980-2005
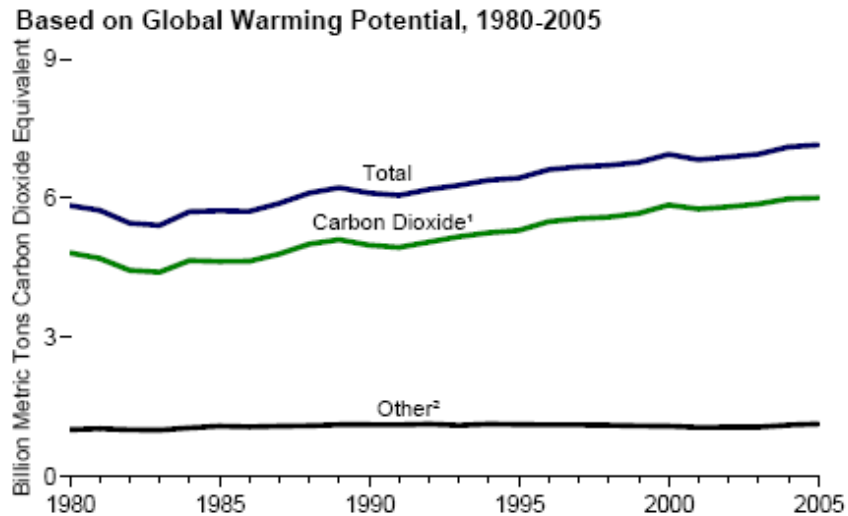
Fig. 1.5   Source of carbon dioxide emission by industry and fuel source
               (Energy Information Administration 2006).

The energy problem is comprised of two parts; consumption and supply. This thesis

investigates solid-state power generation devices designed for niche applications in

both direct power generation and waste heat recovery.

Solid state energy conversion typically refers to thermionic and thermoelectric

devices. Thermoelectrics are arguably the more well known and wide spread example

of solid state energy conversion. There have been many different solid state energy

conversion devices which have been used for both electrical power generation from a

heat source and active refrigeration. Thermoelectric devices are used in high

performance desktop computers (Caswell, 2007), luxury vehicles (Weisbart & Coker,

2001) and numerous other applications. Thermionic devices have been used in more

4

exotic applications such as space exploration where electricity is generated from a radioisotope heat source and the field emission phenomenon is commonly used in the electronics industry, and imaging technologies most notably scanning electron microscopy.

This thesis will introduce two novel field modified emission energy conversion devices that are intended to convert low grade thermal energy to electricity. The goal of this thesis is to analyze performance and efficiency metrics of these devices to determine the feasibility of their use in waste heat applications. To do this, system level models are developed that combine estimates for thermal, electrical and emission behavior.

The following chapters will provide a foundation for system level analysis by developing the models from governing physics and providing a background into potential waste heat applications to identify the boundary conditions. Solid state physics concepts such as material work function; Fermi levels and potential energy barriers are given to compliment this foundation.   A discussion of general emission physics is provided to develop models for electric and magnetic field modified emission.

Using the provided foundation in general emission physics, field modified emission models are then presented. Using these models, parametric studies are performed to illustrate emission dependence upon key parameters. Additionally, a detailed discussion of space charge effects and modeling are presented.

The final modeling effort is the incorporation of emission modeling with detailed thermal models. Again parametric studies are performed and key performance metrics are evaluated. Finally, a chapter dedicated to device fabrication is provided for the proposed nanowire thermal field emission convertor.

2. BACKGROUND

This chapter provides a brief discussion of several potential heat source applications and introduces a reference device that will be used throughout the thesis. An understanding of the application of an energy conversion device is necessary to properly identify and model boundary conditions. The reference device will be used to describe basic thermal and emission concepts.

i.   DIRECT POWER GENERATION

Direct power generation in the context of this thesis refers to a process with the sole intent of converting a raw energy source into electricity. The conversion of indirect process waste heat will be discussed later.

Including the energy source for direct power generation is a key element of a system level modeling approach. A system level model for a solid state energy convertor, such as TE and TI generators, that includes the heat source offers the ability to access the feasibility of efficiently generating power from a given source. Many solid state energy convertors are modeled with constant temperature boundary conditions that don't capture the important interactions between heat source and energy convertor. The following sections will define boundary conditions for a few potential applications that have been investigated for direct energy conversion.

Portable power consuming devices like laptop computers, cell phones, wearable computers, personal mobility systems (electric wheelchairs), and portable refrigerators

are becoming more popular and requiring larger amounts of energy. Batteries currently are the dominant energy source for such applications. Drawbacks of battery technology are the toxic solid waste for disposable batteries and the re-charging time for rechargeable batteries. Solid-state power generation devices offer reliability, low weight and re-fuelable.

a. BATTERY REPLACEMENT

This thesis will investigate the application of solid state energy conversion devices as possible battery replacement technology. The use of these solid state devices as a battery power source is an example of a direct power generation. Solid state electricity generators have the potential to reduce the solid waste and re-charging time of batteries, while increasing the device energy density.

Solid state energy convertors are heat engines that require only a heat source to generate electricity. Potential heat sources could range from process waste heat, to combustion of a fossil fuel like diesel, to the smoldering of a solid fuel stick, to captured solar heat. The energy density of diesel fuel is on the order of 100 times that of a battery (A rechargeable AA battery stores about 10.8 kJ of energy which results in an energy density of 1.2E9 J/m^2). There is a potential to significantly increase on the energy density of current battery technology.

b. PULSE POWER SOURCE

Another example of direct energy conversion is pulse power generation. Pulse heat sources were investigated for use in portable power generation applications similar to a battery. The use of energetic nanomaterials was investigated as a potential pulse heat source. Energetic materials are explosive materials used in various military applications. The energy density of these materials has been shown to be greater than that of TNT. A portion of the energy expelled during the reaction process results in heat dissipation. A numeric and analytic transient thermal model was developed to understand the thermal response of the fast transient burn process associated with the energetic reaction. The total energy release is estimated to determine the potential for a portable pulse power generation device.

Experimentation with the material involved application of a single trace (line) of material on the surface of a glass slide. The material was ignited by heater at one end of the slide. The energetic reaction started at the ignition site and moved across the slide. A moving heat source was used to thermally model this reaction. The thermal penetration into the material was important to characterize in order to help understand the potential to generate power from the thermal energy released by the reaction. Fig. 2.1 shows the analytical results (Q-Step Approx) compared against the numeric simulation (Fluent) which shows agreement. Accurate experimental data was not

available to compare because the thermal instrumentation used was not able to capture the fast thermal transient of the reaction.

Q step verification
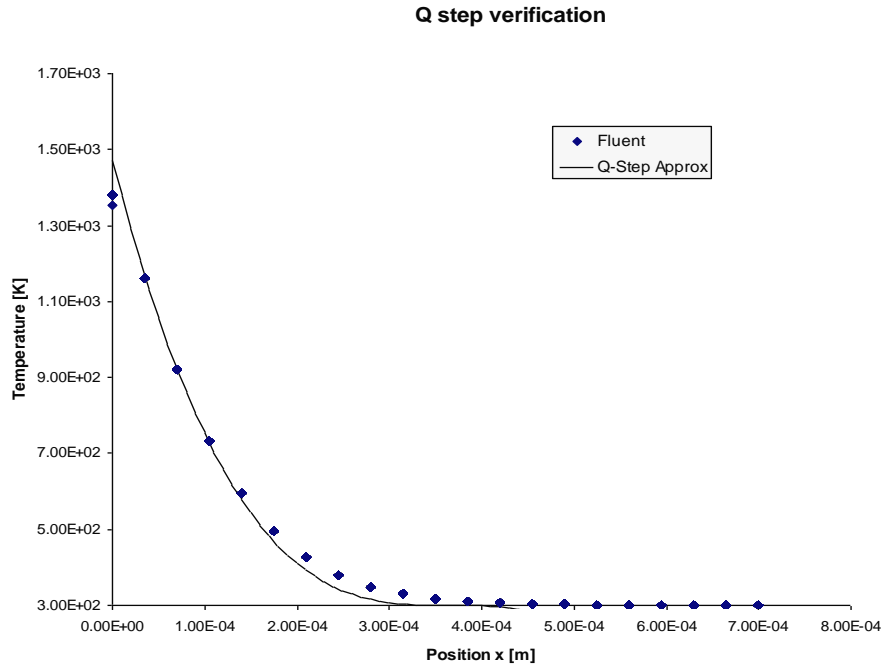
Fig. 2.1   Plot of Analytic and Numeric approximations of the transient thermal response of an energetic material reaction

Experimentation was performed at an attempt to capture the temperature of a substrate during and after the burn process. Multiple temperature measurement methods were deployed to capture this fast transient.

The substrate was first instrumented with a bonded type K thermocouple. The temperature measured of the substrate before and after the burn did not align with our expectations based on the numeric and analytic modeling.   The next step taken was to deploy an infrared camera to capture the thermal radiation emitted from the substrate. The camera interprets the thermal radiation and correlates that to a surface

10

temperature. The refresh rate of the IR camera was too slow to capture the fast response of the burn process. The final method used was to apply phase change materials designed to melt at various temperatures sometimes referred to as "thermal crayons". Each material with a given melting point has a different color. A small amount of each crayon was applied to the substrate. After the burn process a visual inspection revealed that some of the lower melting point crayon marks had vanished leaving only the marks of the crayons with a melting point above the substrate temperature. This allowed us to put bounds on the substrate temperature.

Ultimately the temperature measured was not in agreement with our numeric and analytic modeling. This discrepancy could be attributed to a lower energy density than reported or a greater amount of the reactions energy being expelled as a form of energy other than heat. The analytic and numeric models assumed that all of the reactions energy release was dissipated as heat. Based on the lower than expected temperatures, converting the energetic reaction's heat rejection into electricity was deemed infeasible. As will be discussed later, one key to energy conversion is the source temperature. For a pulse power application, the source temperature must be very high to achieve significant electricity generation.

ii. INDIRECT POWER GENERATION

Indirect power generation is used here to refer to the recovery of a process's thermal byproducts. Reuse or recycling of recovered waste heat is a necessary

ingredient to solve the power consumption crisis. This is because power consuming devices will in general have irreversibilities that reduce the device efficiency and are commonly manifested as acoustical, vibrational and thermal waste byproducts. Some devices produce a considerable amount of low grade waste heat that is typically disposed of by dissipating it into the ambient surroundings resulting in the destruction of exergy. This waste heat is almost by definition comprised of a lower quality energy making it difficult and less efficient to recover. Low quality waste heat is more difficult due to the temperature delta limitations and inherent limitations in generation efficiency as defined by Carnot.

Thermal energy conversion into electrical power is typically performed on a large scale by converting thermal energy into mechanical energy and then into electrical energy using electromagnetic induction. Waste heat has been recovered in coal power plants for decades (Cengel & Boles, 2002). Every steam regeneration cycle reduces the grade of the heat such that there is less useful energy remaining in the steam/water.

Solid-state energy conversion removes the mechanical conversion step from the process. Mechanical losses typically result in lower conversion efficiencies and reduced reliability. Converting heat directly into electricity has the potential to offer higher efficiency energy translation.

Solid-state power generation provides a variety of compelling attributes that make waste heat recovery of low grade energy more attractive in an age of energy awareness. These devices offer low weight, high reliability, and small size, but have traditionally

suffered from low conversion efficiencies and high cost. Given the right application and sufficient optimization solid-state waste heat recovery can be an economical solution to reduce energy consumption.

On a smaller scale, recovery of low grade waste heat can increase the efficiency of hybrid automobiles, computers, power plants, portable generators, solar generators, etc. The following sections provide brief discussions of waste heat sources that have been identified as potential candidates for waste heat scavenging.

a.   AUTOMOTIVE WASTE HEAT

High fuel prices have driven consumers and manufacturers of automobiles to pursue higher efficiency vehicles, as seen in Fig. 2.2. Recovery of engine and exhaust waste heat is one avenue being pursued to enhance fuel mileages.
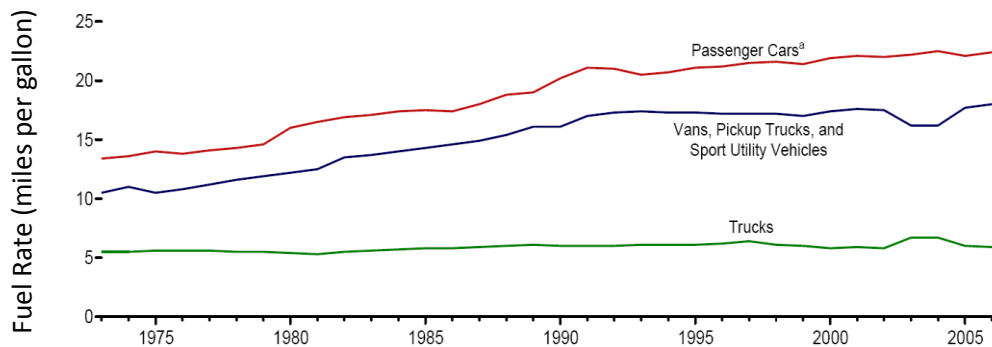
Fig. 2.2   Motor vehicle trending for fuel rate (miles per gallon) (Energy Information Administration 2006)

Car and truck engine exhaust heat recovery can be integrated with hybrid battery and electric motor technologies to stretch fuel mileage. Hybrid automobiles that currently recover braking energy utilizing an electric motor/generator are already

performing waste heat recovery. Kinetic energy during breaking is being converted into

a stored potential energy in the form of a battery instead of generating brake heat.

Hot engine exhaust is another form of waste heat that is generated during

combustion and is typically expelled with the exhaust gases. Thermal waste heat

recovery for engine exhaust can replace the low efficiency alternator on many

automobiles. Efficient thermoelectric devices have been estimated to have the potential

to save 7.1 billion gallons of gas a year (Fairbanks 2006).

Recovery of engine waste heat could also be performed using solid-state energy

conversion. Development of waste heat recovery systems utilizing thermoelectric

power generation are currently being pursued by multiple automobile manufacturers

(Fairbanks 2006).

b. SERVER COMPONENT WASTE HEAT

An area of energy consumption that is being scrutinized is datacenter power

consumption.   Datacenters are estimated to consume 1.5% of U.S. energy

consumption, which cost a total of about $4.5 billion dollars according to a U.S. Energy

Star report (ENERGY STAR program 2007). Fig. 2.3, illustrates that unless new

innovative advances in server/datacenter technology are developed and implemented

this problem will continue to grow. This thesis explores how waste heat from individual

server components can be converted directly into electricity. Component operating

temperatures and heat dissipation requirements are discussed here to help define the

boundary conditions of the problem.
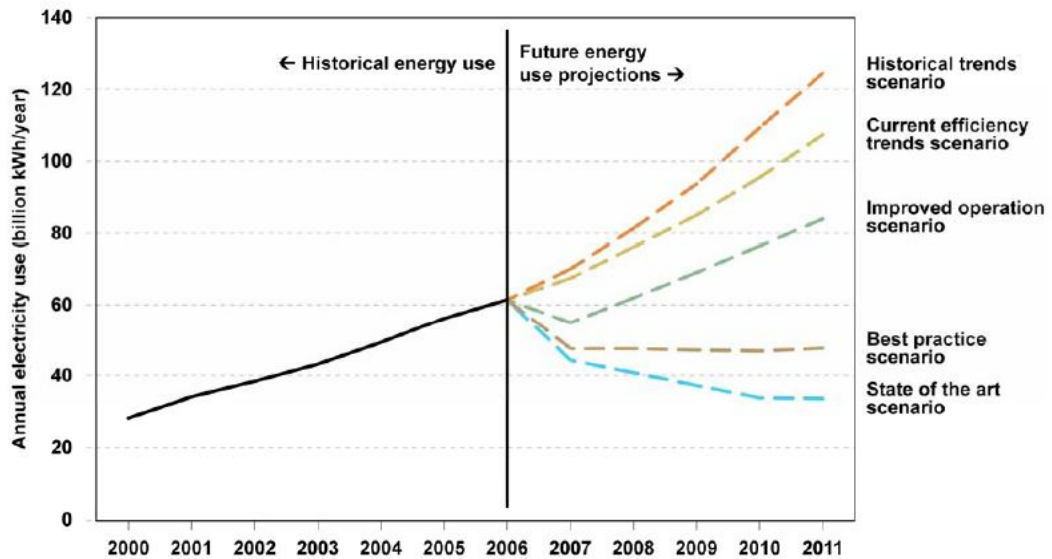
Fig. 2.3   Historical and projected datacenter energy consumption trends (EPA 2007)

Recovered energy is used to offset energy consumption and improve process

efficiencies. In the case of computers, waste heat recovery can be used to drive fans for

the cooling system to reduce the fan power burden on the system and facility cooling

requirements. The vast majority of servers are air cooled with forced convection. This

means that the energy consumed by the server is dissipated into the air. The air is then

typically conditioned by Computer Room Air Conditions (CRAC) or Computer Room Air

Handler (CRAH) which accounts for at least half of most data center's power budget.

The waste heat recovered from a server has at least a 2X effect on power

consumption at the datacenter level. First, generation of electricity replaces a portion

of the power that would have been consumed from the grid by the server. Second, that heat that was converted to electricity no longer has to be removed by the CRACs or CRAHs. Lastly, there will be smaller losses in datacenter and server power distribution due to the reduced load. Therefore, recovery of server waste heat impacts more than just the individual server power consumption and may lead to more than a 2 watt power savings for every 1 watt of recovered power.

The power consumption of individual server components can range from 0-150W. The dominating consumers are generally the microprocessors (CPUs), memory modules, chipset, voltage regulation components, power supplies and hard drives. The maximum operating temperature of most server components ranges from 60°C to 150°C.

Hard drives consume as much as 20W and have a relatively low maximum allowable temperature ~50-60°C. Hard drive densities in a server rack can range from a diskless operation to roughly 200 hard drives in high density storage applications. Their low operating temperatures make them a poor candidate for waste heat recovery.

CPUs consume as much as 150W and operate at junction temperatures between 60-75°C depending on utilization and processor type. A typical server can have anywhere from one to four separate processors. A standard 42U rack with 1U 2S servers will contain 84 processors per rack. This means there can be over 10kW of CPU heat dissipated per rack. It should be noted that CPUs generally have heat sinks with retention hardware lending them to be integrated more readily with energy conversion hardware with minimal changes to existing server hardware.

A single memory module consumes less than 20W of power. However, due to the high number of memory modules available in today's servers, a bank of memory can consume as much or more power than a CPU. The maximum package temperature of most memory modules is around 85-95°C. A rack of high density servers can have round 500 memory modules. The relatively high operating temperature makes an attractive candidate for waste heat recovery. The challenge in recovering the memory waste heat is the dispersion of power over the large surface area of the many modules.

Chipset and other various components typically dissipate under 50W and have temperature limits of up to 125°C. Some of these components are allowed to operate at higher maximum temperatures. However due to the variability of board layouts and components used, a custom recovery solution would be required.

In addition to recovering waste heat, it is necessary to ensure each component temperature is maintained at its specified value. The challenge exists in properly cooling the component and maintaining high enough temperatures for appreciable energy conversion. These competing requirements require a complex thermal solution. It is necessary to integrate the converter design with a thermal solution that can manage the operating temperature of the component without overcooling. Solbrekken, et al (Solbrekken, Kazuaki and Bar-Cohen 2004) has shown one such implementation in his study of waste heat recovery of CPU waste heat in a portable computer.

Thermal energy conversion requires a temperature difference across the converter to produce useful work. Energy converters need to be cooled with the cold temperature

17

provided by the supply air from the data center cold aisle. Data centers generally

operate from 15°C to about 30°C. The temperature ranges and heat loads available in

the server/data center environment are complied in Table 2.1. These boundary

conditions will be used to determine the feasibility of implementing solid-state waste

heat recovery.

Table 2.1   Identified server component specifications

Component	Approximated Operating Temperature [°C]	Approximated Heat Dissipation [W]
CPU	60-75	150
Memory Module	85-95	20
Hard Drive	50-60	25

iii.   REFERENCE CONCEPT

For sake of discussion a reference device is presented in Fig. 2.4. This is a basic

representation of the common elements of an emission based energy converter. This

basic diagram is provided as an example to provide context for future discussions on

emission and thermal modeling.

The reference device includes the typical diode configuration with emitter and

collector electrodes. The emitter is in thermal communication with the heat source and

the collector with the ambient via a heat sink. Electrons are intentionally emitted from

the emitter electrode to be "collected" by the collector electrode. Unintentional "back

emission" is also emitted from the collector and collected by the emitter. The net

difference between the emitter electron emission and collector "back emission" is

equivalent to the electrical current generated by the device. The electrodes are

connected electrically to a load. The voltage potential developed is dictated primarily by

the material work functions of the emitter and collector.

Thermal modeling for the reference concept includes thermal radiation exchange

between the electrodes. Thermal resistances are modeled between the heat source and

emitter as well as between the collector and ambient air. It is important to accurately

estimate the emitter and collector temperatures because electron current emission is

an exponential function of electrode temperature.
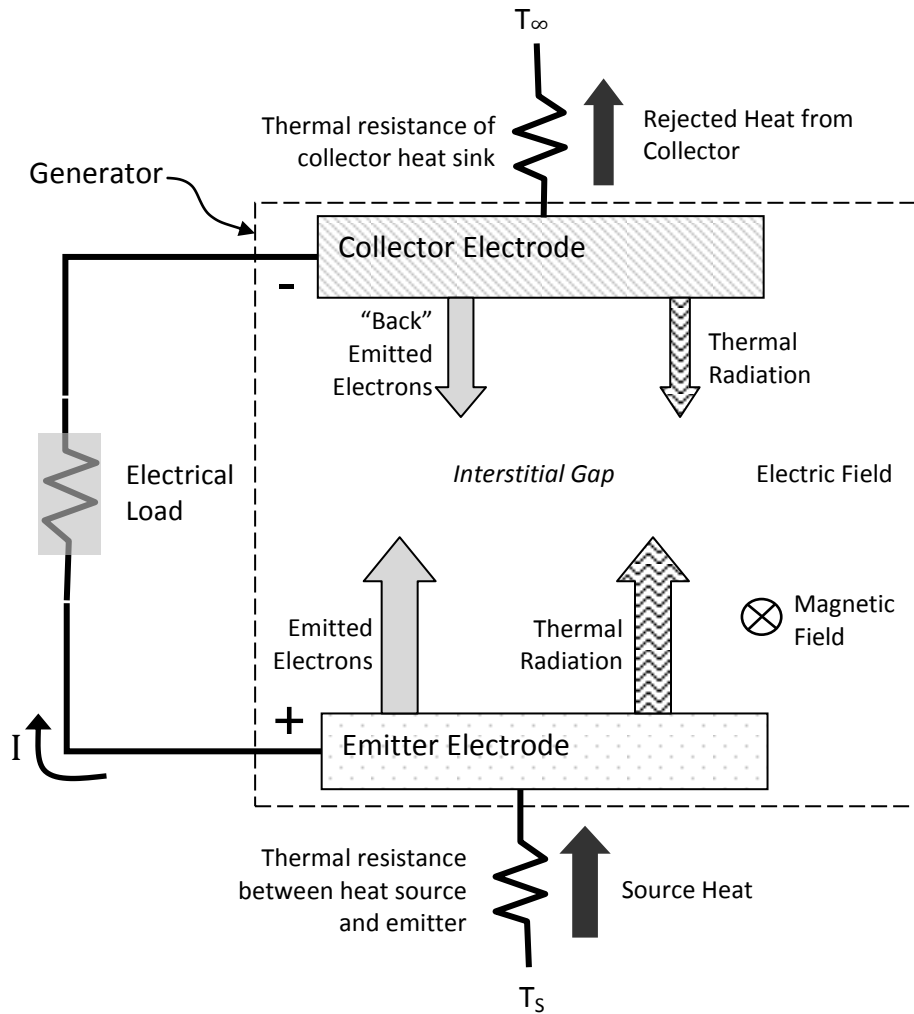
Fig. 2.4   Reference concept – baseline configuration

3. EMISSION PHYSICS

The term emission refers to a process of an object that is expelled, discharged or ejected and in the context of this thesis will be used to refer to the process of electrons being expelled from a material surface. Thermal-to-electric energy conversion is accomplished via thermally excited electron emission currents. At first glance it may seem that the goal of any thermal-to-electric energy conversion system would be to maximize electric current generation. This thesis will show that it is not always best to maximize the generated electron emission current due to inherent losses such as Joule heating, leakage currents and space charge that reduce the efficiency of the converter. Instead an optimization of the efficiency or net power generation of the device is performed using a system level modeling approach.

 The emitted current density can be statistically estimated using various emission models based on a number of parameters including temperature, applied fields and material properties. The following emission models will be based on a flat plate electrode as illustrated in the reference concept (Fig. 2.4).

A key element of all emission models is the potential barrier that exists in the interstitial gap between electrodes (as seen in the reference concept Fig. 2.4). The interstitial gap can be made up of a vacuum, plasma, gas, positive ion cloud, or solid material(s). The potential barrier is the summation of forces inhibiting the escape of an electron from a material, thus reducing the number of emitted electrons.

There are two mechanisms by which an electron can overcome the potential barrier: thermionic (TI) and tunneling emission, as suggested by Fig. 3.1. Thermionically emitted electrons are high energy electrons that have sufficient energy to overcome the opposing force of the potential barrier. Unlike thermionically emitted electrons, tunneling electrons are low energy electrons that have insufficient energy to overcome the potential barrier, but still find their way across the barrier. More detail is provided on these mechanisms in the coming sections.

(A)

Total Electron Energy

Thermionic Emission

"Potential Barrier"

Φ_E

Φ_C

Electron Energy

Kinetic

Potential

Kinetic

Potential

← Emitter → ← Gap → ← Collector →

(B)

"Potential Barrier"

Total Electron Energy

Tunneling Emission

Φ_E

Φ_C

Electron Energy

Kinetic

Potential

Kinetic

Potential

← Emitter → ← Gap → ← Collector →
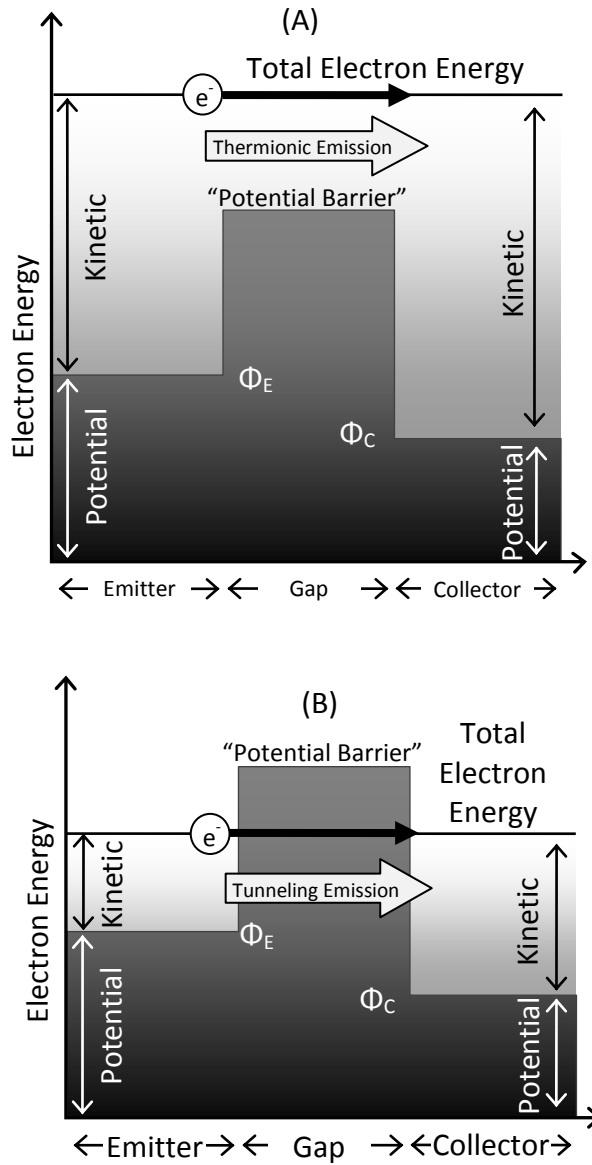
Fig. 3.1   Illustration of thermionic (A) and tunneling (B) emission mechanisms

i.   FERMI LEVEL, WORK FUNCTION & THE POTENTIAL BARRIER

There can be multiple contributors to the magnitude of the potential barrier with

the prominent contributors being the electron's attraction to the material lattice known

23

as the work function and the electron's repulsion to electrons already in the interstitial

gap known as space charge. The material work function is due to the positive charge of

the lattice attracting the electrons to the material and is defined as the amount of

energy required for an electron to be elevated from the Fermi level to the vacuum level

(free space). The Fermi energy level E_f, is the highest electron energy state populated

for a material at absolute zero temperature.

The magnitude of the potential energy barrier, as depicted in Fig. 3.2, is heavily

influenced by material and surface properties.   The electronic properties also influence

the magnitude of the generated voltage potential of the device. The material Fermi

level and work function are the primary properties that determine the emission and

generation behavior for a given material set.
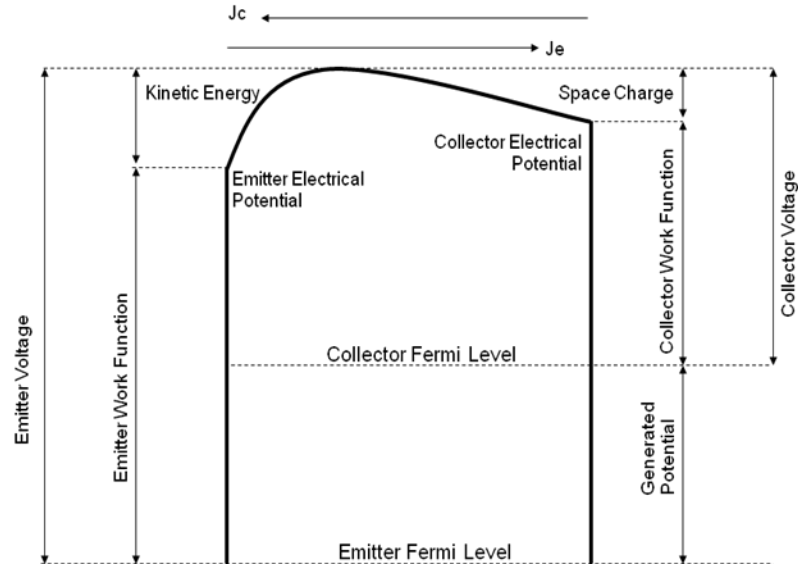
Fig. 3.2   Thermionic potential barrier adopted from (Angrist 1976)

As stated earlier the Fermi energy level E_f, is the highest electron energy state populated when a material is at absolute zero temperature. As the temperature of the material increases a portion of the electrons will attain energy states above the Fermi level. At any temperature above absolute zero the probability of the Fermi level energy state being occupied by an electron is always 50%. The Fermi energy level E_f, is given by:

$$E_f = \frac{h^2}{2m_e}\left(\frac{3n_e}{8\pi}\right)^{2/3}$$

3.1

where h is Planck's constant, n_e is the number of electrons per unit volume, and m_e is the mass of an electron. The probability of an electron being at energy E, for a given temperature is described by the Fermi-Dirac distribution. The Fermi-Dirac distribution f_f at energy E, is given by

$$f_F(E) = \frac{1}{\exp^{(E-E_f)/k_B T_e} + 1}$$

3.2

where k_B is Boltzmann's constant, and T_e is the electron's temperature. For temperatures above absolute zero there is a finite probability that an electron will have an energy greater than the Fermi level, as shown in Fig. 3.3.
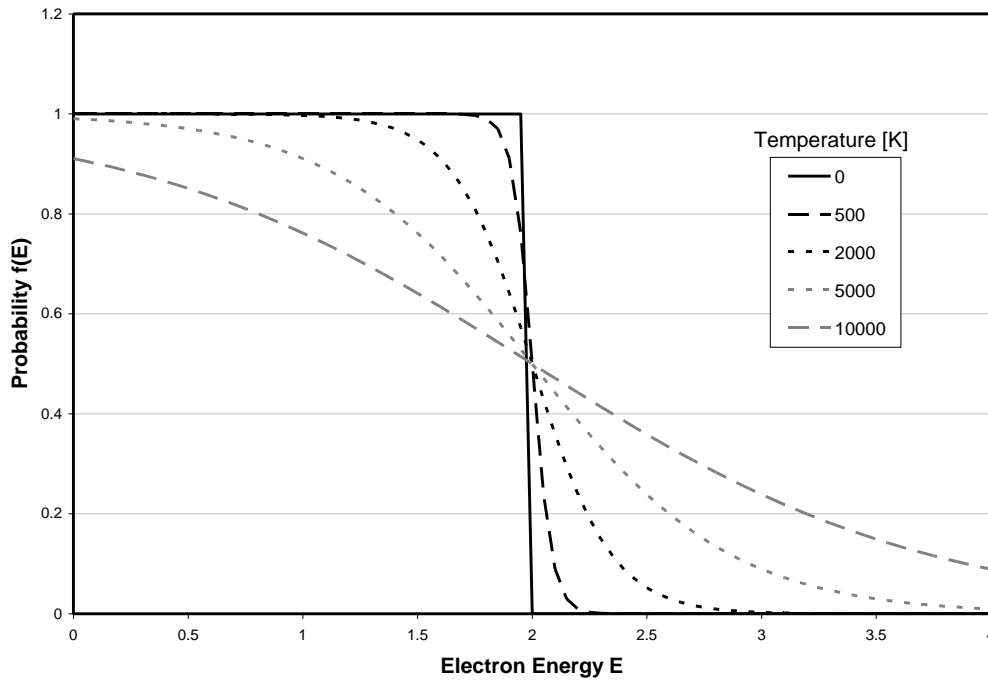
Fig. 3.3   Fermi-Dirac Distribution for a material with a Fermi level of 2 eV

The energy required to remove an electron from a material to a point in a vacuum of

infinite distance away is defined as the material's work function. The typical units for

work function are in electron-volts (eV). This material property can be likened to the

latent heat of vaporization of a solid if one envisions electron emission as a sublimation

process. A low work function results in a low potential barrier which in turn increases

the thermionic emission current. The work function ϕ , is related to the materials Fermi

level E_f and ionization energy χ by:

$$\phi = \chi - E_f$$ 3.3

Ionization energy is amount of work required to remove the outermost electron from an

individual atom in free space. Equation 3.3 is illustrated graphically in Fig. 3.4.
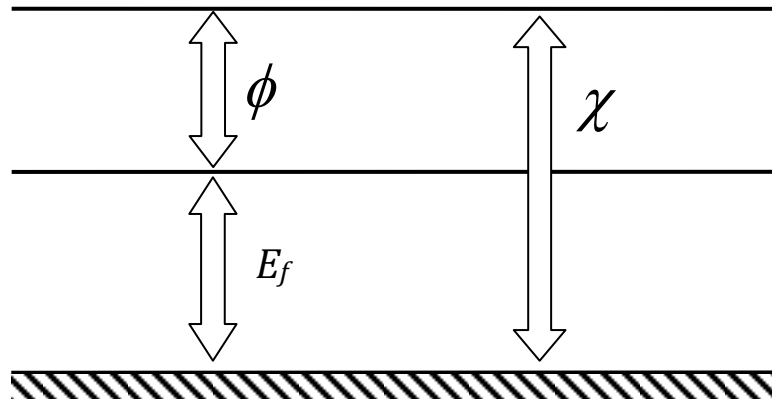
Fig. 3.4   Illustration of the relationship between ionization energy, work function and the Fermi level as described in Equation 3.3

Surface atoms are bonded differently to the lattice as compared with atoms located in the interior of a material. The interaction between the escaping electron and surface atoms are commonly the dominant force driving the magnitude of the work function. To date most accurate work functions are measured empirically. Work functions of various materials are listed in Table 3.1.

Table 3.1   Tabulated values of work functions for various materials

Material	Material Symbol	Work Function, ϕ [eV]	Melting Point [°C]
Cesium	Ce	2.9	798
Gold	Ag	4.26	1064
Molybdenum	Mo	4.6	2617
Platinum	Pt	5.65	1772
Titanium	Ti	4.33	1660
Tungsten	W	4.55	3410
Scandate	-	1.6*	-
Silicon	Si	4.85	1410
Silicon Carbide	SiC	4.4-4.6**	-

(CRC Press, Inc, 1983-1984)
* Estimated based on Scandate emission measured by Gaertner et al (Gaertner, Geittner, Lydtin, & Ritz, 1997)
**(Mackie, Hinricks, & Davis, 1990)

The material work function can also vary as a function of material temperature where the work function ϕ is given by:

$$\phi = \phi^* + \alpha T_{material} \hspace{3cm} 3.4$$

where ϕ^* is the work function at $T = 0$ K, and α is the temperature coefficient ($d\phi/dT$). Fig. 3.5 shows the variation in work function for Tungsten across a temperature range. While the variation appears insignificant, electron emission increases exponentially with work function which results in large changes in current density for small variations in work function. The plot shows that a 0.18 eV increase in work function results in a 50% reduction in current density.

Further emission modeling in this thesis does not include work function variation to temperature, but instead uses a conservative estimate of work function for simplification. This leaves an opportunity to further refine the modeling efforts and perform optimizations.
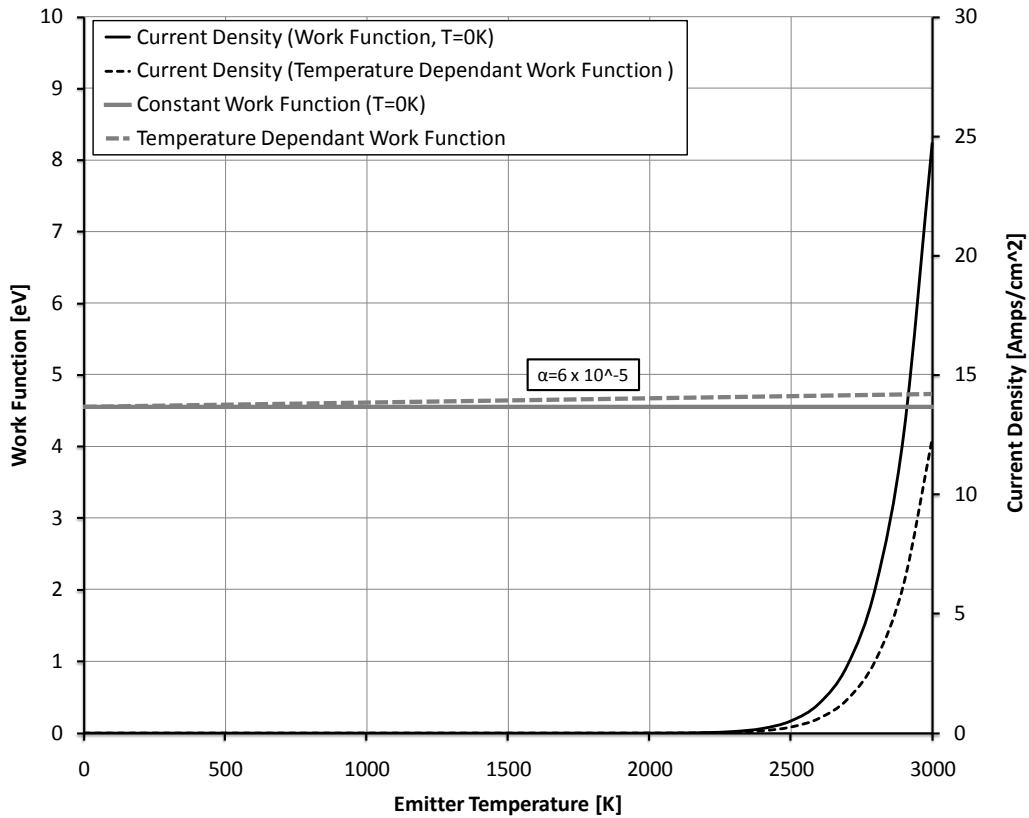
Fig. 3.5   Plot of work function temperature variation for Tungsten, and estimates for TI current densities using a fixed (T=0K) and temperature dependant work functions

ii.   THERMIONIC EMISSION

Thermionic (TI) emission is an emission process used in solid state energy conversion where electrons are typically emitted from a solid material at an elevated temperature.

As previously stated, TI emitted electrons are those with enough total energy to overcome the potential energy barrier.

Thomas Edison through his work on the light bulb was one of the early discoverers of thermionic emission. Commonly considered the father of TI theory and recipient of the 1928 Nobel Prize in Physics for his contribution, Owen Richardson developed an empirical correlation for describing TI electric current density (Richardson 1921):

$$J_{TI} = A_o \sqrt{T_E} \exp^{\left(-\frac{e\phi_E}{k_B T_E}\right)}$$
<div align="right">3.5</div>

where A_0 the emission constant and ϕ_E the work function are material properties specific to the emitter, and T_E is the emitter temperature. This equation matched well with empirical data, however, was not analytically derived.

Shortly thereafter GE Laboratory's Saul Dushman corrected Richardson's empirical equation by fundamentally relating TI emission to evaporation of a monatomic gas (Dushman 1923). Dushman made the assumption that the physical process of sublimation of a monatomic gas is equivalent to that of the TI emission process. Presuming that this assumption holds true the material work function would be equivalent to the latent heat of vaporization. Dushman's equation became generally accepted and the most widely used model for estimating TI current densities and is now well known as the Richardson-Duschman equation (Richardson 1921) (Dushman 1923). The common form of the Richardson-Dushman equation is:

$$J_{TI} = A_0 T_E^{\,2} \exp^{\left(-\frac{e\phi_E}{k_B T_E}\right)}$$
<div align="right">3.6</div>

The Richardson-Dushman equation assumes a Maxwellian electron energy distribution, which limits the use of this equation to regions of high temperature. Other models for predicting TI emission have been developed by Langmuir (Langmuir 1913) (Langmuir 1923), (Langmuir 1929), and Child (Child 1911), but are not as widely used. These models account directly for space charge effects, but tend to overestimate current densities.

TI emission is often likened to the thermodynamic sublimation process where a solid is converted to a saturated gas with the addition of heat/energy. Similarly electrons in a material are converted to an (emitted) electron gas with the addition of the necessary amount of heat/energy. The following illustrates the derivation of the Richardson-Dushman equation for TI emission utilizing the thermodynamic sublimation process. Using the Clausius-Clapeyron equation, the heat of vaporization on a per-mole basis for a monatomic gas $\overline{h}_{fg}$, is

$$\overline{h}_{fg} = \frac{dP_{mg}}{dT_{mg}} T_{mg} v_{fg} \qquad\qquad 3.7$$

where P_{mg} is the vapor pressure at temperature T_{mg}, and v_{fg} is the difference in specific volume between vapor and liquid. Assuming that the monatomic gas obeys the ideal gas law and that the specific volume of gas is greater than that of a liquid:

$$\overline{h}_{fg} = \overline{R}T_{mg}^2 \frac{d\ln P_{mg}}{dT_{mg}} \qquad\qquad 3.8$$

where $\overline{R}$ is the universal gas constant. The heat of vaporization at standard pressure can also be expressed as a function of T_{mg} (Dushman, 1923)

$$\overline{h}_{fg} = \overline{h}_0 + \int_0^{T_{mg}} c_{p,vapor} dT_{mg} - \int_0^{T_{mg}} c_{p,solid} dT_{mg}$$

3.9

where $\overline{h}_0$ is the latent heat of the electrons at absolute zero temperature, $c_{p,vapor}$ is the specific heat of the vapor at constant pressure, and $c_{p,solid}$ is the specific heat of the solid. Combining equations 3.8 and 3.9 and solving for P_{mg} yields

$$\log P_{mg} = -\frac{\overline{h}_0}{\overline{R}T_{mg}} + \frac{1}{\overline{R}}\int_0^{T_{mg}} \frac{\int_0^{T_{mg}} c_{p,vapor} dT_{mg}}{T_{mg}^2} dT_{mg} - \frac{1}{\overline{R}}\int_0^{T_{mg}} \frac{\int_0^{T_{mg}} c_{p,solid} dT_{mg}}{T_{mg}^2} dT_{mg} + C$$

3.10

where C is the constant of integration. The constant C for monatomic vapors is (Dushman, 1923):

$$C = C_0 + \frac{3}{2}\log M$$

3.11

where C_0 is the "universal constant", and M is the molecular weight . Units for this constant are provided by dimensional analysis performed by Tolman (Tolman, 1920).

The specific heat of a monatomic gas is constant and is given by the relation

$$c_{p,vapor} = \frac{5}{2}\overline{R}$$

3.12

and the specific heat of the solid is assumed to be negligible. Therefore equation 3.10 becomes

$$\log P_{mg} = -\frac{\overline{h}_0}{\overline{R}T_{mg}} + \frac{5}{2}\log T_{mg} + C_0 + \frac{3}{2}\log M$$

3.13

Reducing this equation and taking the exponential provides

$$P_{mg} = M^{3/2} T_{mg}^{5/2} \exp^{\left(-\frac{\bar{h}_0}{\bar{R}T_{mg}}\right)} \exp^{(C_0)}$$

The molecular weight of an electron is given by:

$$M = N_A m_e$$ 3.15

where N_A is Avagadro's number (6.0221415 x 10^{23}). Equation 3.13 becomes

$$P_{mg} = (N_A m_e)^{3/2} \exp^{(C_o)} T_{mg}^{5/2} \exp^{\left(-\frac{\bar{h}_0}{\bar{R}T_{mg}}\right)}$$ 3.16

and the current density J_{TI}, is given by

$$J_{TI} = n_e e$$ 3.17

The kinetic theory of gases predicts that the number of electrons n_e, incident on a unit

area of material is given by

$$n_e = \frac{P_E}{\sqrt{2\pi m_e k_B T_E}}$$ 3.18

Assuming

$$T_{mg} = T_E$$ 3.19

$$P_{mg} = P_E$$ 3.20

then

$$J_{TI} = \left(\frac{N_A^{3/2} m_e e \exp^{(C_0)}}{\sqrt{2\pi k_B}}\right) T_E^2 e^{-\frac{\bar{h}_o}{\bar{R}T_E}}$$ 3.21

Comparing Equation 3.21 with the Richardson-Dushman equation (equation 3.6) yields

the following relation:

$$\frac{\phi}{k_B} = \frac{\bar{h}_o}{\bar{R}}$$

3.22

 This relationship illustrates the similarity between enthalpy and work function. Both

are a measure of the energy required for a particle, be it a monatomic particle or an

electron, to be released from a solid material. The gas constant is equivalent to the

Boltzmann constant, but is expressed on per molar as opposed to per particle basis as

illustrated by:

3.23

$$\bar{R} = N_A k_B$$

The emission constant A_0 for a material is defined as:

$$A_0 = \frac{16\pi^4 k_B^2 m_e e}{\hbar^3}$$

3.24

where $\hbar$ is the reduced Plank constant.

Other forms of the derivation have been presented by (Angrist 1976), (Waterman

1924), (Dushman 1923), (Soo 1962), and (Richardson 1921). The Richardson-Dushmann

equation (equation 3.6) can be derived using other techniques including statistical

thermodynamics.

To obtain significant electron emission, and hence electric current the emitter must

be held at a high temperature (on the order of 1000's K) and have a relatively low work

function. Fig. 3.6 shows the electron current density as estimated by the Richardson-

Dushman Equation 3.5 for thermionic emission as a function of temperature and work

function. The plot illustrates that at low temperatures thermionic emission will be

negligible unless lower work functions are achieved. Appreciable power generation at

low temperatures either requires further developments in material science that produce

lower work function materials or very large surface areas.
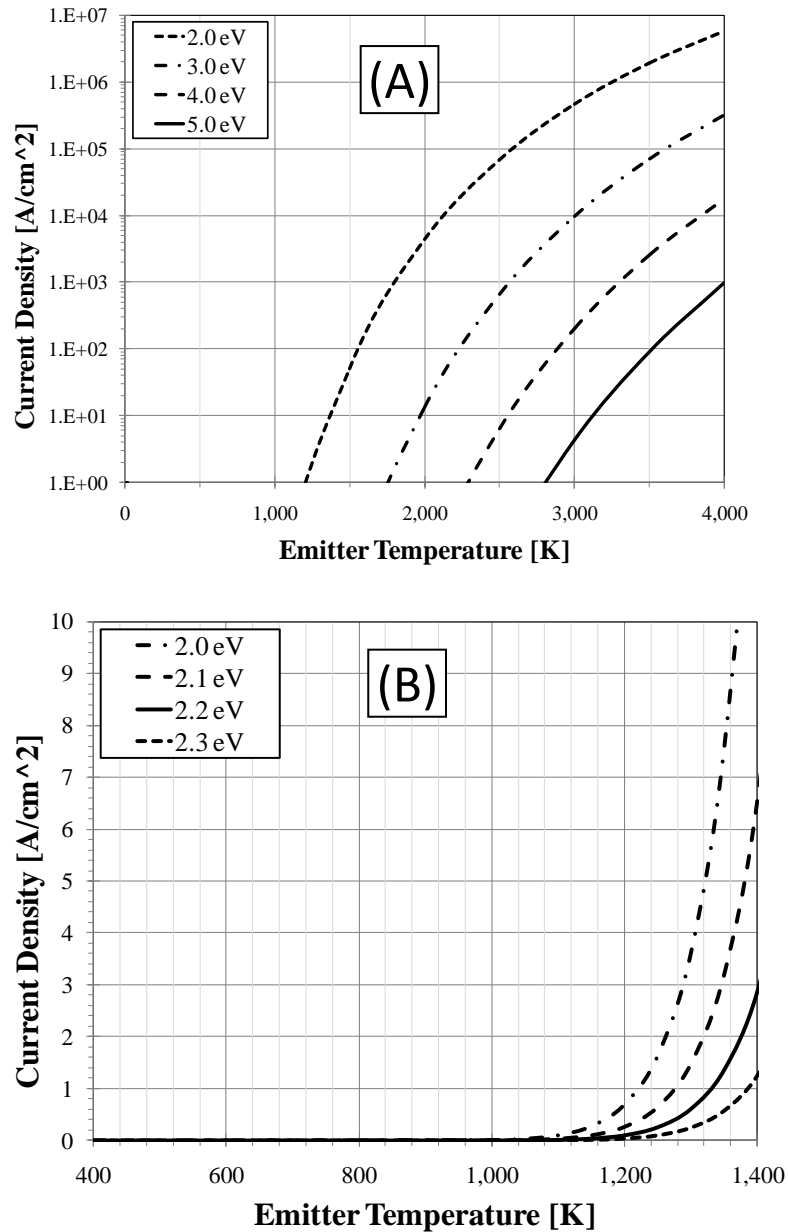
Fig. 3.6   Plots of flat plate thermionic emission currents for (A) work functions ranging from 2 eV to 5 eV to illustrate high temperature emission, and (B) work functions ranging from 2.0 eV to 2.3 eV to illustrate low temperature emission

Power generation devices based on TI emission include the cesium diode (Angrist 1976), magnetic triode (Hatsopoulos and Gyftopoulos 1973) and superlattice (Mahan and Woods 1998), (Shakouri and Bowers 1997) among others.

iii.   TUNNELING

As the previous section on TI emission highlighted, only high energy electrons can be thermionically emitted. Electrons with insufficient energy can also be emitted via a mechanism known as tunneling. Classical mechanics predict that an electron with an energy level less than the potential energy barrier cannot escape the emitter material or penetrate the barrier and suggests that all such electrons will be reflected by the barrier. However, quantum mechanics developed in the late nineteenth and early twentieth century predicts a finite probability that a low energy electron can "tunnel" though the potential barrier as seen in Fig. 3.1.

The probability of tunneling is formulated by considering a thin potential barrier as illustrated in fig 3.7. Consider electrons in Region I of the figure that have higher potential energy than the barrier. The electron can freely travel from Region I, through Region II into Region III. As previously discussed, this is the TI emission process.

Now assume that electrons with lower potential energy than the barrier exist in Region I of Fig. 3.7. As stated previously, these electrons cannot thermionically traverse the barrier, but have a finite probability of tunneling through the barrier based on

quantum physics. The Schrodinger's one dimensional time independent wave equation

can be solved for the three regions to determine the probability of tunneling.
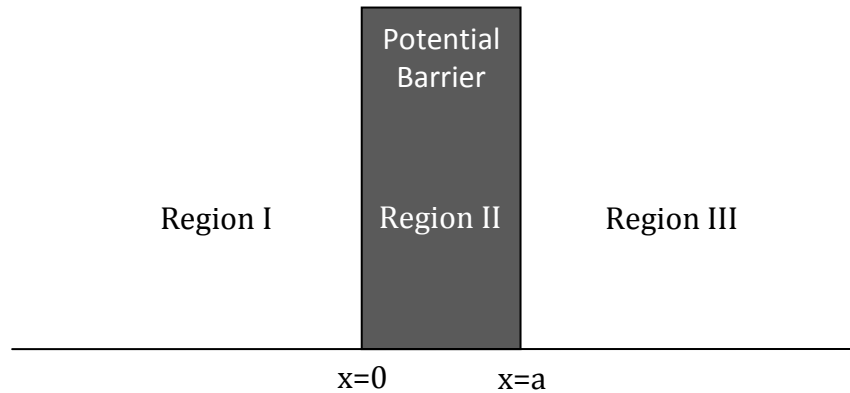
Fig. 3.7   Theoretical thin potential barrier

This finite probability has been experimentally validated and is generally accepted as

a fundamental behavior of nature. It should be noted that both classical and quantum

mechanics predicts and accounts for higher energy thermionic electron emission.

The probability of an electron tunneling is a function of the potential barrier and its

magnitude. The chances for tunneling decrease as the potential energy barrier becomes

wider. The profiles for the potential barriers vary in shape and size and can be

influenced by electric field, electrode material selection and the makeup of the

interstitial gap. The potential barrier profile for tunneling emission from a flat plate

(refer to the reference concept Fig. 2.4) is more accurately given by $V(x)$ (Hishinuma,

Geballe, & Moyzhes, 2001):

$$V(x) = \frac{\phi}{e} - \underbrace{V_{bias}\frac{x}{d}}_{E-field} - \underbrace{\frac{e}{4\pi E_0}\left[\frac{1}{4x} + \frac{1}{2}\sum_{n=1}^{\infty}\left(\frac{nd}{n^2d^2 - x^2} - \frac{1}{nd}\right)\right]}_{Image}$$

3.25

where V_{bias} the voltage difference between the emitter and collector (or gate in the case of field emission), x is the distance from the emitter surface, E_o is the permittivity of free space and d is the distance between electrodes. An example voltage profile for a flat plate is illustrated in Fig. 3.8. The figure illustrates how the electric field reduced the potential barrier height, and changes the profile shape. In the absence of an electric field (i.e. pure tunneling) the image force (or space charge) defines the potential barrier profile.
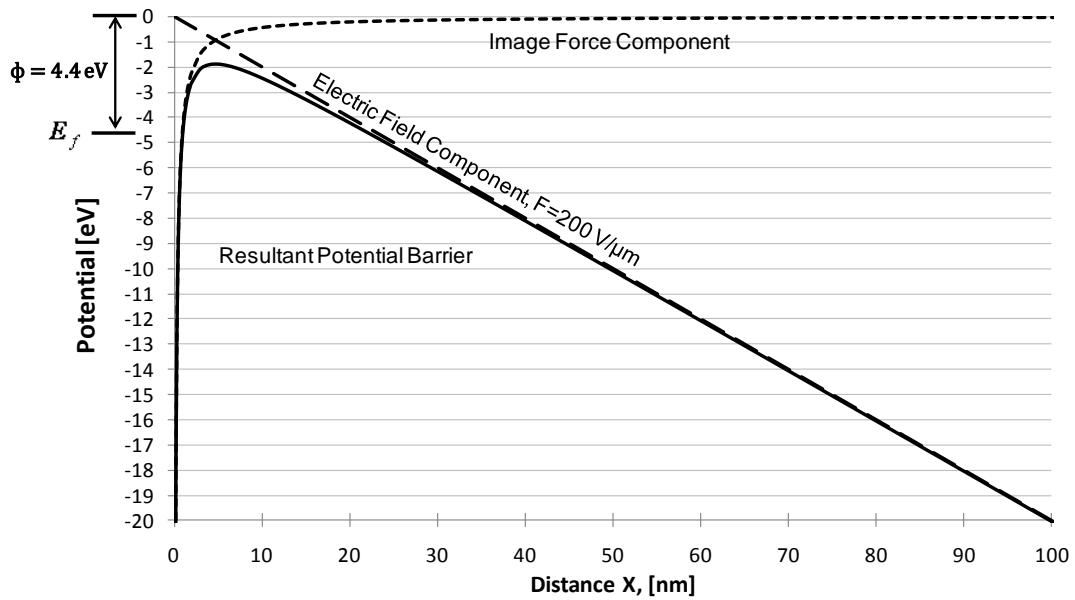
Fig. 3.8   Flat plate potential barrier example

a. FIELD EMISSION

Applying an electric field to the emitter material to enhance tunneling emission is a method known as field emission (FE). This process requires a gate electrode to apply the electric field that effectively thins the potential barrier. This thinning of the barrier increases the probability of tunneling electron currents. FE electrons are emitted via the tunneling process and are therefore at a lower energy state than TI electrons. Current display technologies rely upon field emission as a source of electrons.

Low temperature or "cold cathode" field emission is possible with use of an externally applied electric field via a gate electrode at the emission site (Nation, et al. 1999) which thins the potential barrier and increases the probability of tunneling currents. Modeling of field emission has been performed and is classically derived as follows.

Cold cathode field emission current density J_{FE}, can be estimated using probability distributions:

$$J_{FE} = e \int_0^\infty N(E_x) D(E_x, V_{bias}) dE_x \qquad \text{3.26}$$

where $N(E_x)$ is the electron supply function, $D(E_x, V_{bias})$ is the barrier transparency function (or transmission function), V_{bias} is the applied voltage between the emitter and collector, and E_x is the electron energy normal to the surface (x-direction). The electron number density is a product of the available quantum states and the probability that that state is occupied by an electron:

$$N(E) = g_c(E)f_F(E)$$
3.27

As discussed earlier the probability that a state is occupied by an electron is dictated by

Firmi-Dirac distribution as shown in Equation 3.5.

The number density of electrons is given by (Westover & Fischer, 2006):

$$N(E_x) = \frac{m_e k_B T_E}{2\pi^2 \hbar^3} \ln\left[1 + \exp\left(-\frac{E_x}{k_B T_E}\right)\right]$$
3.28

where m_e is the mass of an electron, k_B is Boltzmann's constant, T_E is the temperature of

the emitter surface, E_x is the kinetic energy in the x direction of an electron, and $\hbar$ is

the modified Planck constant.

The tunneling transmission coefficient $D(E_x)$, is the probability that an electron at

energy E_x, will pass through the potential barrier. Using the Wentzel–Kramers–Brillouin

approximation of the Schrödinger time-independent wave equation the tunneling

transmission coefficient is given by (Westover & Fischer, 2006):

$$D(E_x) = \exp\left[-\int_{x_1}^{x_2} \sqrt{\frac{8m_e}{\hbar^2}} |eV(x) - E_x| dx\right]$$
3.29

where x_1 and x_2 are the roots of $eV(x) - E_x$.

The Fowler-Nordheim (F-N) equation predicts the cold cathode electron emission in

the presence of electric fields at absolute zero temperature and is the solution for

equation 3.26. Experimental data has shown that field emission at low temperatures

(i.e. room ambient) can be closely modeled by the F-N equation for current density. The

current density J_{FE}, for T_E = 0 is

$$J_{FE} = \frac{1.5 \times 10^{-6} \beta^2 F^2}{\phi} \exp\left[-6.83 \times 10^7 \frac{\phi^{3/2}}{\beta F}\right]$$

where β is the field geometrical enhancement factor and the variable F is the applied electric field. Fig. 3.9, shows the electron current density as estimated by the Fowler-Nordheim equation for field emission as a function of electric field and work function. The figure illustrates that very high current densities can be achieved using cold cathode field emission. However, this emission mechanism is not suitable for thermal-to-electrical energy conversion since emission is not being driven or enhanced by temperature.
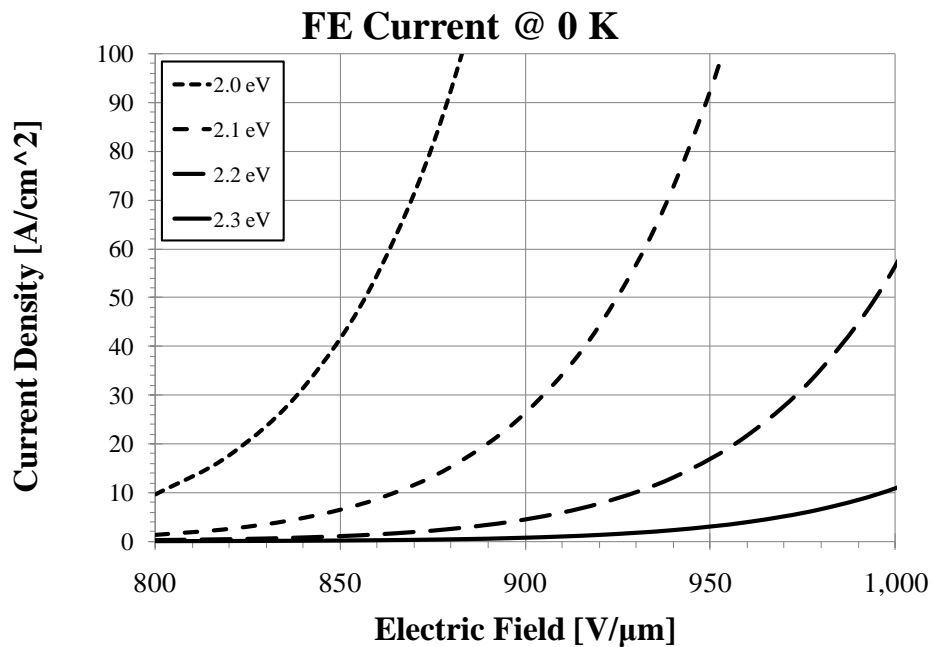
Fig. 3.9   Plot of flat plate (β=1) cold cathode field emission current densities for work functions ranging from 2.1 eV to 2.3 eV

The geometric enhancement factor accounts for non flat plate geometries such as tip emission. The electric field is concentrated at a sharp point, tip or sphere. It is

therefore possible to achieve high electric fields around a sharp point with a relatively

low gate voltage. This factor is typically determined empirically (Zuber, Jensen, &

Sullivan, 2002)(Teo, et al., 2002) .

A simple model for the geometric enhancement factor of an emitter tip is

approximated by (Zuber, Jensen, & Sullivan, 2002)

$$\beta = \frac{1}{r}$$
3.31

where r is the radius of the emitter tip.

A study by Brodie et al suggests the following geometric enhancement factor for

the spherical tip illustrated in Fig. 3.10 (Brodie & Schwoebel, 1994):

$$\beta = \frac{R}{r(R-r)}$$
3.32

where R is the radius of the outer sphere representing the gate electrode, and r is the

radius of the inner sphere representing the emitter tip.

Actual   Model
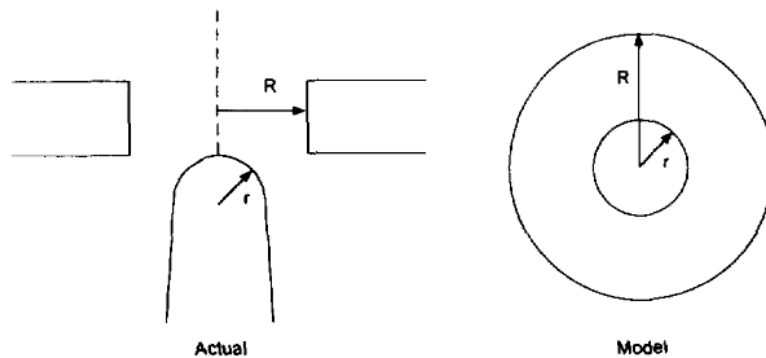
Fig. 3.10   Illustration of a (a) spherical tip emitter and gate electrodes and (b)
                 electric field model using concentric spheres (Brodie & Schwoebel, 1994)

A more complex and accurate treatment of the geometric enhancement factor

for a microtip is provided by Zuber et al where the factor is analytically derived based on

a prolate-spheroidal coordinate system (Zuber, Jensen, & Sullivan, 2002). Using the coordinate system in Fig. 3.11 the enhancement factor is given by

$$\beta(\xi) = \frac{1}{a \sin \theta\, Q_0(\cos \theta)\sqrt{\xi^2 - \cos^2 \theta}}$$

3.33

where $2a$ is the foci distance, θ is the tip half-angle , ξ is an orthogonal coordinate that defines prolate-spheriodial surfaces. The terms a and Q_0 can be determine from

$$a = \frac{d}{\cos \theta},$$

3.34

and

$$Q_0 \cos \theta = \tfrac{1}{2} \ln \left[\frac{1+\cos \theta}{1-\cos \theta}\right].$$

3.35
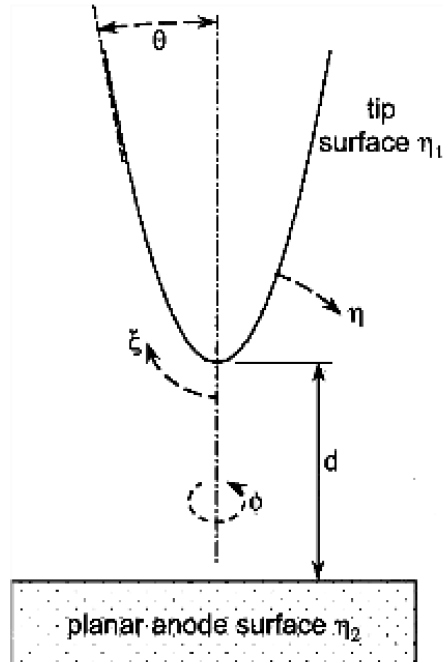
Fig. 3.11   Illustration of the prolate-spheroidal coordinate system used to derive the geometric enhancement factor in equation 3.37 (Zuber, Jensen, & Sullivan, 2002)

The 2D Folwer-Nordheim equation can be applied to 3D structures using the geometric enhancement factors, but due to the assumption that the emitter is at absolute zero temperature the Folwer-Nordheim equation for emission is only applicable for low temperature "cold cathode" emission. There exists an "intermediate region" between cold cathode FE and TI emission as illustrated in Fig. 3.12. The so called "intermediate region" is where a high temperature emitter in the presence of an electric field produces what has been named thermal-field emission (TFE).
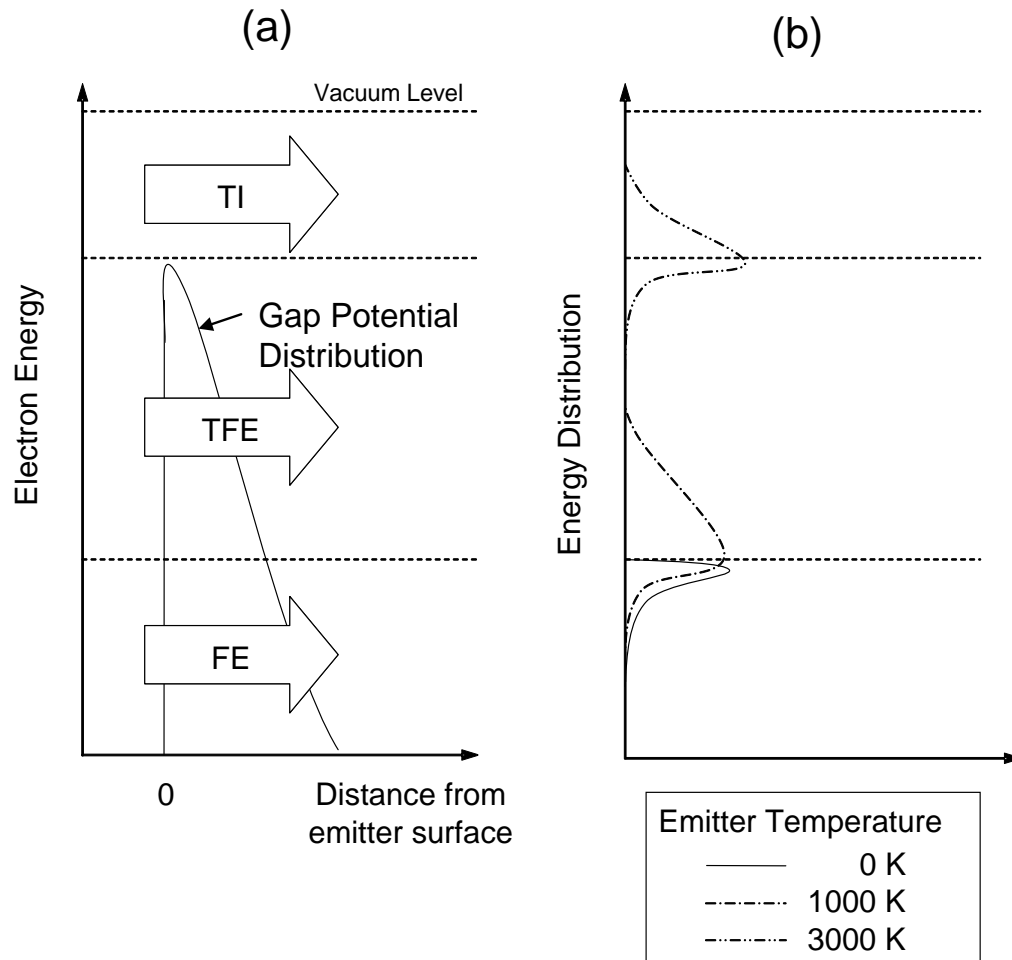
Fig. 3.12   Electron Transport Mechanisms: (a) Thermionic (TI), Thermal-Field (TFE), and Field (FE) Emission, (b) Approximate Energy Distributions for Emitted Electrons

b.   THERMAL-FIELD EMISSION

Thermal-field emission (TFE) was first presented in a study by W. W. Dolan and W. Dyke (Dolan and Dyke 1954). TFE is in essence field emission of electrons at above nominal temperatures.   TFE is of particular interest because it has the potential to produce significant currents at considerably lower temperatures than TI emission.

Unlike the Fowler-Nordheim model the solution for TFE includes the emission temperature. Solving the probability distribution integrals for current density is more complex when temperature effects are included.

An analytic model approximating TFE is presented by (Murphy and Good Jr. 1956). The thermal-field emission current density J_{TFE}, is defined by the analytic model:

$$J_{TFE} = \beta J_{FE} \qquad 3.36$$

where the scaling factor λ must be less than 5 and is defined as:

$$\beta = \frac{\pi \omega}{sin(\pi \omega)} \qquad 3.37$$

where ω is defined as:

$$\omega = \frac{4\pi \sqrt{2m_e \phi} k_B T_E t(y)}{heF} \qquad 3.38$$

and $t(y)$ is defined as:

$$t(y) = \theta(y) - \left(\frac{2y}{3}\right)\left(\frac{d\theta(y)}{dy}\right) \qquad 3.39$$

The Nordheim elliptical function $\theta(y)$ is given by:

$$\theta(y) = \frac{\sqrt{1 + \sqrt{1 - y^2}}}{\sqrt{2}} \left[E(k) - \left\{ 1 - \sqrt{1 - y^2} \right\} \right] K(k) \qquad 3.40$$

where

$$y = \frac{\sqrt{(e^3 F)}}{\phi} \qquad 3.41$$

$$E(k) = \int_0^{\pi/2} \frac{d\alpha}{(1-k^2 sin^2 \alpha)}$$

<div align="right">3.42</div>

<div align="right">3.43</div>

$$K(k) = \int_0^{\frac{\pi}{2}} \sqrt{(1-k^2 sin^2 \alpha)} d\alpha$$

and

$$k^2 = \frac{2\sqrt{(1-y^2)}}{1+\sqrt{(1-y^2)}}$$

<div align="right">3.44</div>

To a good approximation ω can be given by:

$$\omega = 9.22 \times 10^3 \sqrt{\phi} \frac{T_E}{F} < 0.7$$

<div align="right">3.45</div>

Equation 3.45 is plotted for various work functions and electric fields in Fig. 3.13. The plot illustrates that for the approximation is good for high electric fields.

Fig. 3.14 shows the TFE approximation, using the ω approximation given by equation 3.45, plotted as a function of electric field and work function for a given emitter temperature of 400K. Similarly, Fig. 3.15 shows the TFE approximation plotted as a function of emitter temperature and work function for a given applied field of 800 V/μm (or 8x10^6 V/cm). The figures illustrate that significant current densities can be achieved at relatively low temperatures. For this reason TFE conversion is believed to have a distinct advantage over TI conversion.
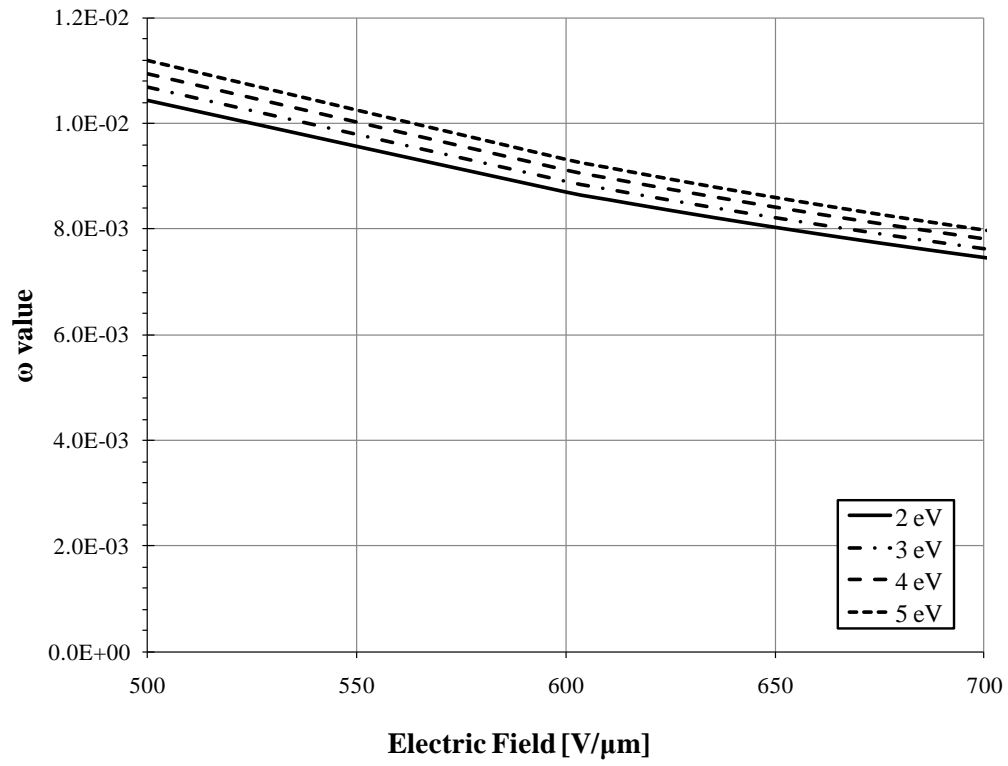
Fig. 3.13   Plot of approximated ω values based on equation 3.45 at constant temperature 400 K
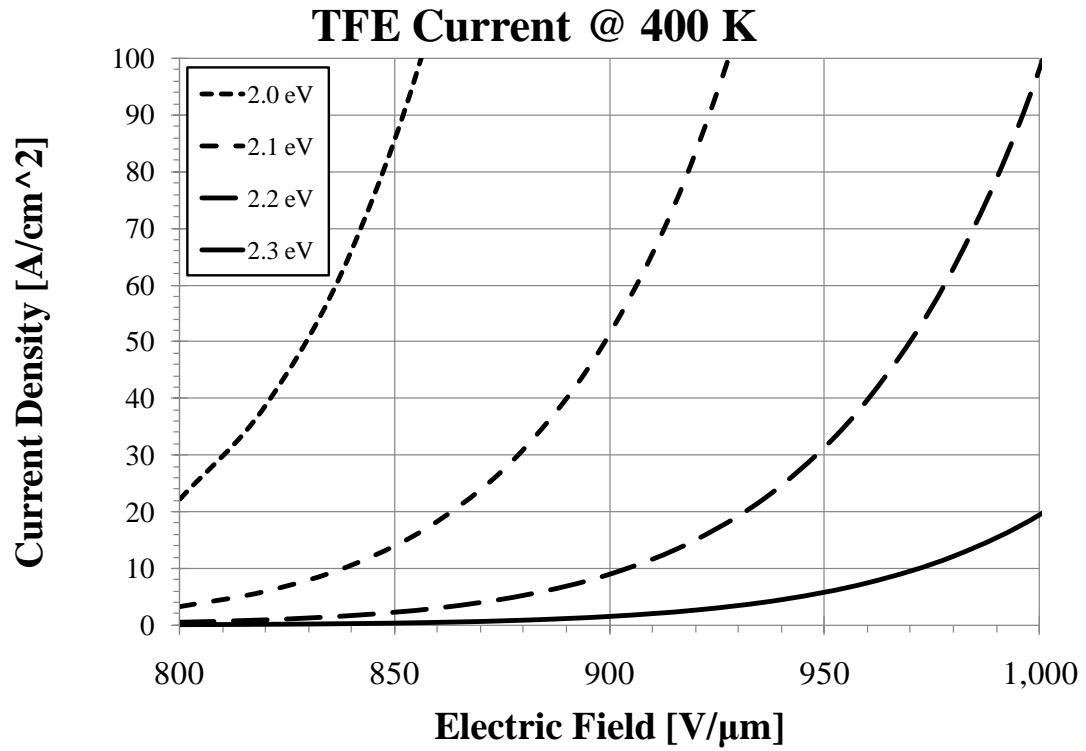
Fig. 3.14   Plot of thermal field emission current densities for various work functions
              (2.0 – 2.3 eV) with respect to applied electric field

TFE Current @ 800 V/μm
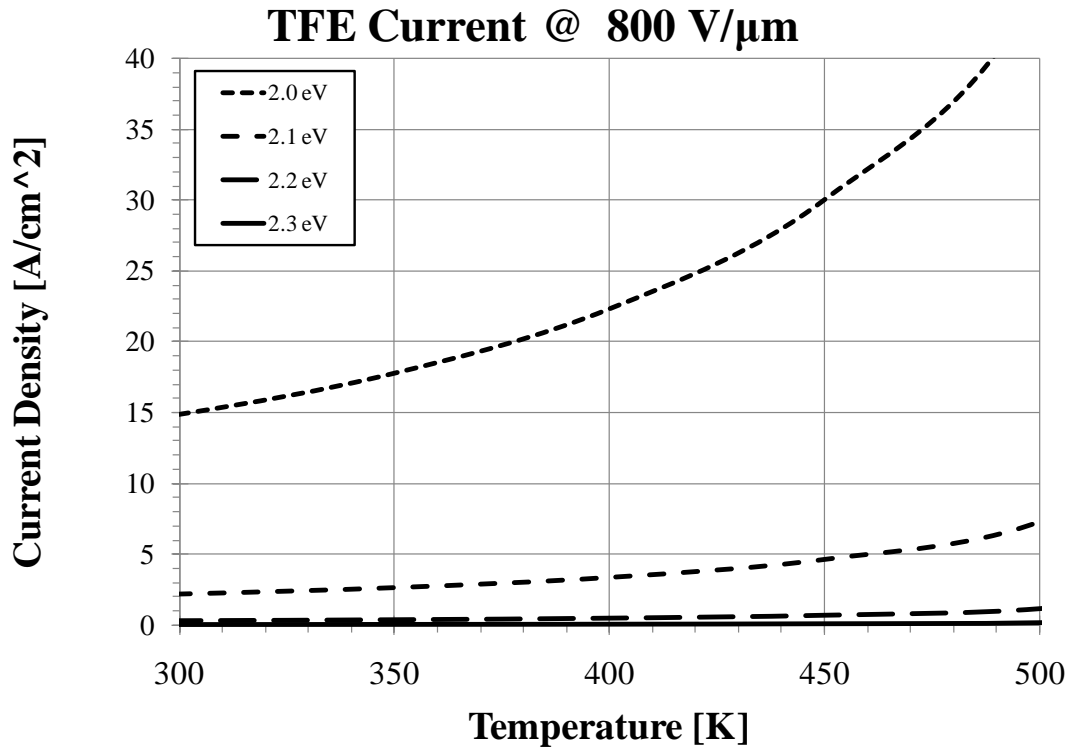
Fig. 3.15   Plot of thermal field emission current densities for various work functions (2.0 – 2.3 eV) with respect to temperature

TFE has other less obvious benefits over TI generation. The energy carried by

electrons from the emitter to the collector will increase the temperature of the

collector, increasing the thermal losses from the collector. Since TI emitted electrons

carry more thermal energy to the collector than TFE (Burstein et al., 1969, and Dolan et

al., 1954), it is expected that TFE will have smaller thermal losses, and hence a higher

efficiency then a TI generator. The lower temperature (< 1000K) operation of the TFE

generator is expected to also reduce the radiation losses from the emitter surface

relative to a TI generator.

50

The TFE modeling equations 3.36 through 3.45 describes a temperature dependant modification factor to FE. FE emission does not convert thermal energy into electricity and it is assumed that all energy transferred due to FE is balanced by energy consumed by the gate electrode to produce the electric field. Therefore, the net power generation and thermal energy conversion is only due to the additional electron current produced by TFE enhancement.

iv. EMISSION COMPARISON

Studies by Dolan, Dyke, Murphy and Good compare TI, TFE, and FE emission (Dolan & Dyke, 1954)(Murphy & Good Jr., 1956). The study by Dolan and Dyke illustrates that the three different emission types occur at different levels of the potential barrier. This is shown in Fig. 3.16, by plotting the electron number density on the left at 0°C, 1000°C and 3000°C correlating to FE, TFE, and TI emission temperatures, respectively. On the right hand side of the figure the potential barrier is plotted and broken up into the three regions of emission.
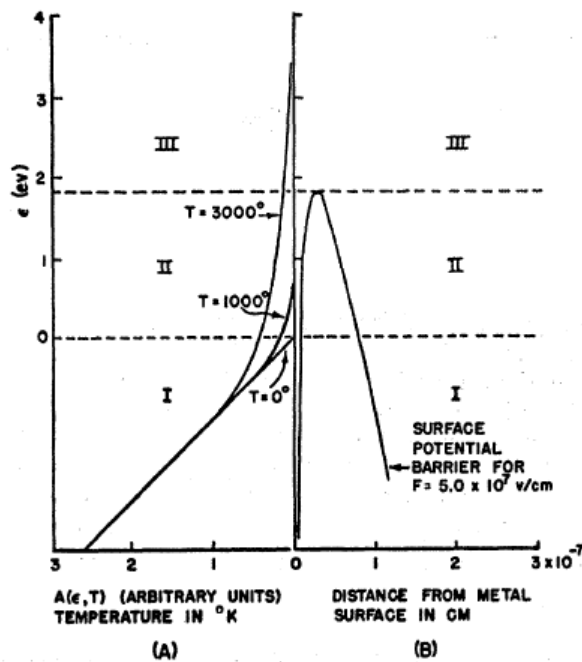
Fig. 3.16   Plot of potential energy barrier ("SURFACE POTENTIAL BARRIER") that includes the FE region (Region I), the TFE region (Region II) and the TI region (Region III). (Dolan & Dyke, 1954)

In the same study by Dolan et al, energy distributions of emitted electrons are plotted with respect to the three emission regions for a matrix of temperatures and applied electric fields, shown in Fig. 3.17. The plot illustrates that at low temperature (0 K), independent of field magnitude, a majority of the electrons are in region I which corresponds to FE. For intermediate temperatures (1000 K - 2000 K) the electron distribution transitions to higher concentrations of region II electrons as the field strength increases. For high temperatures (3000 K) the electron energy distribution transitions from region II to region III or, TFE to TI.

52
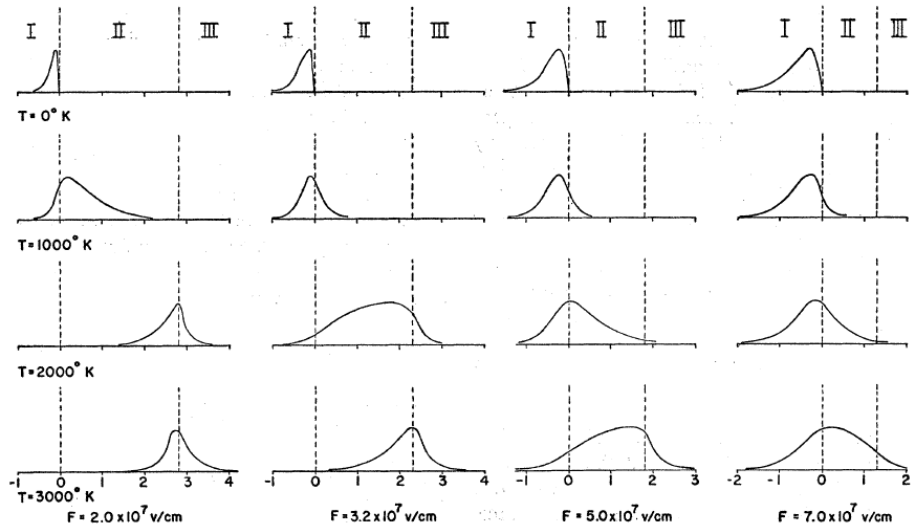
Fig. 3.17   Plots of the energy distributions for emitted electrons at various temperatures and applied electric fields (Dolan & Dyke, 1954)

In a different study, Murphy et al shows for a given temperature and electric field the regions where TI, TFE and TE are dominant, as shown in Fig. 3.18, where TFE is referred to as the "Intermediate Region". Murphy's regions are in relative agreement with the emitted electron energy distributions shown in Fig. 3.17.

53
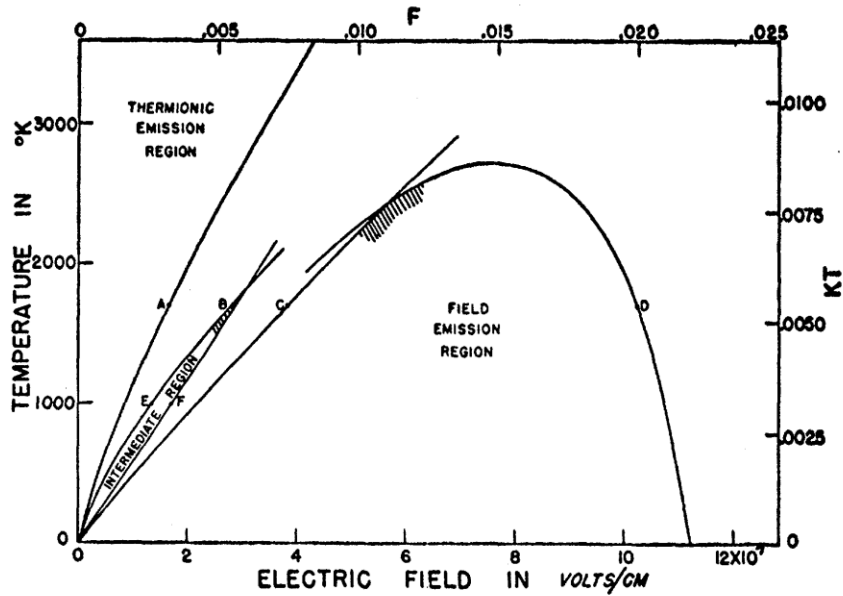
Fig. 3.18   Plot of the three emission regions as a function of temperature and
electric field (Murphy & Good Jr., 1956)

v.   SPACE CHARGE

TI, FE, and TFE can all be impeded by space charge effects. Space charge is an

inhibiting force on electron emission caused by electron screening in the interstitial gap.

This phenomenon has an additive effect on the magnitude of the potential barrier, but

there are several methods of reducing space charge such as introducing positive ions

into the gap or decreasing the distance between the emitter and collector.

As electrons are emitted into the inter-electrode gap a "space charge" develops due

to the electrons in transit from the emitter to the collector. The space charge causes a

repulsive effect on the electrons still in the material. The electrons must overcome both

the attractive forces of the lattice (work function) and repulsive forces of the space

charge. If no emission has occurred and hence no electrons are present in the

54

interstitial gap, no space charge is present as illustrated in Fig. 3.19 (a). As the number

of electrons in the interspatial region increase the repulsive force on electrons in the

lattice also increases as illustrated in Fig. 3.19 (b).
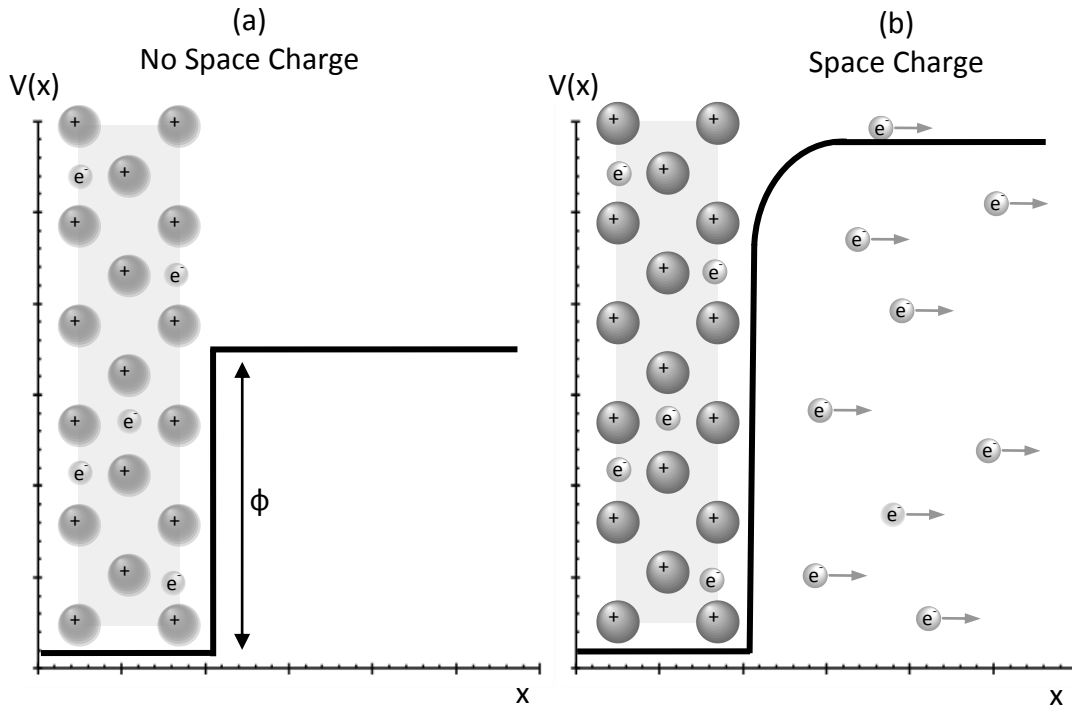
Fig. 3.19   Metal lattice (a) prior to emission with no space charge, and (b) after
             emission with space charge caused by emitted electrons

As current increases so does space charge and therefore high current designs are

more affected by space charge. From this benefit can be seen for higher voltage lower

current operation.

a. DERIVATION OF CHILD-LANGMUIR EQUATION

Deviations from the current predicted by Richardson at high temperatures led many

researchers to believe that TI emission was not a real phenomenon. Many believed that

the source of the electrons was a result of chemical reactions occurring between the

electrodes and interspatial gases. This belief was backed by low currents when emission

occurred in a high vacuum. In a study by Irving Langmuir (Langmuir 1913) it was

determined that the real culprit of the reduced current was a space charge build up due

to electrons in the interspatial region. At low temperatures emission followed

Richardson's predictions, as illustrated in Fig. 3.20. When current reached some critical

point, space charge build up was sufficient to reduce the emission and resulted in a

plateau. As higher voltage was applied to the collector the current was allowed to follow

Richardson's prediction until the current reached a new critical point.
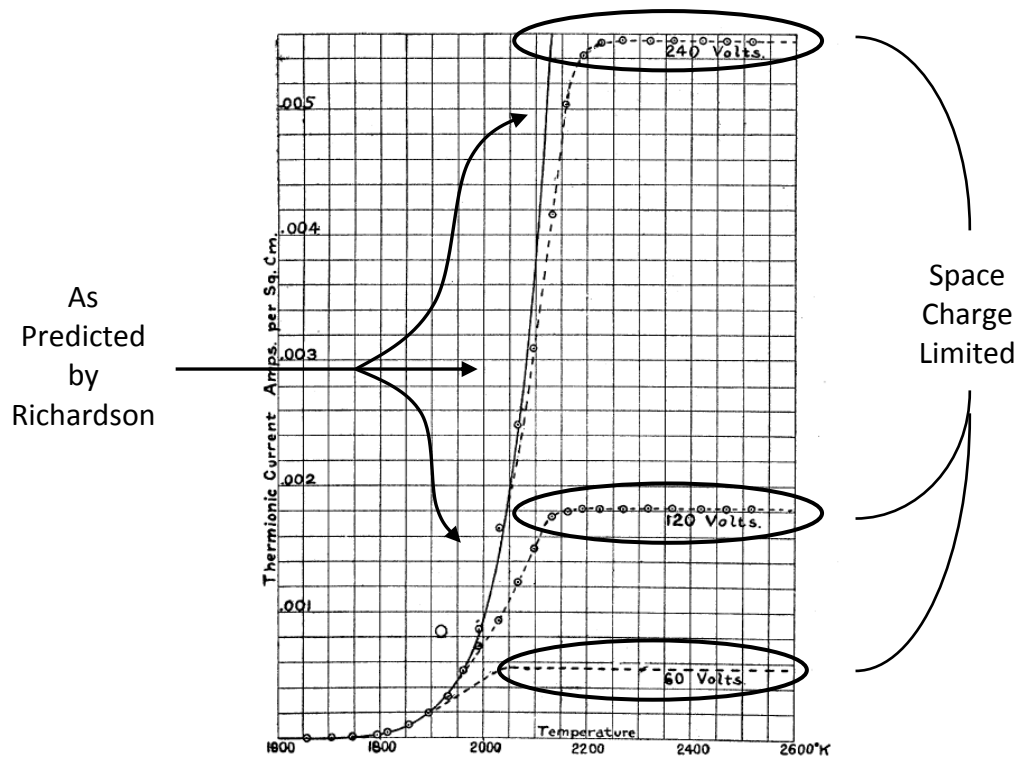
Fig. 3.20   Langmuir's findings for current at various emitter temperatures and
                 collector voltages with a gap of 1.2 cm (Langmuir 1913)

At high vacuums no gases are present to counter the charge of the electrons. Langmuir's study illustrated that that current could be increased by increasing the voltage of the collector, decreasing the interspatial distance between electrodes or increasing the area of the collector.

The following is a derivation of the Child-Langmuir equation for space charge limited electron emission. First, consider two electrodes separated by some distance d, where a vacuum is present in between electrodes, as illustrated in Fig. 3.21. The left electrode is biased to zero voltage and is elevated to a temperature such that appreciable electrons are thermionically emitted. The right electrode is biased to a positive voltage, and held at nominally room temperature, such that there is no appreciable electron emission. The assumption is made that emitted electrons have no initial velocity.
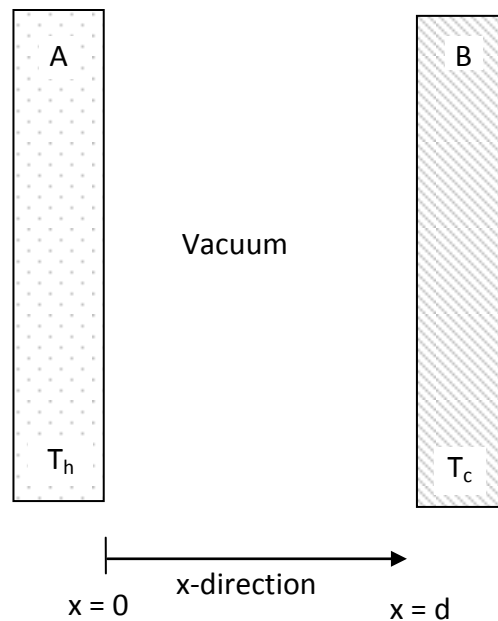
Fig. 3.21   Case for derivation of Child-Langmuir space charge model

From the Poisson equation:

$$\nabla^2 V = \frac{\partial^2 V}{\partial x^2} + \frac{\partial^2 V}{\partial y^2} + \frac{\partial^2 V}{\partial z^2} = -4\pi\rho \qquad \text{3.46}$$

where *V* is the potential at distance x from plate A, *x* refers to the x-direction as illustrated in the figure, *y* is the y-direction, *z* is the z-direction, and ρ is the space charge density. Assume that no emission occurs in the y and z directions and the equation reduces to:

$$\frac{d^2 V}{dx^2} = 4\pi\rho \qquad \text{3.47}$$

The kinetic energy of an electron traveling in the x-direction is given by:

$$\frac{1}{2} m_e v^2 = Ve \qquad \text{3.48}$$

where v is the velocity of the electron. The current density J, is given by:

$$J = \rho v \qquad \text{3.49}$$

v is eliminated from the preceding equations as follows:

$$v = \sqrt{\frac{2Ve}{m_e}} \Rightarrow J = \rho\sqrt{\frac{2Ve}{m_e}} \qquad \text{3.50}$$

thus

$$\frac{d^2 V}{dx^2} = 4\pi \frac{J}{\sqrt{\dfrac{2Ve}{m_e}}} \qquad \text{3.51}$$

Some algebra yields:

$$\frac{d^2V}{dx^2} = 2\pi\sqrt{\frac{2m_e}{e}}\frac{J}{\sqrt{V}}$$

<div style="text-align:right">3.52</div>

Both sides are now multiplied by *dV/dx* and integrated with respect to *x* from 0 to *d* to yield:

$$\left(\frac{dV}{dx}\right)^2 = 8\pi\sqrt{\frac{2m_eV}{e}}J + C$$

<div style="text-align:right">3.53</div>

where *C* is a constant. At the point *x* = 0, the potential distribution is horizontal

$$C = \left(\frac{dV}{dx}\right)^2_{x=0} = 0$$

<div style="text-align:right">3.54</div>

If the distribution where not horizontal the system would not be in equilibrium.

Therefore,

$$\left(\frac{dV}{dx}\right)^2 = 8\pi\sqrt{\frac{2m_eV}{e}}J$$

<div style="text-align:right">3.55</div>

which if integrated and solved for current density $J_{C\text{-}L}$ results in:

$$J_{C-L} = \frac{\sqrt{2}}{9\pi}\sqrt{\frac{e}{m_e}}\frac{V^{3/2}}{d^2}$$

<div style="text-align:right">3.56</div>

known as the Child-Langmuir equation. This model is accurate for cases when the thermionically emitted electron's velocity is negligible compared to the velocity produced by the voltage potential between electrodes. The initial velocities can be predicted based upon a Maxwellian distribution given by:

$$\bar{v} = \left[\frac{8k_BT_E}{\pi m_e}\right]^{1/2}$$

<div style="text-align:right">3.57</div>

Fig. 3.22 shows the voltage required for the electron initial and potential voltage induced velocities to be equivalent. As previously stated Equation 3.56 is accurate when the initial velocities are negligible compared to those induced by the potential voltage. The figure also shows the voltage required for the potential voltage velocity to me an order of magnitude larger than the initial velocities. The magnitude of these voltages indicates that the Child-Langmuir equation is accurate when the voltage potential is on the order of a volt.
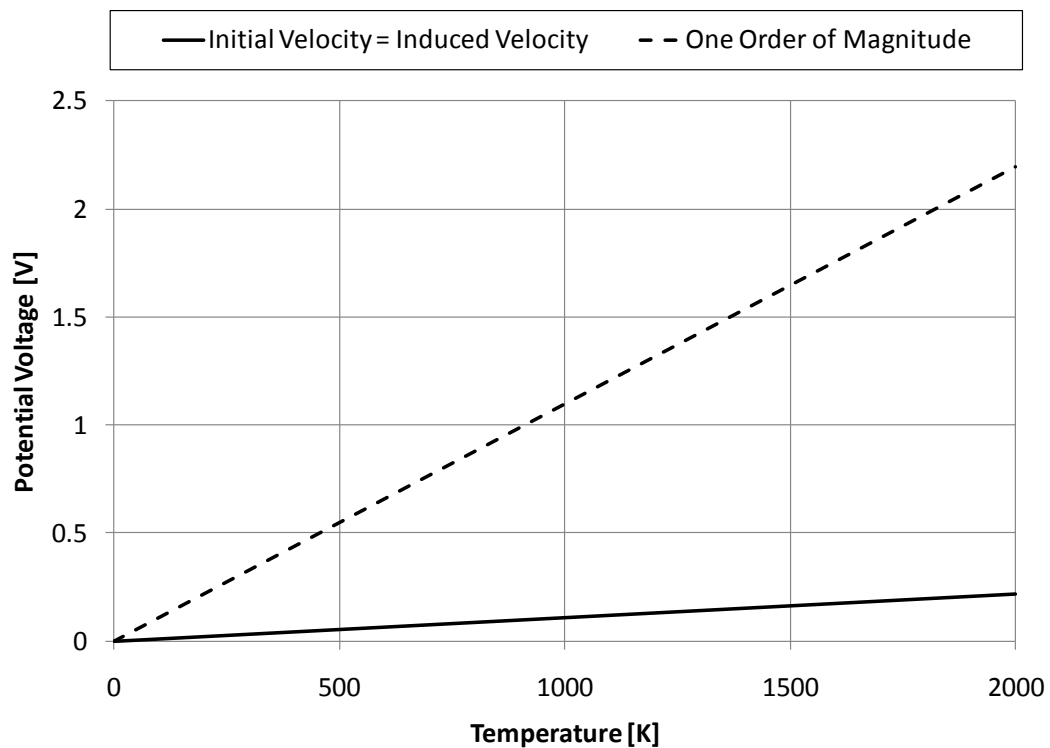
Fig. 3.22   Plot illustrating the voltage required for the initial velocity to equal the potential voltage induced velocity at a given temperature, and the voltage required for the initial velocity to be one order of magnitude less (negligible) than the potential voltage induced velocity for a given temperature

For this space charge model the current density is a function of the voltage difference and interspatial distance of the electrodes. This approximation is a conservative approximation of space charge effects. A comparison of the Child-Langmuir model and the Richardson model for TI emission is illustrated in Fig. 3.23 that shows the cross over point causing Langmuir's plateau as shown in Fig. 3.20.

Fig. 3.23 shows that as the gap between emitter and collector increases the current predicted by Child-Langmuir decreases due to increasing space charge. The Richardson equation is independent of gap size and is therefore constant. There is a crossover point at a gap size of d* where the models predict the same current draw for the given conditions. For gaps larger than d* current will be limited by space charge and follow the Child-Langmuir prediction, and for gaps less than d* current will follow the Richardson prediction. This illustrates that reducing electrode gap is an effective way to eliminate the negative effects of space charge.

The figure illustrates that the saturation current predicted by Richardson does not change with gap spacing because the prediction is only dependent upon the lattice in which electrons are emitted. Richardson does not directly account for space charge and the collector plate's effect on emission. The Richardson equation predicts the maximum emission from a material of work function ϕ , into a pure vacuum. Space charge is accounted for in the Richardson model by adding a value to the work function. This value must be predicted using a space charge theory.

Child-Langmuir Law: Space Charge

V = 0.5 V

T = 1500 K

Φc+δ = 1.3 eV

Child-Langmuir

Richardson-Dushmann

d*

I [Amps]

d [nm]
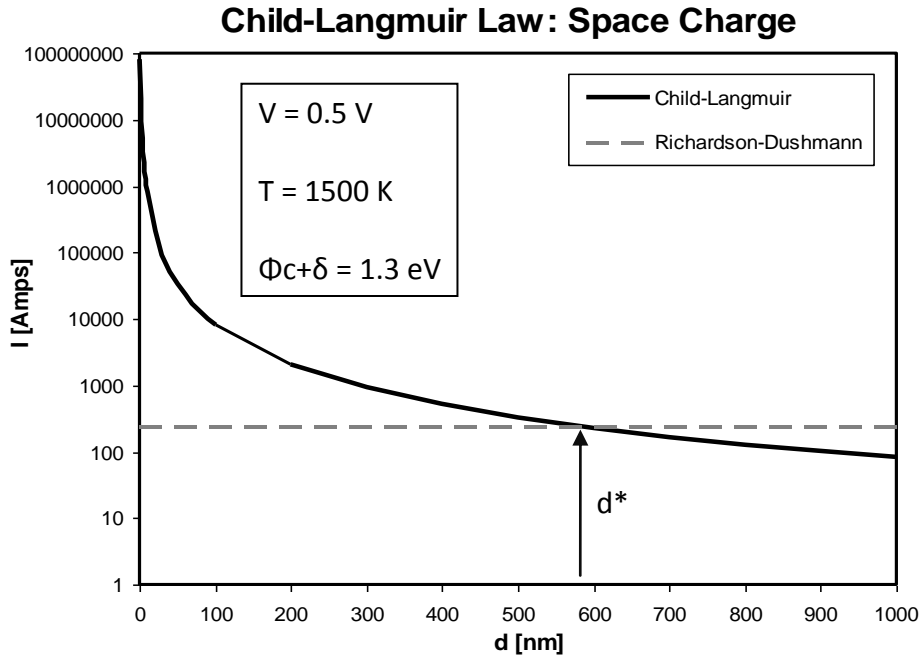
Fig. 3.23   Comparison of the Child-Langmuir model with the Richardson model

A more accurate model that includes initial velocities is presented by Langmuir.

Much of the work was performed by E. Q. Adams, and presented by Langmuir. The

Langmuir theory that includes initial velocities is dependent upon the emitter

temperature T_E as given by:

$$J = 7.728 \times 10^{-12} \frac{T_E^{3/2}}{d^2}$$

3.58

This is a more liberal estimate of space charge limited current density.

Fig. 3.24, illustrates the over prediction of the Langmuir theory for low

temperatures. At these temperatures the current follows the Richardson model

because the current emission is limited by work function. Beyond the cross over point

of the models space charge dominates and the current saturates and follows the

Langmuir model.
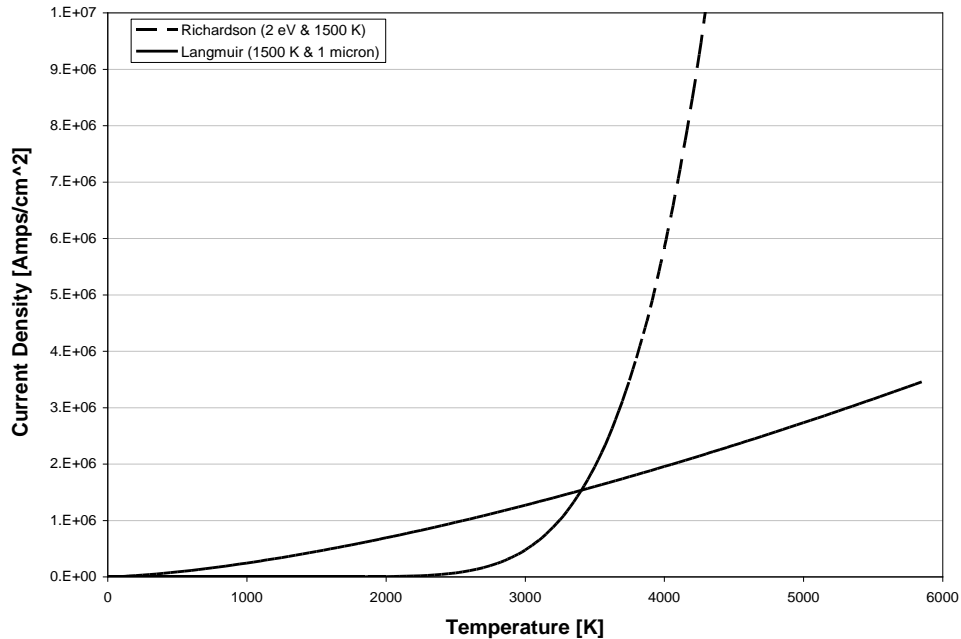
Fig. 3.24   Comparison of the Langmuir model (including initial velocities) with the
                Richardson model

b.   METHODS FOR CONTROLLING SPACE CHARGE

Many methods have been successfully used to reduce space charge. These methods

include reducing the amount of electrons in the gap by reducing the gap size, increasing

the velocity of the electrons with an electric field, or screening the gap with positive

ions.

The space charge theory suggests that reducing the interspatial gap will reduce

space charge. All else being equal, reducing the interspatial gap dimension results in

fewer electrons within the gap, as illustrated in Fig. 3.25. During early investigations of

TI devices, dimensions and tolerances were limited by manufacturing processes.

Current state of the art technologies allow for devices to be built on the nanoscale with much tighter tolerances.
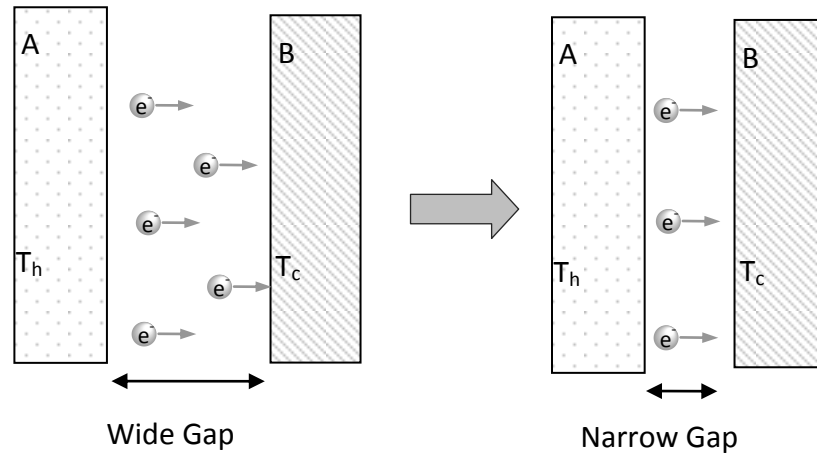
Fig. 3.25   Space charge control utilizing narrow gap dimensional constraint

Reducing the interspatial gap beyond a certain point will result in a finite probability of tunneling currents. Tunneling may prove to be advantageous in power generation; however, if the device is being used for cooling application tunneling will result in a reduction in the effectiveness of the device as illustrated in a study by (Hishinuma, Geballe and Moyzhes 2001). For cooling purposes it is important to remove only the high energy electrons that carry more heat.

Another method commonly used is introducing ionized particles into the gap to reduce the negative charge, as shown in Fig. 3.26. A common gas utilized in this method is cesium for its low work function. Issues related to this method include supply of positive ions to the gap, surface ionization, and electron scattering, (Angrist 1976).

Wide Gap
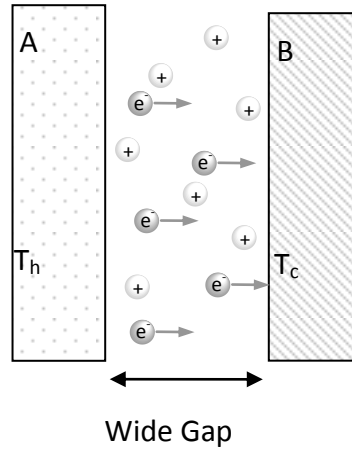
Fig. 3.26   Space charge control utilizing positive ions

Electric fields have successfully reduced space charge using a separate accelerating electrode sometimes referred to as a gate electrode as illustrated in Fig. 3.27. The primary limitation for using an accelerating electrode is the loss of power due to electrons being inadvertently collected by the high voltage electrode (Hatsopoulos & Gyftopoulos, 1973).

Accelerating
Electrodes
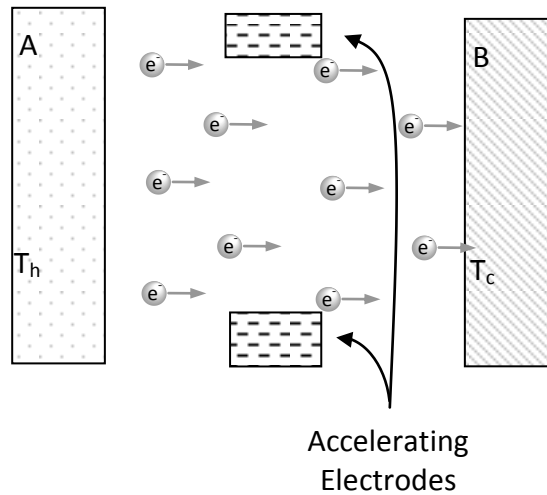
Fig. 3.27   Space charge control using a gate electrode

Table 3.2 provides a summary of the space charge models.

Table 3.2   Space charge model summary

Model	Equation	Description
Richardson-Dushman	$J_{TI} = A_0 T_E^{\,2} e^{\left(-\frac{e\phi}{k_B T_E}\right)}$	This model does not directly account for space charge, but space charge is sometimes modeled by adding an empirically derived value to the work function. The model provides a good estimate of emission when not space charge limited.
Child-Langmuir	$J = \dfrac{\sqrt{2}}{9\pi} \sqrt{\dfrac{e}{m_e}} \dfrac{V^{3/2}}{d^2}$	This model over estimates emission when not space charge limited, but accurately describes emission when limited by space charge.
Langmuir	$J = 7.728 \times 10^{-12} \dfrac{T_E^{3/2}}{d^2}$	This model also over estimates emission when not space charge limited, but to a less extent.

4. INTEGRATION OF EMISSION BASED DEVICE INTO A SYSTEM

i. THERMODYNAMIC BACKGROUND

Metrics are needed to compare the relative performance of a power generation device or design. Unfortunately the electron emission studies to date have focused primarily on maximizing current generation with little focus on device efficiency. For this reason this thesis with use thermodynamic efficiencies to evaluate the proposed devices.

Energy conversion efficiencies are a function of the required input to achieve the desired output of the system. In the case of a solid state electrical generator the input would be the heat source and the output is the generated electrical power. The first law efficiency is given by:

$$\eta_I = \frac{output}{input} = \frac{W_{elecrical}}{Q_{in}}$$ 4.1

where $W_{electrical}$ is the generated electrical power and Q_{in} is the heat source input to the system. The highest conversion efficiency is achieved for high amount of generated electricity for a small amount of heat input.

Carnot cycle heat engines cannot achieve 100% efficiency for low temperature power generation. The second law of thermodynamics requires that the power generation device operate between two temperature reservoirs and that it is impossible

to convert all waste heat into useful work. A portion of the waste heat must be dissipated into the lower temperature reservoir.

Carnot efficiency is the limit of a thermodynamic heat engine operating between two thermal reservoirs: T_h is the hot reservoir temperature, and T_c is the cold reservoir temperature. The heat engine, as illustrated in Fig. 4.1, requires a coupling between the input and output which limits the efficiency of Carnot cycle.
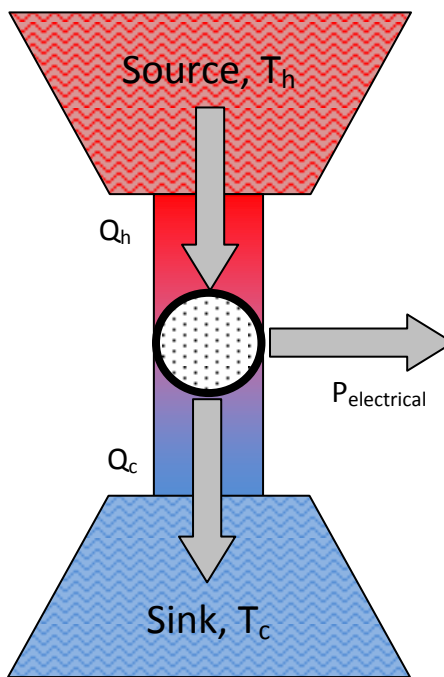
Fig. 4.1   Thermal heat engine operating between two thermal reservoirs

$$\eta_{carnot} = 1 - \frac{T_c}{T_h}$$

4.2

The total achievable efficiency goes up with an increase in the temperature delta

between the two reservoirs. A first law efficiency does not take into account this Carnot

limit, however, the second law efficiency given by:

$$\eta_{II} = \frac{\eta_I}{\eta_{carnot}}$$

4.3

is a more representative way to compare efficiencies of a system because it is based on

the Carnot limit. A highly efficient Carnot device may be misconstrued as a low

efficiency device if the first law efficiency is not compared against the Carnot limit.

Solid state energy conversion follows the Carnot heat cycle and is subject to its

limitations. The preceding efficiency discussions will be used in future sections to

evaluate and benchmark device performance and effectiveness.

ii.   MAGNETIC DIODE

a. SYSTEM DESCRIPTION

The first device proposed in this thesis utilizes a magnetic field to alter

thermionic emission to reduce thermal radiation exchange between emitter and

collector. It will be shown that reducing this exchange enables lower collector

temperatures and back emission which improves conversion efficiencies. Fig. 4.2 is a

simple diagram of the device illustrating the unique electrode orientation employed.

The following sections will explain the thermal radiation exchange between the

electrodes and the system level enclosure modeling approach.
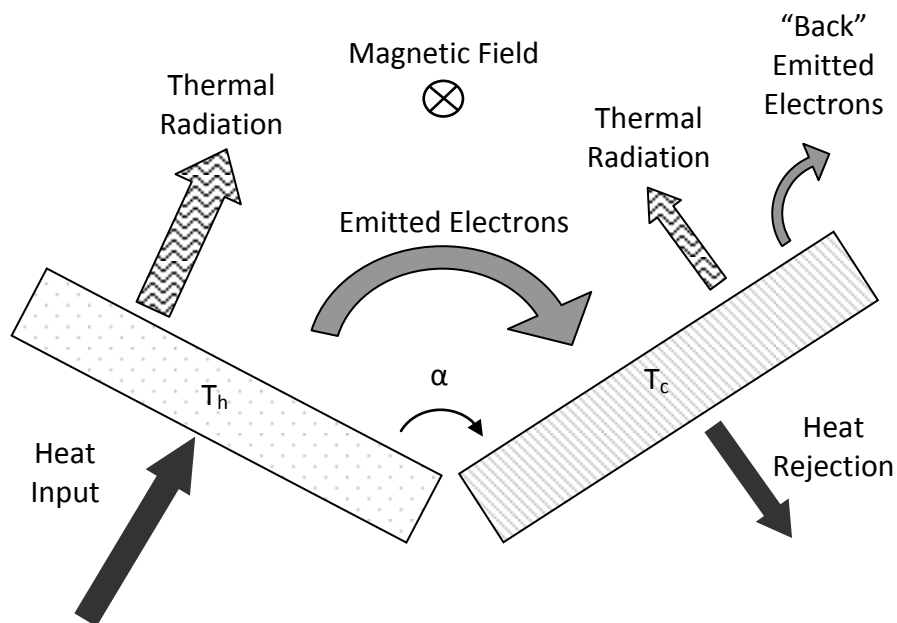
Fig. 4.2   Simplified magnetic diode

b. THERMAL RADIATION VIEW FACTOR

Thermal radiation exchange between emitter and collector is a dominant source of loss and inefficiency for a TI generator. The traditional TI diode is sufficiently modeled by assuming all radiation leaving the face of an electrode is "seen" by the other electrode. As discussed previously the implementation of the magnetic field allows for unconventional electrode orientations that reduce thermal radiation exchange between the emitter and collector. A thermal radiation view factor is used to model and account for the radiation exchange between unconventionally oriented electrodes. This section describes the unique contribution of using thermal radiation view factors to minimize the thermal radiation exchange between the emitter and collector.

The thermal radiation view factor is used as a modifier constant that accounts for geometric orientations in thermal radiation exchange. Parallel plate devices have a view factor of nominally 1 because all radiation emitted by one plate will be "seen" by the other plate. Fig. 4.3 illustrates a few possible orientations of the emitter and collector.

Parallel Orientation   Perpendicular Orientation   Same Plane Orientation
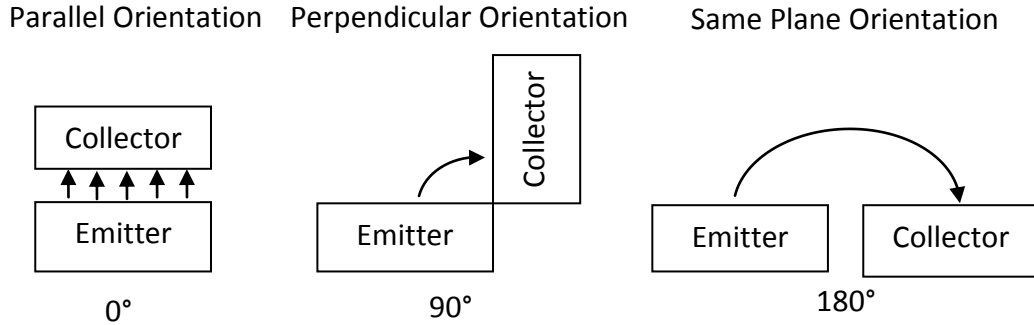
Fig. 4.3   Illustration of parallel, perpendicular and 180° plate orientations

The following will show how the magnitude of a thermal view factor can be reduced geometrically. (Inropera and Dewitt 2002) provide a view factor F, for two inclined plates of equal dimension:

$$F = 1 - \sin\left(\frac{\alpha}{2}\right)$$
                    4.4

where α is the angle between plates. The calculated view factor for varying angles is illustrated in Fig. 4.4. It can be concluded from the figure that the minimum amount of thermal radiation exchange between the flat plate electrodes is experienced at 180 degrees.
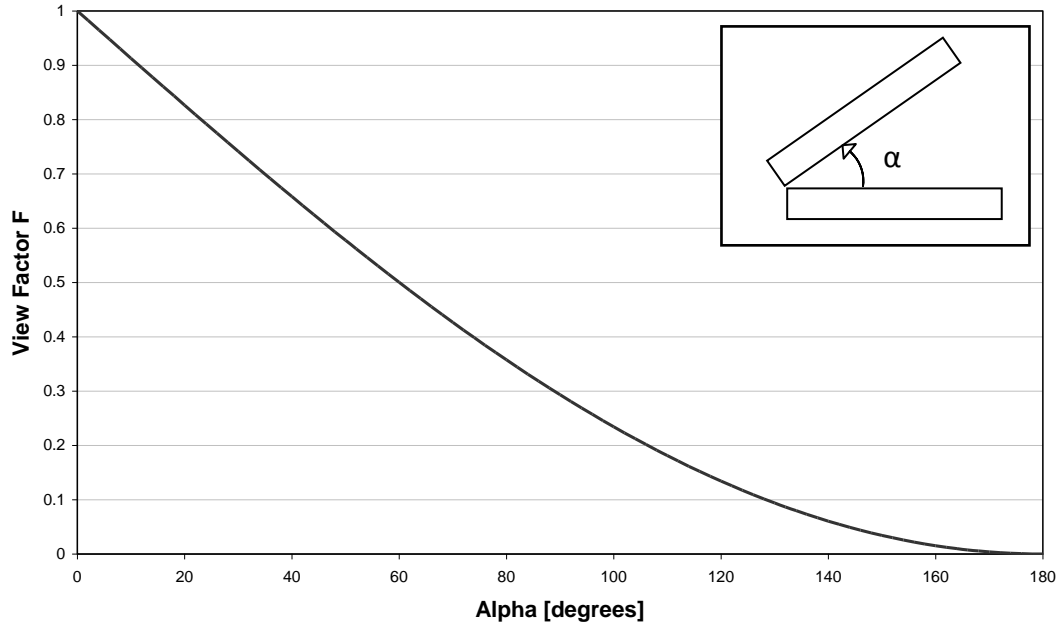
Fig. 4.4   Thermal radiation view factor for angles between emitter and collector varying from 0 to 180 degrees

It is assumed that the emitter and collector are gray bodies. The net thermal radiation $Q_{Rad,net}$, for the inclined plates is given by:

$$Q_{Rad,net} = \frac{F A_c \sigma \left(T_E^{\;4} - T_C^{\;4}\right)}{\left(\dfrac{1}{\varepsilon_E} + \dfrac{1}{\varepsilon_C} - 1\right)}$$

4.5

where A_C is the cross sectional area of a plate, σ is the Stefan-Boltzmann's Constant, ε_E is the emissivity of the emitter surface, and ε_C is the emissivity of the collector surface.

c. ENCLOSURE MODELING

For a simple diode with a parallel orientation the view factor between the electrodes is effectively one, and radiation exchange with other surfaces can be neglected. However, when the plate orientation is altered to reduce this view factor

72

between electrodes, thermal radiation exchange with the enclosure becomes relevant.

Therefore, this section will provide analysis of the radiosity exchange between the

enclosure and the electrodes. The radiosity resistance network is illustrated in Fig. 4.5.

As illustrated in the Fig. 4.4 the view factor between the electrodes F_{H-C} is zero.

Therefore heat transfer via the direct radiation path between electrodes is negligible.
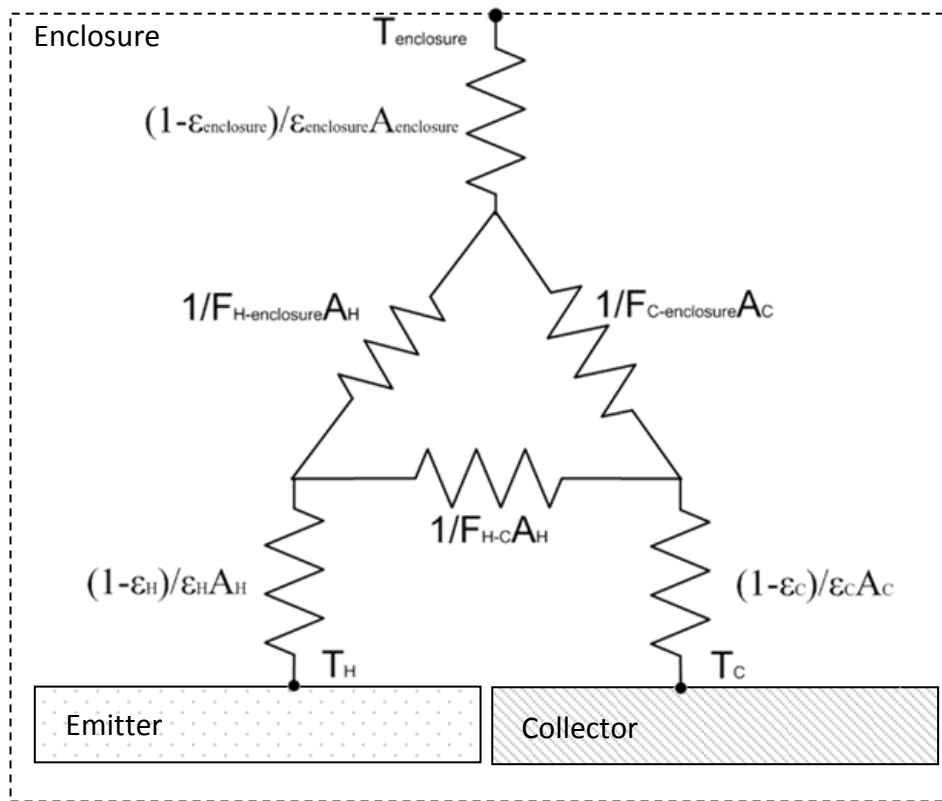
Fig. 4.5   Radiosity resistance network of a Magnetic converter within an enclosure

This analysis assumes blackbody radiation. A gray surface would emit less radiation

than a blackbody and would likely help reduce the parasitic losses associated with

thermal radiation. There is an opportunity to further develop this analysis based on real

surfaces however for this analysis the blackbody assumption is assumed to be worst

case and allows for simplified modeling.

Given these assumptions the radiosity resistance network simplifies to that

illustrated in Fig. 4.6. This analysis will look at three separate enclosure boundary

conditions; a constant 0 K enclosure temperature, a fully insulated reradiating

enclosure, and an intentionally non-insulated enclosure.
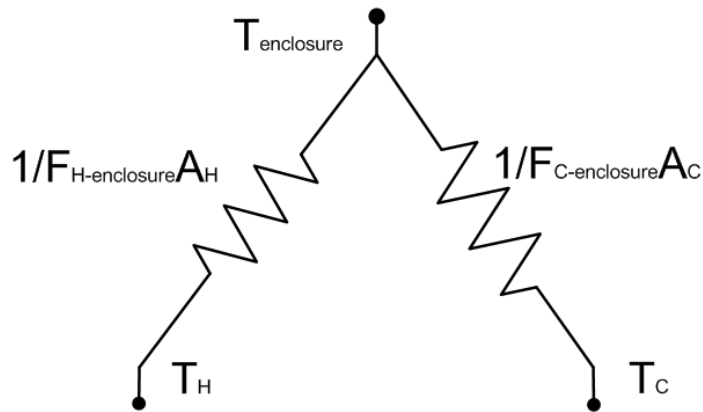
Fig. 4.6   Simplified radiosity network

The first condition that assumes that the enclosure is at a constant 0 K is not a

realistic scenario but provides an upper bounds in terms of device efficiency. In this

case all thermal radiation emitted by the electrodes will be absorbed by the enclosure

and there is no irradiation on the electrodes.

In the second condition, that assumes a fully insulated reradiating enclosure, there is

no heat into or out of the enclosure. Therefore all incident radiation is reradiated to the

electrodes. Therefore the effective view factor between electrodes is unity and the

device is essentially the same as the simple diode configuration. It is evident that the

enclosure thermal resistance to ambient should be minimized to reduce radiation

exchange between the electrodes.

The last condition assuming a non-insulated enclosure that sinks to the ambient is

the most realistic scenario. In this case the enclosure temperature is not constant and

sinks to the ambient as illustrated in Fig. 4.7.
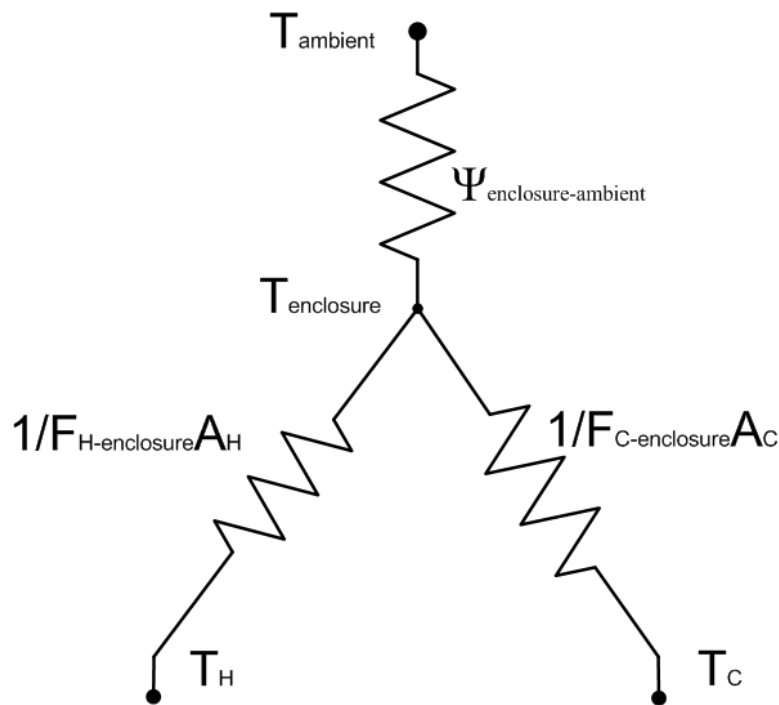
Fig. 4.7　　　Non-insulated enclosure radiosity network

The enclosure analysis reveals that simply reducing the view factor between

electrodes and eliminating the direct radiation path does not necessary prevent thermal

communication between the electrodes. Care must be taken in the design of the

enclosure to optimize energy conversion efficiencies. The next section proposes a

method to eliminate heat loss through the enclosure.

d. THERMAL RADIATION RECOVERY METHOD

Reducing the thermal radiation exchange between emitter, collector, and enclosure will enhance both performance and efficiency by maintaining the electrodes at optimal temperatures. Further enhancement can be obtained by recovering the radiation losses from the emitter and preventing it from being reradiated off of the enclosure to the collector. This can be accomplished by placing plates of nominally the same temperature across from the emitter and collector as illustrated in Fig. 4.8.
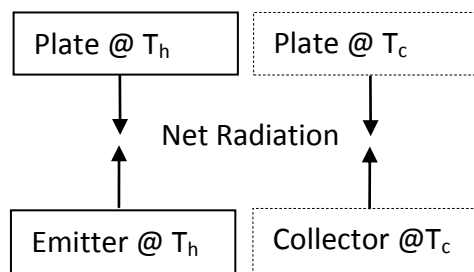
Fig. 4.8   Thermal radiation recovery orientation

The view factors for radiation exchange between the emitter and cold plate or the collector and hot plate are equivalent to each other. To determine this view factor consider the resultant view factor in Fig. 4.9, where view factors plates of unequal dimension and plates of equal dimension plates are known.

76

Plates of unequal dimension	Plates of equal dimension	Resultant view factor
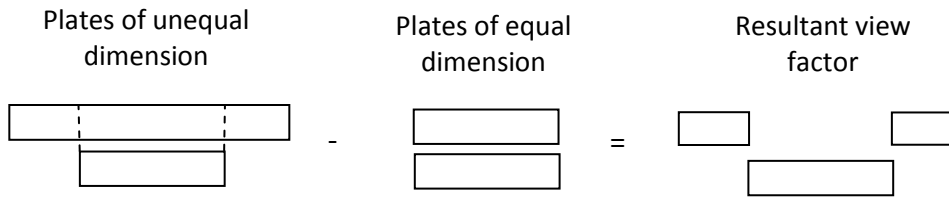
Fig. 4.9   Method for determining the view factor between the emitter and collector plates for the thermal radiation recovery orientation

Thermal view factor for plates of unequal dimension separated by some distance

L, as illustrated at the top of Fig. 4.10.
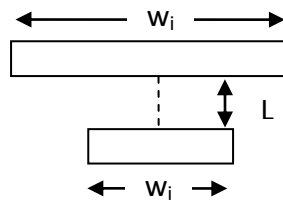
Fig. 4.10   Thermal radiation view factor for plates of unequal dimension separated by some distance L

The thermal view factor F_{ij}, for plates of unequal dimension (shown in Fig. 4.10), is given

by (Serway and Beichner 2000)

$$F_{ij} = \frac{\sqrt{(W_i + W_j)^2 + 4} - \sqrt{(W_j - W_i)^2 + 4}}{2W_i}$$ 4.6

where W_i and W_j are

$$W_i = \frac{w_i}{L}$$ 4.7

and

$$W_j = \frac{w_j}{L} \qquad\qquad 4.8$$

respectively.

The resultant view factor is plotted at various separation distances in Fig. 4.11. The figure illustrates that the thermal radiation exchange between the emitter and collector can be significantly reduced in comparison with the usual diode configuration and can be made negligible with a sufficiently small gap L. The view factor between the hot plates as well as between the cold plates will approach unity as the gap is reduced. Like the simple diode design there will be negligible radiation exchange with the enclosure.
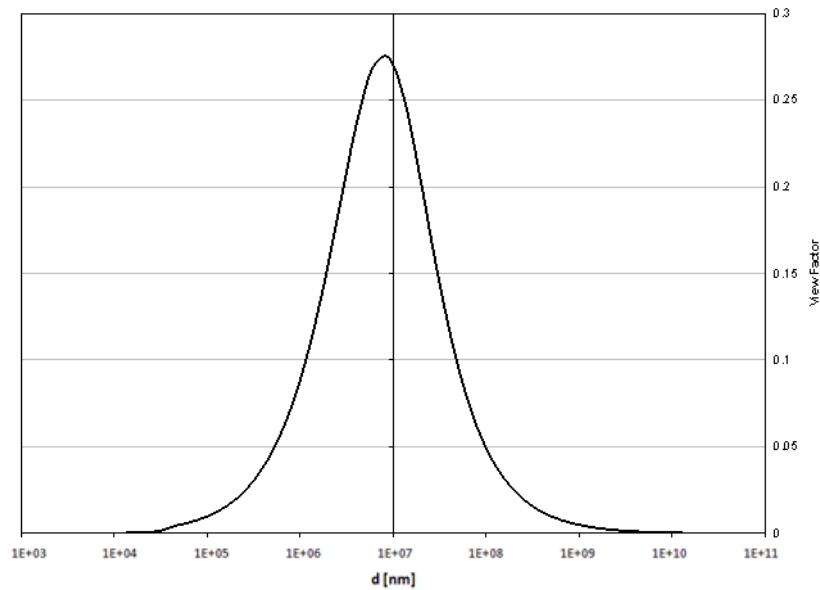
Fig. 4.11   Thermal radiation view factor for varying plate separation distances

iii. TFE NANOWIRE CONVERTOR

a. SYSTEM DESCRIPTION

The second proposed device utilizes TFE from nanowire emitters. Fig. 4.12 shows a simplified diagram of the TFE nanowire convertor. The diagram shows the nanowire emitters, gate, and collector electrodes. The following sections will describe the system level thermal modeling approach taken for the TFE nanowire convertor.
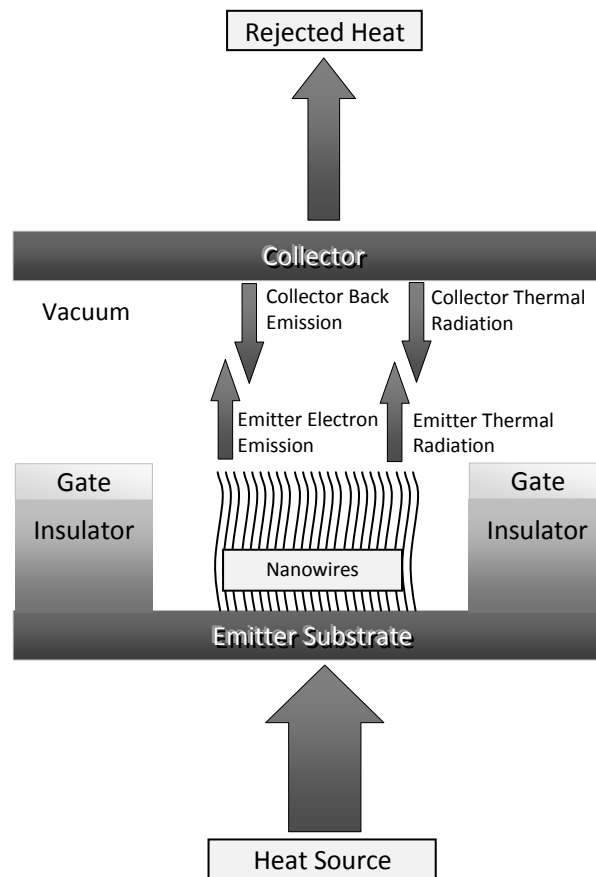
Fig. 4.12   Simplified TFE nanowire convertor

b. THERMAL MODELING

This section will focus on thermal modeling of the TFE nanowire convertor. Many energy conversion studies assume constant temperature boundary conditions for their analysis of energy convertors. This type of modeling approach reduces complexity of the model, but also reduces the accuracy of the prediction as shown with in the Magnetic Diode example. Most real world applications typically include some level of thermal impedance between the source and convertor. For this reason this model will include thermal resistances between the temperature reservoir and the convertor. This additional thermal modeling improves the accuracy between theory and practice and allows for optimization of the converter performance based on application.

In addition to the system level modeling approach this device concept will be modeled based on a server waste heat source to help illustrate both the benefits of system level modeling and the applicability of recovering server waste heat.

Two types of boundary conditions are considered for the thermal model: constant source temperature and constant source heat flux. Determining the appropriate boundary condition is application/heat source dependant. In the case of processor waste heat recovery application either boundary condition could effectively be used. The processor has a relatively constant heat flux for a given stress load, but the reliability requirements of the processor require that the processor not exceed a specific temperature. Overcooling of the processor consumes unnecessary energy commonly in

the form of fan power. A shunt heat sink is used in parallel with the convertor to

regulate the processor temperature to within its operating specification. Based on the

application and source the constant heat flux boundary condition should be assumed for

a system level modeling approach. However a more myopic view of the converter

would suggest that using a constant temperature heat source would provide for

simplified modeling. In this case it is assumed that the shunt resistor is varied to

provide the necessary cooling to maintain the processor temperature specification. It is

important to ensure that the heat flux through the convertor does not exceed that

produced by the source.

c. THERMAL RESISTANCE NETWORK

The conduction, convection and radiation heat transfer for such a device is well

understood and based on fundamentals of heat transfer theory with the exception of

the emission process. A certain amount of energy will be transported from the emitter

to the collector via net electron currents. Electron emission heat transfer is modeled as

a black box. Determining how to treat the emission black box in a thermal resistance

network is not entirely explicit. Therefore the more common approach to thermal

modeling of an electron emission device is to perform separate energy balances around

the emitter and collector.

As an exercise to illustrate the thermal complexity of the device a thermal resistance

network for the TFE convertor is presented in Fig. 4.13. The network assumes that all

contact resistances are lumped into the various conduction resistances for

simplification.
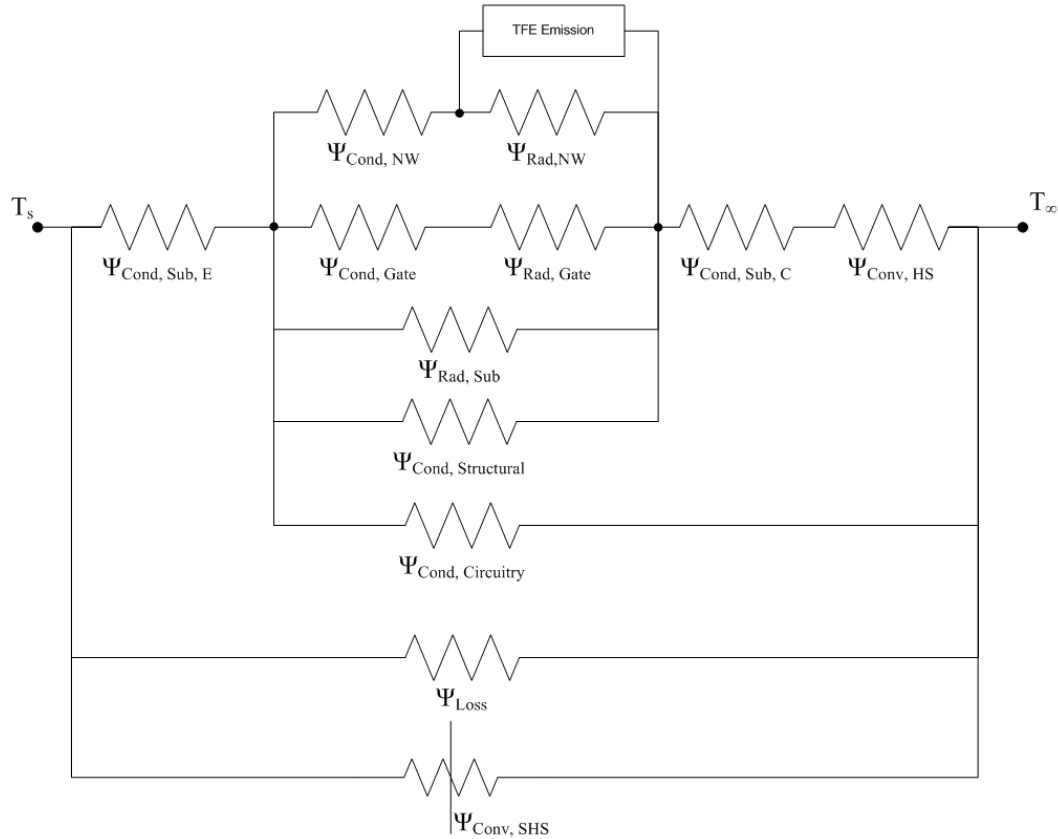
Fig. 4.13   Detailed TFE convertor thermal resistance network

The thermal resistances shown in Fig. 4.13 figure are as follows:

- $\Psi_{Cond,\,Sub,\,E}$: Thermal conduction through the emitter substrate. The contact resistance between the substrate and the heat source is lumped into this term.

- $\Psi_{Cond,\,NW}$: Bulk thermal resistance of the oriented SiC nanowires.

- $\Psi_{Cond,\,Gate}$: Thermal conduction of the gate insulator, gate electrode, gate circuitry (which is a function of the ambient temperature, but is neglected for simplicity), and contact resistances.

- $\Psi_{Cond,\,Structural}$: This is the thermal resistance of the mechanical structure and housing for the device.

- $\Psi_{Cond,\,Circuitry}$: This is the thermal resistance of the electrical circuit that attaches the emitter and collector. Depending upon the magnitude of current, joule heating may occur in the lead wires of the circuitry.

- $\Psi_{Cond,\,Sub,\,C}$: Bulk thermal resistance of the collector and contact resistance between the collector and the heat sink.

- $\Psi_{Rad,\,NW}$: This is the thermal resistance of the thermal radiation emitted by the nanowires

- $\Psi_{Rad,\,Gate}$: Thermal resistance of the thermal radiation exchange between the gate and the collector.

- $\Psi_{Rad,\,Sub}$: This is the thermal resistance of the radiation exchange between the emitter substrate and collector surfaces.

- $\Psi_{Conv,\,SHS}$: This is a variable thermal resistance of the shunt heat sink designed to keep the heat source within a specified temperature range.

- $\Psi_{Conv,\,HS}$: The thermal resistance of the heat sink used to keep the collector cool by expelling heat transferred from the emitter.

- Ψ_{Loss} : This thermal resistance represents the culmination of the remaining parasitic heat losses (such as heat loss to the ambient from the emitter directly to the ambient)

The TFE generator is illustrated in the resistance network as a "black box". The

generator includes those elements between the emitter and collector temperatures.

The generator cannot be depicted as a thermal resistance because of the conversion of

thermal energy into electricity. A portion of the source heat will be converted into

electrical energy that is consumed at the electrical load. The remaining amount of

energy carried from the emitter to the collector will be dissipated through the collector

heat sink. The heat transfer between the emitter and collector is a result of thermal

radiation and electron emission energy exchanges.

There are several assumptions made in developing the thermal resistance network.

It is assumed that the device is perfectly insulated from the ambient in all areas other

than the heat sink and electrical load. This assumption will not affect the accuracy of

the model since the magnitude of this heat loss is negligible. It is also assumed that

conduction and convection within interstitial gap is negligible due to the ultra high

vacuum environment. This resistance network also assumes no power loss through the

gate circuitry. In practice there will be losses associated with emitted electrons being

inadvertently collected by the gate electrode. This will be discussed later in greater

detail.

The thermal resistance model illustrated in Fig. 4.13 is not necessary to create an

accurate thermal model for a TFE convertor. Fig. 4.14 shows a reduced network that

lumps resistances together reducing the complexity without sacrificing model accuracy.

The thermal resistance network is necessary to accurately predict the emitter and

collector temperatures which relate to electron emission and power generation.
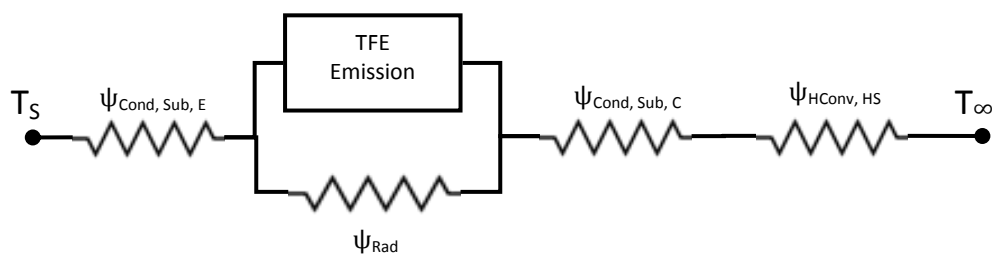
Fig. 4.14   Simplified TFE convertor thermal resistance network

The net thermal radiation exchange between the emitter side surfaces and the

collector surface is modeled as $\Psi_{Rad.}$ Thermal radiation from the emitter substrate,

nanowires and gate are modeled as a flat plate of the same projected area and assumed to emit thermal radiation at the emitter substrate temperature.

d. ENERGY BALANCE

To precisely model and characterize the performance and efficiency of the TFE converter it is necessary to keep an accurate balance of all energy transactions. It is customary to form separate control volumes around the emitter and collector or a control volume around the interstitial gap. The following emitter and collector control volumes and associated energy balances roughly correlate to the control volumes indicated in the thermal resistance network shown in Fig. 4.13. This control volume assumes the device has perfect insulation in order to neglect insignificant heat transfer to the surroundings.
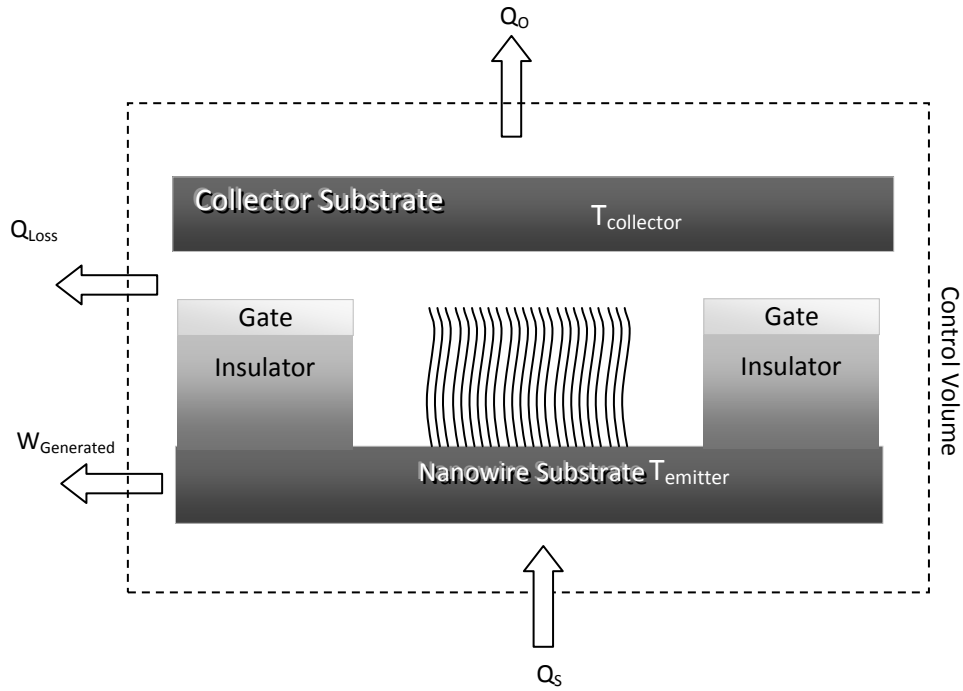
Fig. 4.15   Device level energy balance
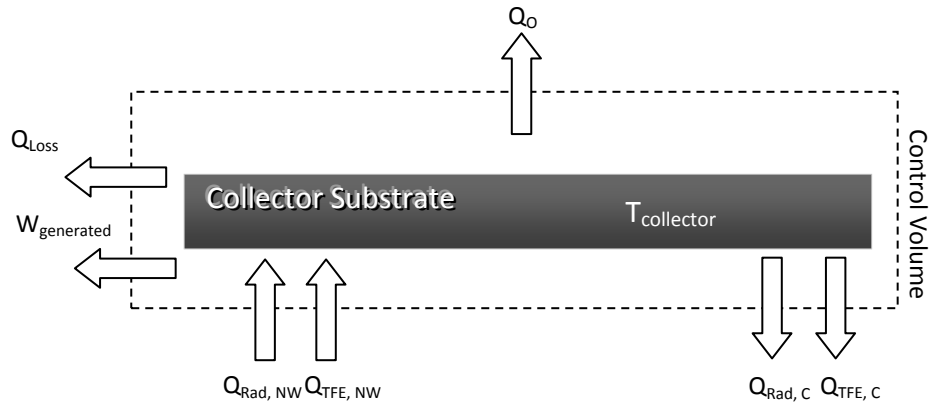
Fig. 4.16   Detailed collector side energy balance.
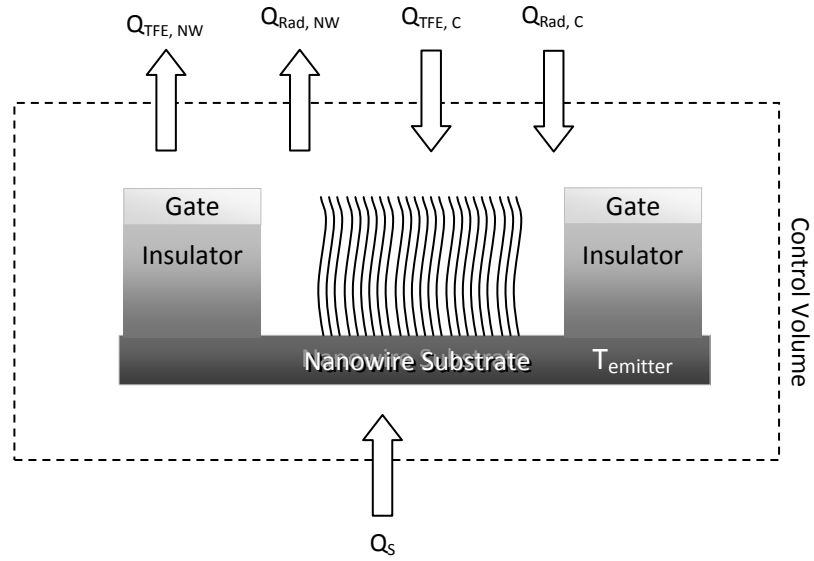
Fig. 4.17   Detailed emitter side energy balance

Simplified energy balances are performed around the emitter and collector, as shown in Fig. 4.18 and Fig. 4.19 respectively. Simplification of the energy balances is useful in performing a device feasibility study.
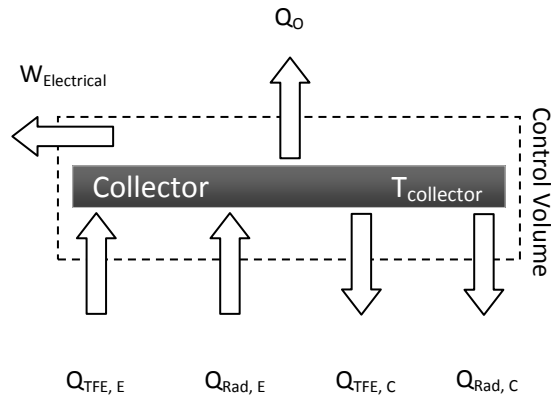
Fig. 4.18   Simplified collector side energy balance

$$Q_{TFE,C} + Q_{Rad,E} = Q_{TFE,C} + Q_{Rad,C} + Q_o + W_{Electrical} \qquad \text{4.9}$$
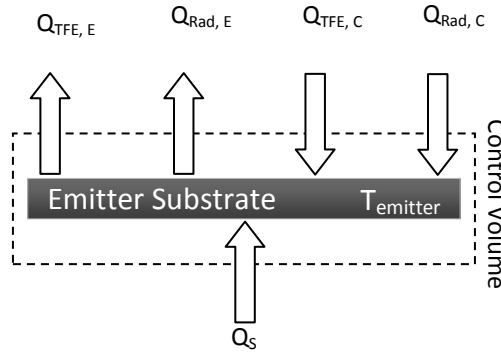
Fig. 4.19   Simplified emitter side energy balance

$$Q_{TFE,E} + Q_{Rad,E} = Q_S + Q_{TFE,C} + Q_{Rad,C} \qquad \text{4.10}$$

The energy carried by electrons from the emitter to the collector will increase the temperature and thermal losses of the collector. Since TI emitted electrons carry more thermal energy to the collector than TFE (Burstein et al., 1969, and Dolan et al., 1954) (Dolan and Dyke 1954), it is expected that TFE will have smaller thermal losses, and potentially a higher efficiency then a TI generator. The lower temperature (< 1000K) operation of the TFE generator is expected to also reduce the radiation losses from the emitter surface relative to a TI generator.

5. ANALYSIS OF SYSTEM

i. ITERATIVE SOLVING

Solving the energy balances, emission equations and thermal resistance networks for the Magnetic Diode and TFE Nanowire Convertors required multiple iterations to converge on a solution as illustrated in the flow chart in Fig. 5.1. The process required making an initial guess of electrode temperatures to acquire first pass estimates of emission current densities. Then the energy balance calculations are performed based on the emission approximation to estimate new electrode temperatures. The new electrode temperatures are used to update the emission current estimates and the process is repeated until the temperatures converge on a solution. This iterative process is also repeated for each unique set of emission and thermal parameters.

The iterative solution of the device models were performed using Matlab programs and Microsoft Excel.   Some of the Matlab programs used to solve the modeling can be found in the appendix. Excel solutions required starting with constant temperature electrodes to perform the emission current approximations. Then thermal components of the analysis were added one by one to the calculations. Each time a component was added Excel would reiterate until a solution was found. Once all components were added a solution was found. Adding all thermal components at one time resulted divergence.
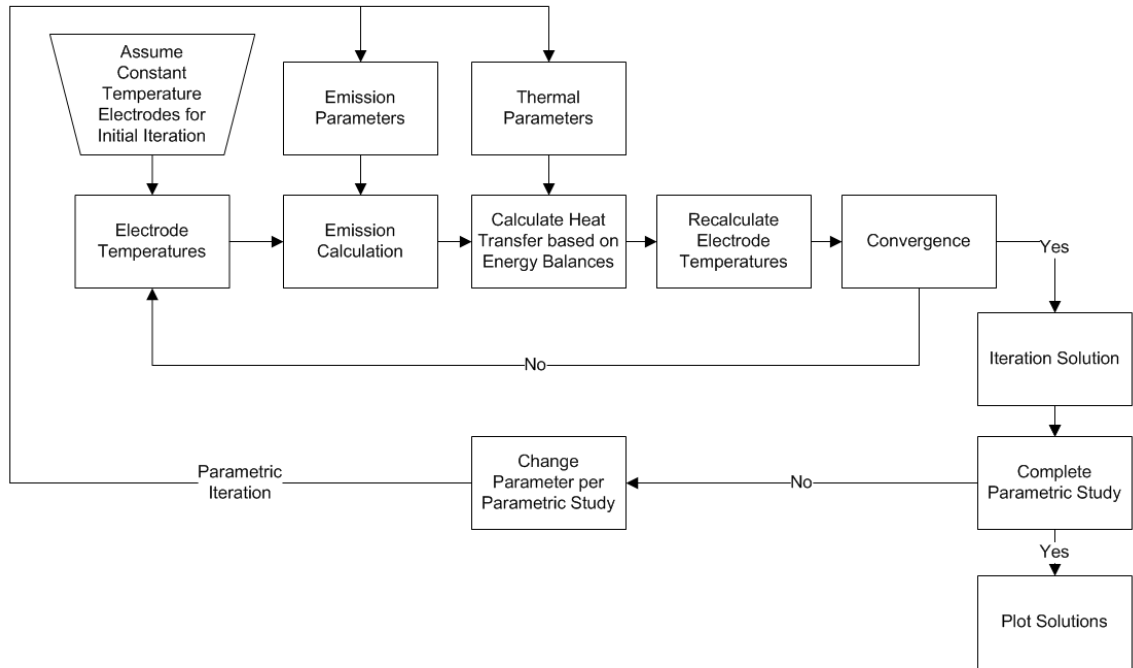
Fig. 5.1   Flow chart illustrating iterative method used to solve electromechanical models

ii.   MAGNETIC DIODE CONVERTOR

a.   MAGNETIC FIELD

A magnetic field (or B-field) alters the trajectory of the emitted electrons and is proposed in order to reduce thermal radiation losses. The force exerted on a particle F_B, by a magnetic field B, is described by the equation:

$$F_B = qv \times B \qquad\qquad 5.1$$

where q is the charge of the particle, and v is the velocity of the particle. The magnetic field required to cause an electron moving at velocity v, in a straight line to an arc of radius, r, is:

$$B = \frac{m_e v}{|e|r}$$

5.2

Motion of an electron in the presence of a B-field into the page is illustrated in Fig. 5.2.
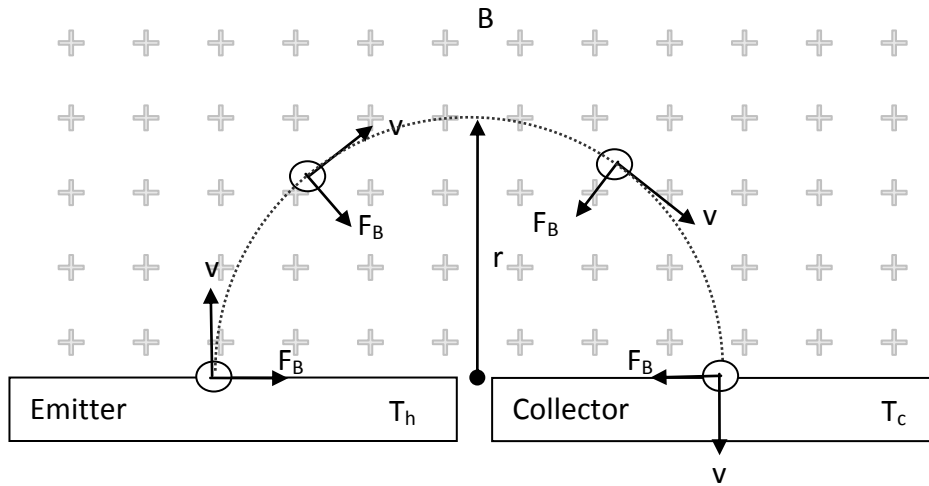
Fig. 5.2   Illustration of electron trajectory due to B-field

Recall that the average velocity $\bar{v}$, of an emitted electron from a material at temperature T_E, is described by the Maxwellian distribution as provided in space charge chapter in Equation 3.48. The Maxwell distribution is suitable when dealing with high temperatures. A Bose-Einstein distribution is more suitable when dealing with low temperatures.

In order to reduce space charge the minimum possible electron trajectory radius is desired. However, as Fig. 5.3, shows the smaller the radius the higher the B-field required. In order to use a realistic B-field common field sources, as shown in Table 5.1, are plotted in figure Fig. 5.3. The strong conventional laboratory magnet would produce a radius of less than 1 micron for electrons emitted from a 1000 K source. The resulting radius for the all of the magnetic field sources are also provided in Table 5.1.
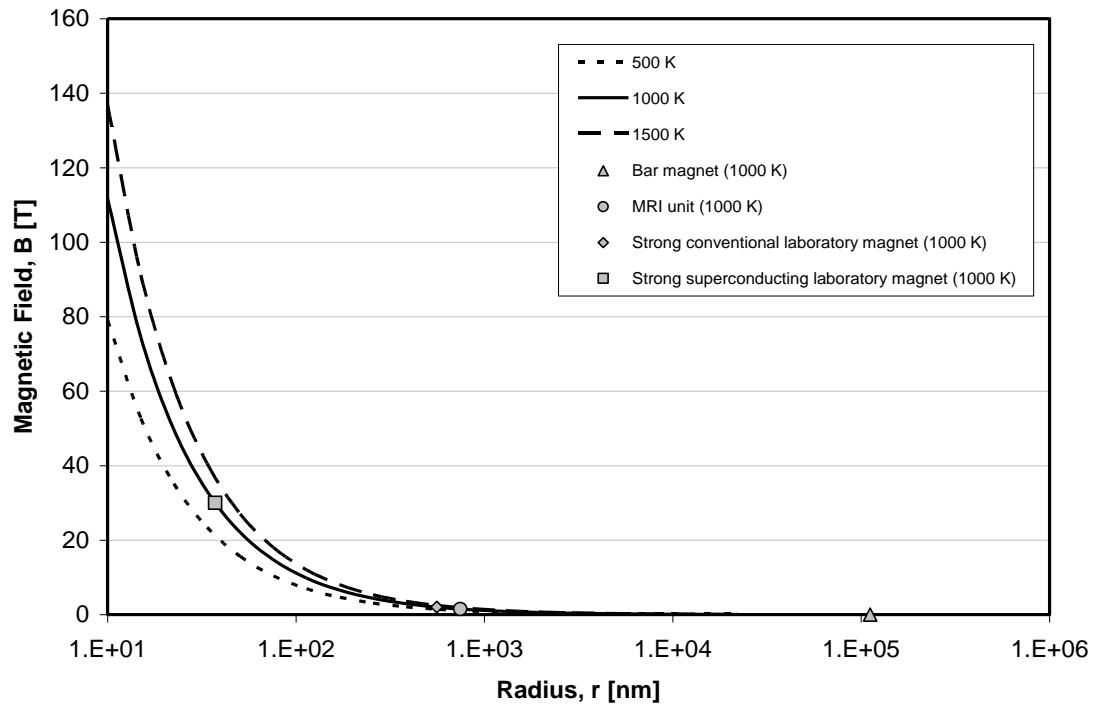
Fig. 5.3   Magnetic field, B required for an electron radius, r emitted from a surface at 500K, 1000K, and 1500K

Table 5.1   Approximate magnetic field sources (Serway and Beichner 2000)

Field Source	Field Magnitude [T]	Radius [nm]
Bar Magnet	10^{-2}	10^5
MRI unit	1.5	745
Strong conventional laboratory magnet	2	560
Strong superconducting laboratory magnet	30	37

The first design concept explored in this thesis encompasses the use of flat plate

thermionic emission in the presence of a magnetic field. Conventional TI emission

based energy conversion devices are oriented in the traditional fashion of a diode where

electrodes are aligned face to face. The magnetic field is employed to alter the

trajectory of the electrons such that the collector can be oriented in unconventional

orientations as illustrated in Fig. 5.4. This section will show how altering the electrode

orientation can enhance conversion efficiencies.
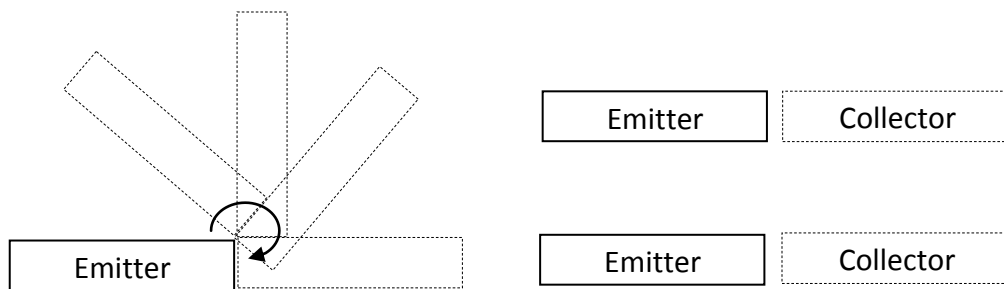
Fig. 5.4   Collector orientations considered with the presence of a magnetic field

In a previous study, a similar concept using a magnetic field to alter electron trajectories

and electric fields to reduce space charge effects was investigated (Hatsopoulos and

Gyftopoulos 1973). A device was developed in that study that was named the

"Magnetic Triode", and is illustrated in Fig. 5.5 that uses a magnetic "B" field to provide

the arced trajectory of the electron. The accelerating electrode is biased to a higher

voltage potential to generate an electric field that was used to reduce space charge

effects by accelerating the emitted electrons. Acceleration of the electrons removes the

electrons from the inter-electrode region faster and thus reduces the space charge.

Hatsopoulos et al found that when leakage current (i.e. stray electrons) are

inadvertently collected by the accelerating electrode, power losses on the order of that

generated are incurred (Hatsopoulos and Gyftopoulos 1973). Fig. 5.6 shows the

modeling results from Hatsopoulos's Magnetic Triode modeling.
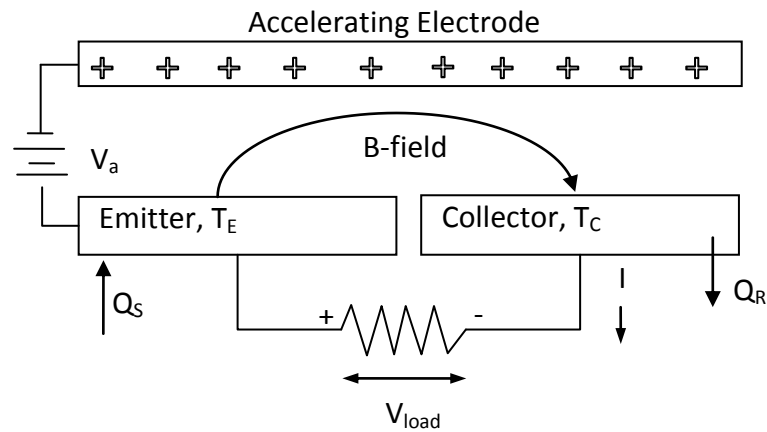
Fig. 5.5   Magnetic triode as adopted from (Hatsopoulos and Gyftopoulos 1973)
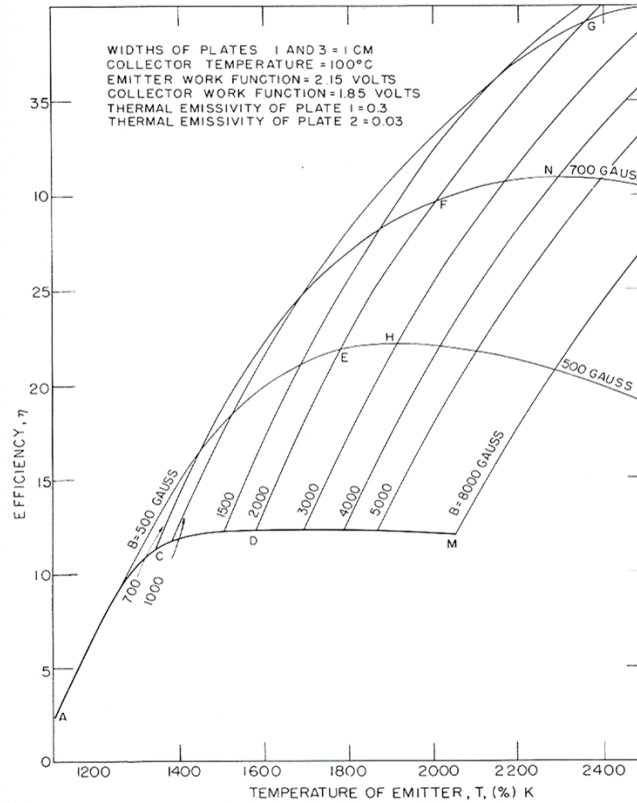
Fig. 5.6　　　　Magnetic triode efficiency (Hatsopoulos and Gyftopoulos 1973)

Hatsopolous's study showed promise in reducing both radiation losses and space

charge. However, the space charge reduction came with the tradeoff of gate leakage

current. This thesis proposes a similar design that uses extremely small dimensions to

control space charge instead of the accelerating electrode. Later modeling will also

illustrate that thermal radiation can still be transmitted from the emitter to the collector

via the accelerating electrode. This thesis will propose a method that eliminates this

heat path.

When the magnetic triode was devised the ability to dimensionally control space

charge was beyond the capability of manufacturing techniques. Today we have the

ability to manufacture devices at much smaller scales allowing for the control of space charge via dimensional constraints as an alternative to the accelerating electrode.

b. SPACE CHARGE

The trajectory of the electrons must be small enough to negate the effects of space charge. The space charge current density predicted by Childs and Langmuir is a one dimensional model that does not account for an electron with a curved trajectory. However it stands to reason that reducing the trajectory distance will result in a reduced space charge.

Hatsopolous uses the same assumption in his work on the magnetic triode (Hatsopolous, 1956), where he states, "The power output becomes appreciable only for the very small gaps of 0.01 cm and 0.001 cm. At the present time no technique is know by which one can obtain these small gaps in practice." These spatial limitations drove Hatsopolous to use an electric field to reduce space charge. Today's technology provides for fabrication techniques that can achieve these microscale dimensions.

The Child-Langmuir space charge and Richardson equation are plotted in Fig. 5.7 for a work function of 2.0 eV and emitter temperature of 1000 K. Space charge becomes a limiting factor when the Child-Langmuir predicted current is lower than that predicted by the Richardson model. In other words the current is no longer limited by emission, but is limited by space charge. The figure illustrates that this does not occur for dimensions below 100 microns.

Child-Langmuir Law: Space Charge
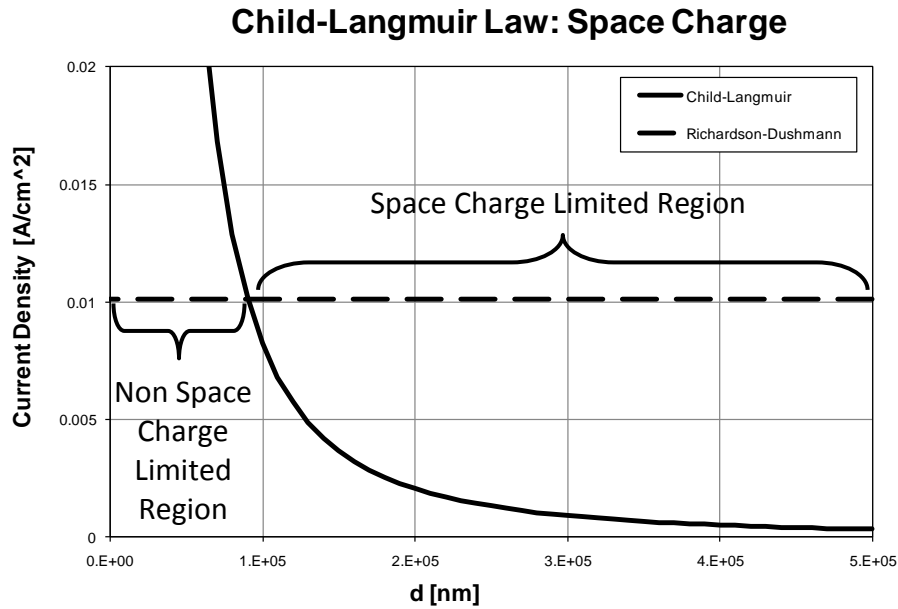
Fig. 5.7   Illustration of space charge limitation for an emitter at 1000 K with a work function of 2 eV

c.   1ST ORDER ANALYSIS

Many emission studies assume constant temperature boundary conditions and neglect the effects of the enclosure. This first order model assumes no space charge, constant temperature electrodes and an enclosure temperature of 0 K to illustrate the problems associated with the typical emission modeling assumptions. An illustration of these assumptions and the device configuration are provided in Fig. 5.8. Electron emission was calculated based on the projected area of the flat plate emitter.
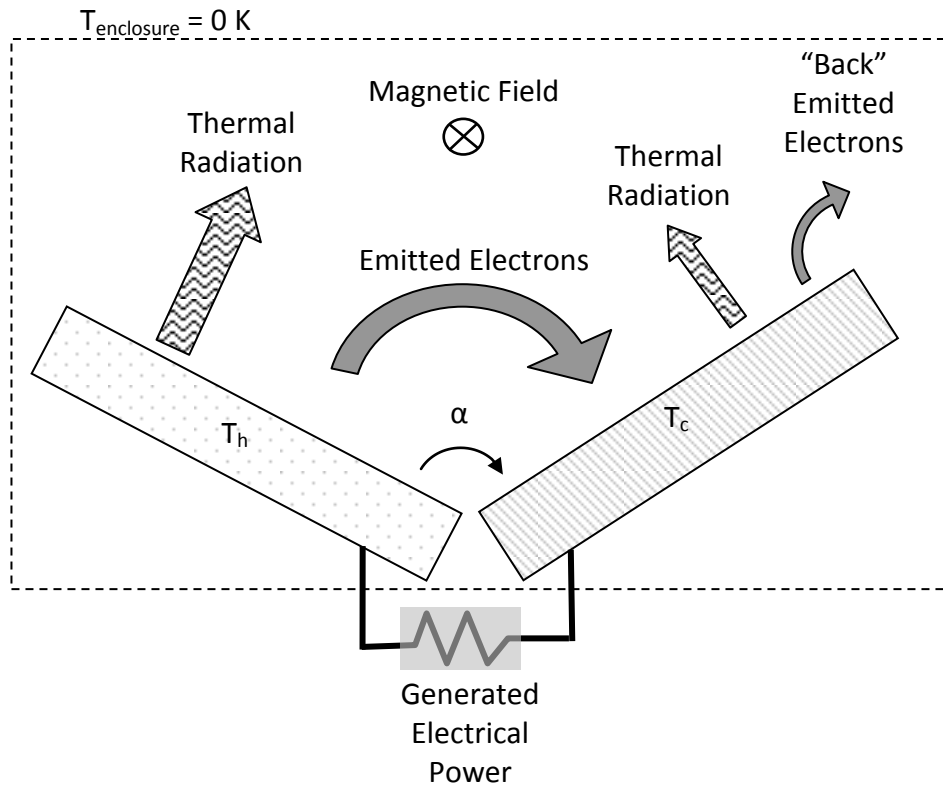
Fig. 5.8   Magnetic converter first order analysis with constant temperature
electrodes

One of the primary metrics used to evaluate an energy convertor is efficiency.

As discussed in Thermodynamic Background section on efficiency there are two

separate types of efficiency. The 1st law thermal efficiency η_I, for this model is given by

$$\eta_I = \frac{\left(J_E - J_C\right)\left(\phi_E - \phi_C\right)}{Q_{Rad,net} + J_E\left(\phi_E + \frac{2K_B T_E}{e}\right) - J_C\left(\phi_E + \frac{2K_B T_C}{e}\right)}$$ 5.3

where J_E is the emitter saturation current, J_C is the collector saturation current, ϕ_E is the

emitter work function, and ϕ_C is the collector work function. The thermal efficiencies for

the 1st order model are shown in Fig. 5.9 for varying emitter temperatures. Interestingly,

the efficiency curves take the same shape as those predicted by Hatsopoulos et al in Fig.

5.6. Under identical conditions minus the electric field Hatsopoulos used to control

space charge (assuming dimensional space charge control) the modeling aligns

perfectly.
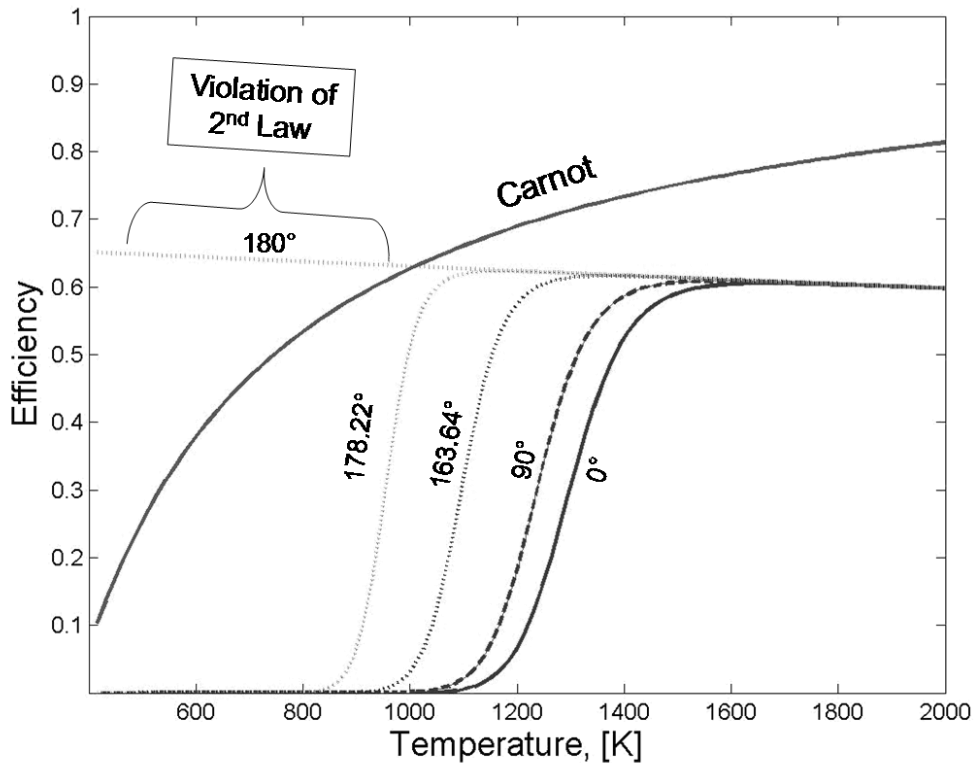
Fig. 5.9   Efficiency of magnetic triode for varying emitter temperatures and angles. The collector plate is assumed to operate at 400 K and the work functions for the emitter and collector being 3 eV and 1 eV respectively. The enclosure is assumed to be a constant 0 K.

Violation of the 2nd law of thermodynamics occurs for large angles due to the

lack of "thermal communication" between the emitter and collector. The assumption of

constant temperature electrodes and an enclosure temperature of 0 K results in a

decoupling of heat transport and electrical power generation which results in an

overestimation of the efficiency. In reality heat would be lost from the emitter and

gained by the collector resulting in a lower emitter temperature and higher collector

99

temperature. As the emitter temperature is reduced TI emission is reduced, and as the collector temperature increases back emission increases. Heat loss between the emitter and collector as well as heat loss from the emitter to its surrounds would result in a higher input heat to maintain a constant emitter temperature. More heat input would further lower the predicted efficiency. These factors are considered more closely in the next section detailing the 2nd order analysis. This 1st order design approach was performed to illustrate the inherent deficiencies in the modeling approach assumed in other studies that focus primarily on the emission process and ignore detailed thermal modeling.

d. 2ND ORDER ANALYSIS

Results from the first order analysis illustrate a need to refine the modeling efforts. A second order analysis is performed with more complete and accurate boundary conditions by using a system level design approach which includes non-constant temperature electrodes and a better enclosure estimate. The emitter and collector plates are thermally coupled to constant temperature sources through thermal resistances. This provides a more representative modeling attempt while adding to the level of complexity of the model.   Fig. 5.10 illustrates the magnetic diode with thermal resistances added between the heat source and between the collector and ambient temperature.
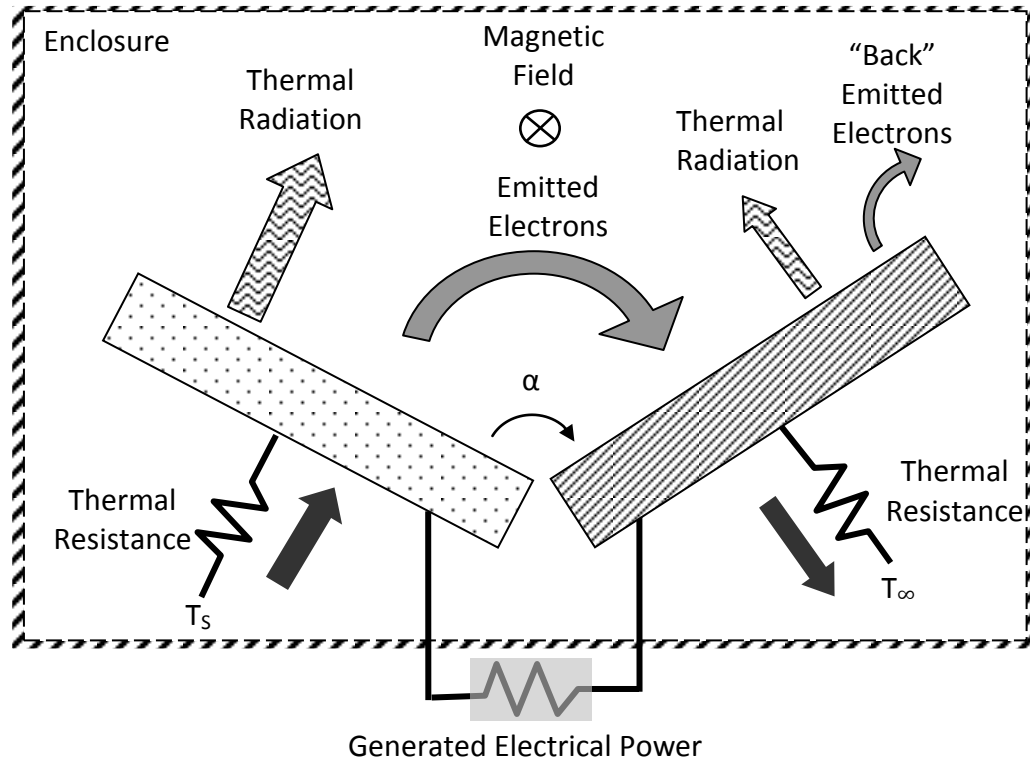
Fig. 5.10   Illustration of magnetic converter with non constant temperature
boundaries and an insulated enclosure

The thermal energy input into the converter must equal the energy that exits the

converter. Energy exits the converter in two forms: thermal and electrical. The

efficiency of the system is dependent upon the amount of electrical and thermal output

of the device. Efficiency is higher for a lower heat rejection and or higher electrical

output device. The energy balance for the system is

$$W_{Electrical} = Q_S - Q_R \qquad\qquad 5.4$$

where Q_R is the heat rejected from the device. The heat supplied to the device must be

determined using an iterative process. Energy balances of the emitter and collector are

used to determine the heat supplied, rejected, emitter, and collector temperatures. The

energy balance around the emitter and collector are illustrated in Fig. 5.11 and Fig. 5.12,

respectively.
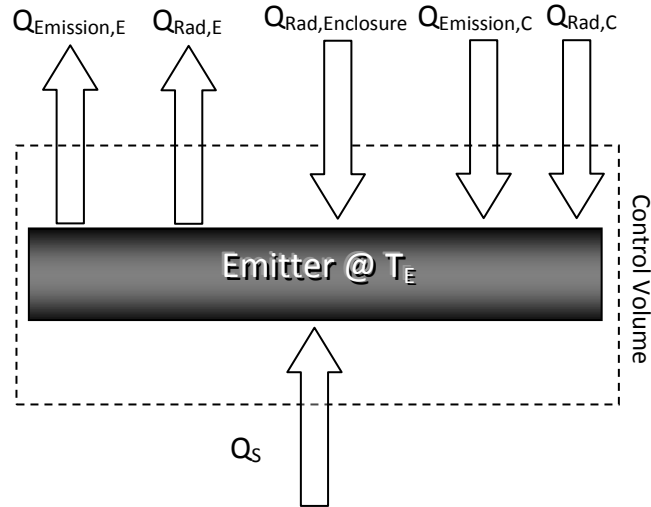
Fig. 5.11   Emitter energy balance assuming no temperature distribution within
               emitter material
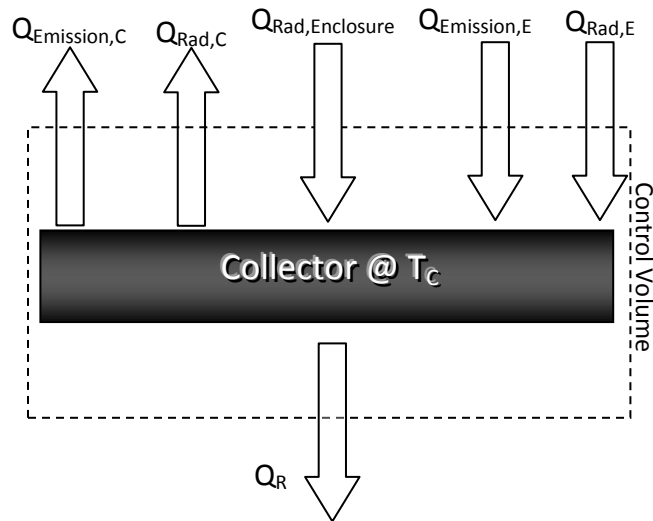
Fig. 5.12   Collector energy balance assuming no temperature distribution within
               collector material

The thermal energy associated with those electrons emitted from the emitter $Q_{Emission,E}$ is given by:

$$Q_{Emission,E} = J_E A_E \left(\phi_E + \frac{2k_B T_E}{e} \right)$$ 5.5

where J_E is the current density as predicted by the Richardson equation for the emitter at temperature T_E, and A_E is the projected emitter area. Similarly, the energy associated with those electrons emitted from the collector $Q_{Emission,C}$, is given by:

$$Q_{Emission,C} = J_C A_C \left(\phi_C + \frac{2k_B T_C}{e} \right)$$ 5.6

where J_C is the current density of back emission as predicted by the Richardson equation for the collector at temperature T_C, and A_C is the projected collector area. The heat supplied to the emitter Q_S, is given by:

$$Q_S = \frac{(Ts - T_E)}{\psi_E}$$ 5.7

where ψ_E is the thermal resistance between the source temperature T_S and the emitter temperature T_E. The heat rejection of the collector Q_R, is given by

$$Q_R = \frac{(T_C - T_\infty)}{\psi_C}$$ 5.8

where ψ_C is the thermal resistance between the collector temperature T_C and the ambient temperature T_∞. The thermal radiation emitted by the enclosure $Q_{Rad,Enclosure}$ is given by:

103

$$Q_{Rad,Enclosure} = F_{enclosure} A_{electrode} \sigma T_{Enclosure}^4$$ 5.9

where $F_{enclosure}$ is the view factor between the electrode and the enclosure, $A_{electrode}$ is

the area of an electrode (the emitter and collector are assumed to be of equivalent

dimensions), and $T_{enclosure}$ is the temperature of the insulated enclosure. The thermal

radiation emitted by the collector $Q_{Rad,C}$ is given by:

$$Q_{Rad,C} = F_{E-C} A_{electrode} \sigma T_C^4$$ 5.10

where F_{E-C} is the view factor between the emitter and collector. The thermal radiation

emitted by the emitter $Q_{Rad,E}$ is given by:

$$Q_{Rad,E} = F_{E-C} A_{electrode} \sigma T_E^4$$ 5.11

The preceding energy balances around the emitter and collector were performed as

part of the system level modeling along with estimates for emission.

Analytic modeling of the system described was performed using an iterative method

to determine surface temperatures. Thermal radiation was assumed to be emitted from

a blackbody maximizing the effect of thermal radiation on the system. Results from the

modeling showed that the efficiency changes very little for greater angles of separation.

Thermal radiation exchange between the electrodes and insulated enclosure coupled

with non constant electrode temperatures resulted in a device efficiency of

approximately zero. Thermal radiation leaving the emitter cooled it down such that

emission was greatly reduced, and reradiation from the enclosure heated the collector

greatly reducing the temperature gradient between electrodes.

Contrasting these results from those attained in the 1st order model (Fig. 5.9) reveals

that the constant temperature boundary condition results in hugely inflated efficiencies.

The 1st order model suggested a very efficient device that in certain cases violated the

Carnot limitation whereas the more accurate model presented in this section estimates

that the device will be very inefficient.

e. RADIATION RECOVERY ANALYSIS

The 2nd order analysis from the last section suggests that radiation exchange with

the enclosure reduces the device efficiency. Thermal radiation losses can be reduced by

aligning emitter electrodes across from one another as illustrated in Fig. 5.13 and

suggested in Thermal Radiation Recovery Method section. Thermal radiation emitted

from the emitter is predominantly radiated to the emitter plate directly aligned with it.

The temperature difference between emitter plates will be negligible resulting in little

net energy exchange between the electrodes. A very small loss of thermal energy will

occur between the emitters and collectors due to small view factor.
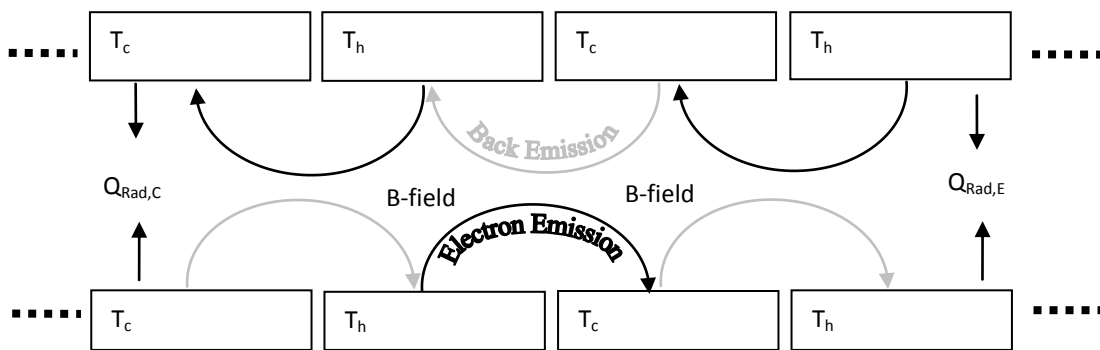
Fig. 5.13   Magnetic device concept minimizing thermal radiation losses

Thermal radiation in this model was assumed to be black body radiation. This assumption was made to provide a worst case analysis which ultimately accentuates the orientational effects observed in the results. Analysis of the system is limited to the boundary illustrated in Fig. 5.14. This boundary captures all necessary characteristics for a unit analysis. Symmetry allows for scaling of the results obtained from this boundary to any number of emitters and collectors oriented in the same fashion.
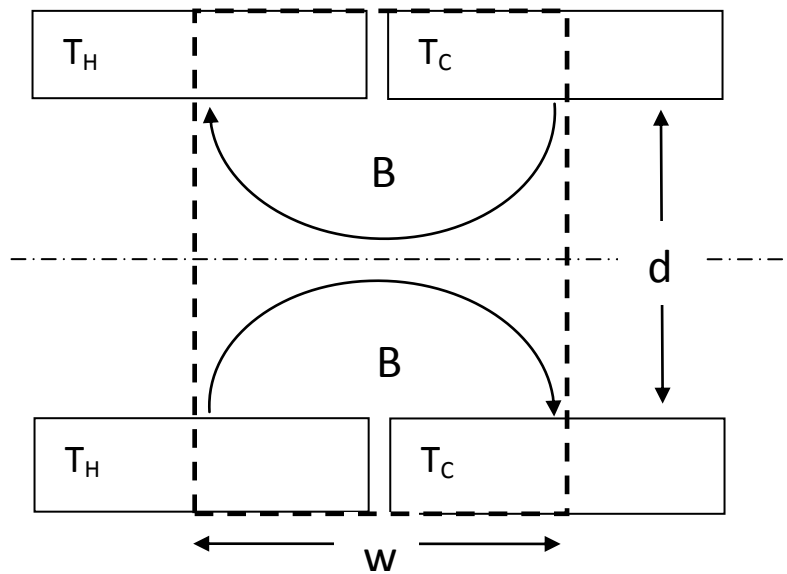
Fig. 5.14   Unit cell boundary used to analyze device concept

Analysis was performed in the same iterative manner as the previous case. The main difference in modeling is the collection (or reduction) of thermal radiation. The separation distance between plates was again varied to illustrate that efficiency increases as the separation decreases; illustrated in Fig. 5.15. The electron trajectory's radius of curvature must be half the plate separation distance to minimize electron path collisions. These collisions would result in a certain amount of electrons contributing to

back emission. Back emission reduces the net current and thus reduces power and efficiency.
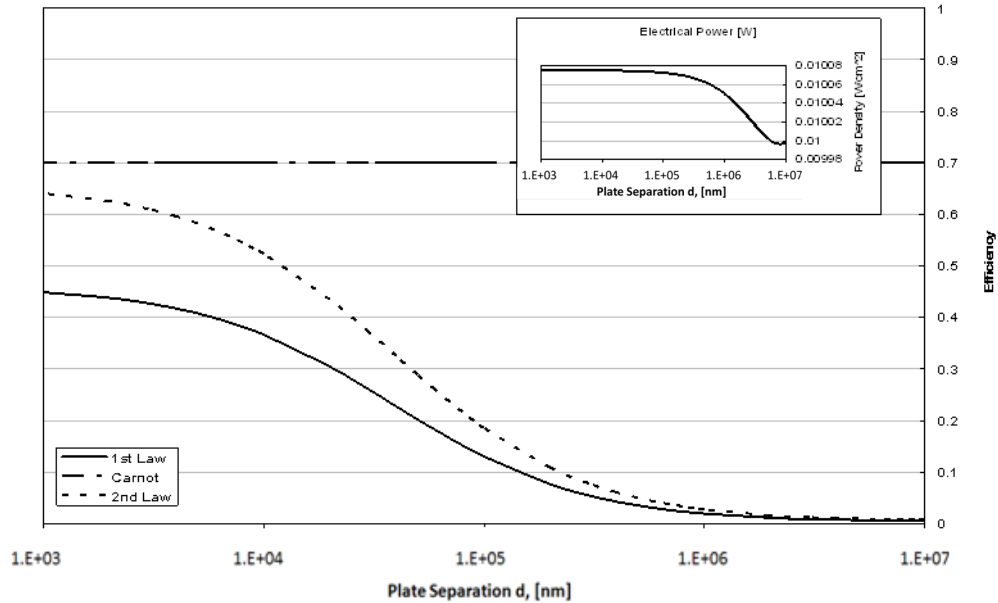
Fig. 5.15   Device efficiency for varying plate separation. The emitter and collector temperatures are 1000 K and 300 K, respectively. The emitter and collector work functions are 2 eV and 1 eV, respectively.

The efficiency for varying emitter source temperatures is illustrated in Fig. 5.16 and is calculated using equation 3.6 to estimate thermionic emission, equations 5.5 - 5.11 to estimate heat transfer and equations 4.1 - 4.3 to calculate efficiencies. Interestingly the efficiency profile is similar to that obtained in the 1st order modeling effort where the only thermal losses where those due to radiation exchange between electrodes. An obvious efficiency optimum is obtained for a certain emitter source temperature. The Carnot efficiency is no longer violated because there is thermal communication via small amounts of thermal radiation exchange between electrodes.
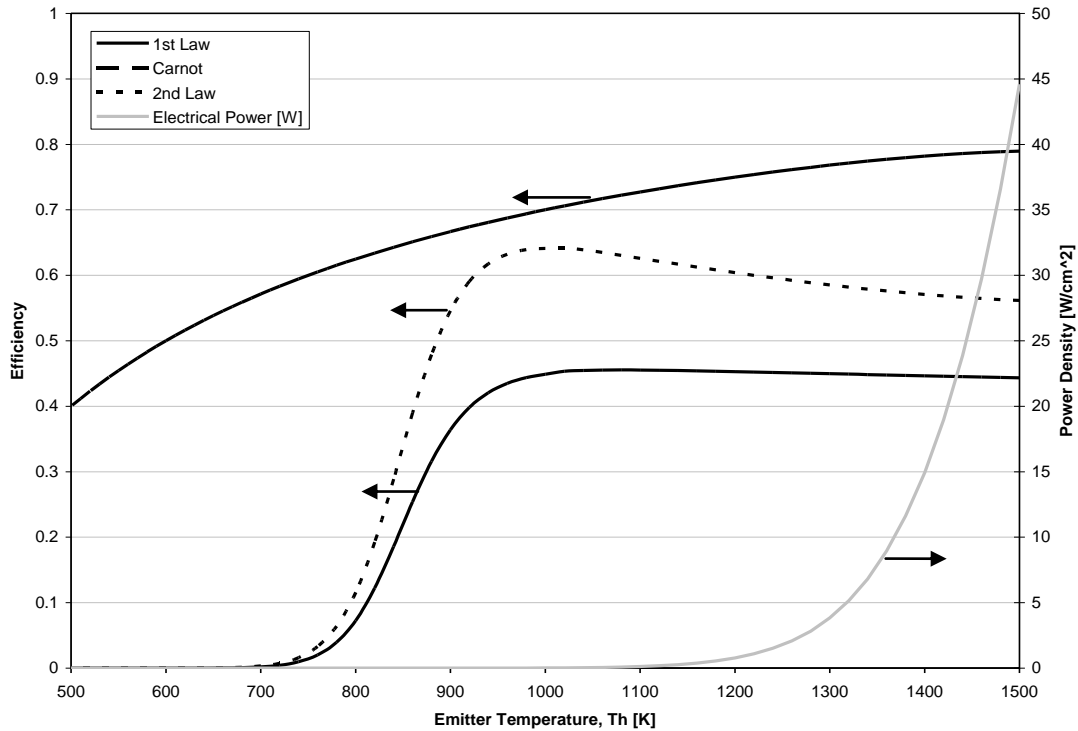
Fig. 5.16   Device efficiency and power density for varying emitter temperatures.
The emitter and collector work functions are 2 eV and 1 eV, respectively.

The device efficiency for varying emitter work functions is illustrated in Fig. 5.17.

The collector work function is assumed to be 1 eV. The emitter and collector source

temperatures are held at 1000 K and 300 K, respectively. An optimum emitter work

function occurs due to an increase in emission current. As the work function is reduced

higher emission currents are realized, however at the same time the device voltage is

decreasing because the work function is decreasing. This is the primary reason for the

optimum efficiency. Operating at the optimum efficiency will not provide the highest

power density. As both Fig. 5.16 and Fig. 5.17 illustrate the maximum power densities

occur for the highest emitter operating temperatures and lower emitter work functions.
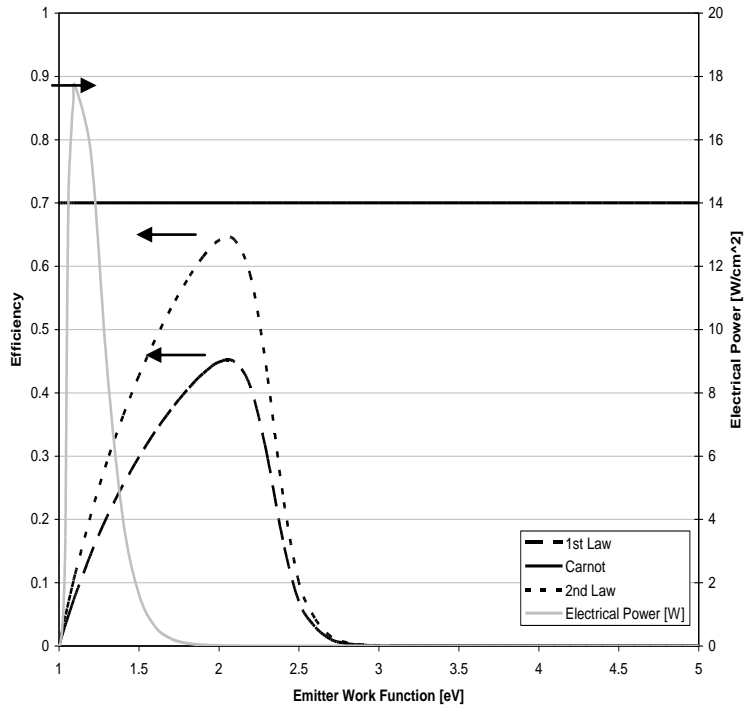
Fig. 5.17   Device efficiency and power density for varying emitter work functions. The collector work function is assumed to be 1 eV. The emitter and collector source temperatures are assumed to be 1000 K and 300 K, respectively.

The previous results illustrate the potential for optimization of both operating temperatures and work functions. The design concept shows promise for higher operating efficiencies; achieving 2nd law efficiencies in the 60th percentile would make this device competitive with other current power generation technologies. Although the power densities in the results were very small the cross-sectional area of the model unit is very small and would be scaled up based on application to achieve appreciable amounts of power generation.

Strict dimensional constraints are imposed on the design due to alignment with electron trajectories and reduction of space charge. The device could be operated with a

magnetic field similar to that of a strong laboratory magnet. The electron trajectory's radius of curvature would be roughly 0.5 microns which will result in a plate width and separation distance of 1 micron. The space charge is not significant for these dimensions due to the low current density. These device dimensions are within the fabrication limits of the current state of the art.

Alternating hot and cold plates would require a design that isolates the hot from cold plates. Spreader technology such as heat pipes, vapor chambers, and microchannels could provide the link between the source and hot plates as well as the link between the cold plates and collector heat sink.

iii.   TFE NANOWIRE CONVERTOR

Small scale dimensions are also an attribute of the second device investigated in this work; which has been named the TFE Nanowire Converter. TFE has been shown to have distinct advantages over TI emission. Specifically the addition of the electric field reduces the required operating temperature and work function to achieve appreciable current densities. One of the challenges in implementing TFE is achieving a sufficient electric field to enhance emission. Many studies have shown that the use of the strong electric field around a sharp point can provide a suitable field at relatively low applied voltages.

A stronger electric field can be generated around a very small radii point source. The point sources can be arranged in an array to achieve maximum power densities. For

this reason an array of oriented SiC or Si nanowires has been chosen for this

investigation. The nanowire diameter is on the order of 5nm. This small tip size

provides for very concentrated electric fields for relatively low applied gate voltages.

Fig. 5.18 shows an illustration of the proposed TFE nanowire convertor.
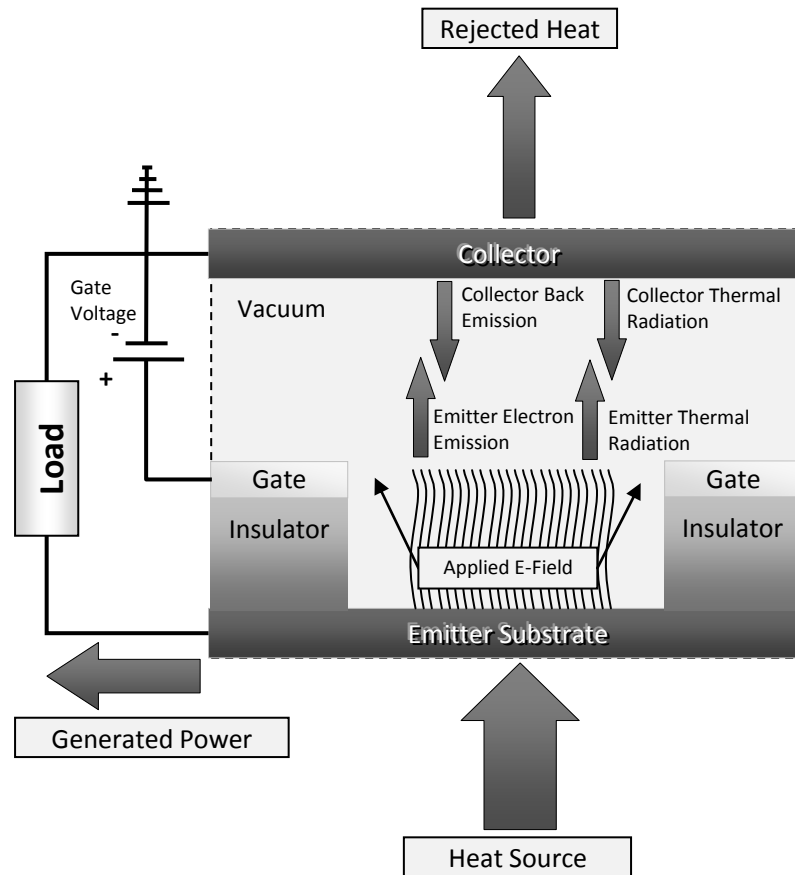
Fig. 5.18   An illustration of the proposed TFE nanowire convertor

    Utilizing the gate electrode to enhance electron emission creates an intrinsic

challenge to minimizing current loss. As Hatsopolous realized in his magnetic triode, if

the accelerating electrode at a much higher operating voltage than the emission

potential, collects stray emission current the power loss through the gate/accelerating

electrode can greatly reduce the overall device efficiency. The gate voltage is typically

one to two orders of magnitude greater than the built in voltage of the

emitter/collector. Small amounts of emitted electrons collected by the gate will result

in significant power losses. Too much current leakage can even result in a device that

consumes more power than it generates rendering the device useless. Therefore it is

imperative to minimize both the applied gate voltage and reduce the amount of gate

leakage current.

a. ELECTRIC FIELD

The high electric fields required to obtain field emission are only achievable with

extreme voltages for flat plate cathodes. One method to reduce the required gate

voltage is to utilize the high electric fields that concentrate around a sharp point or tip.

The electric fields achieved around a sharp tip are illustrated by Fig. 5.19 based on the

field enhancement factor provided in equation 3.31. The figure shows that as the tip

radius is decreased the required voltage to obtain a specific electric field is reduced.
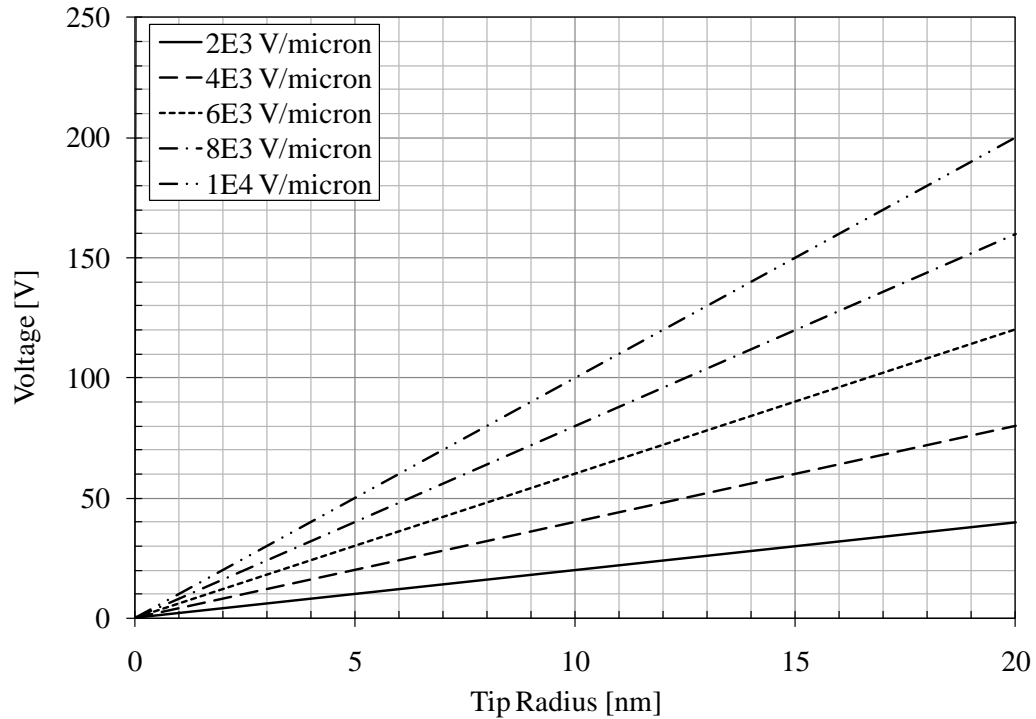
Fig. 5.19   Electric field strength for various tip radii and operating voltages

b.   TIP EMISSION & FIELD EMITTER ARRAYS

Tip emission has been thoroughly investigated for use as field emission cathodes. Carbon nanotube field emission has been demonstrated by (Zhu, et al. 1999). Nanowire field emission has been illustrated by (Liu, et al. 2005) (Z. Pan, et al. 2000).

The plot in Fig. 5.20 was developed using the simplified TFE model for a potential barrier between parallel plates (equations 3.36 through 3.45) for 3C silicon carbide (SiC) with a work function of 4.4 eV (Wu, et al. 2002). Emission was estimated based on a projected emitter area as opposed to the profile area of the nanowires. The chart

113

shows that TFE varies exponentially with applied electric field. Therefore it is important

to achieve very high electric fields while minimizing the applied gate voltage.
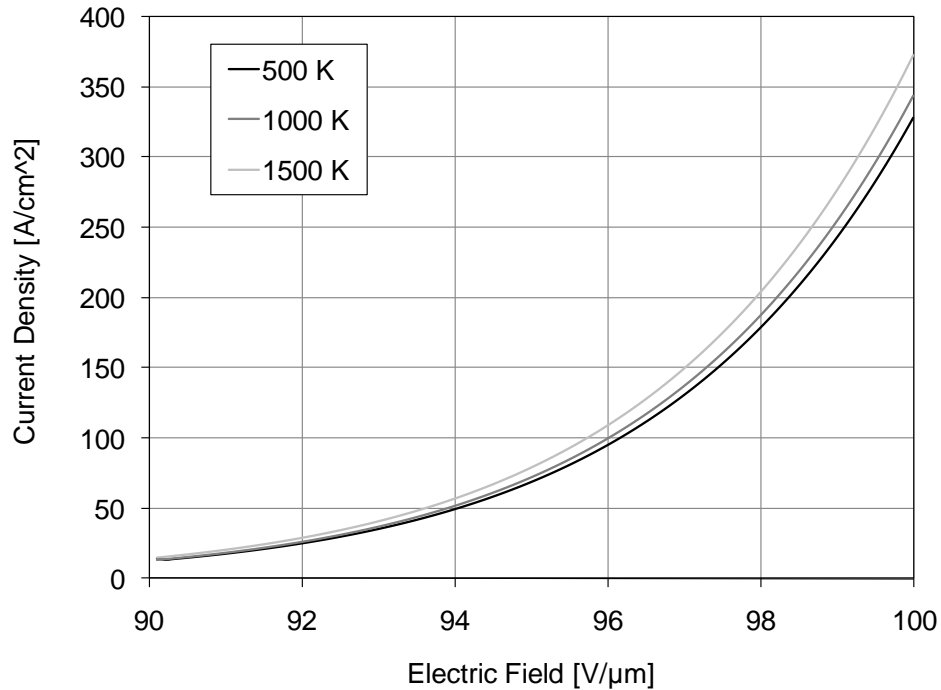
Fig. 5.20   Thermal-Field Emission using 3C SiC (Work Function ~ 4.4 eV) based on
                the projected emitter area

Field Emitter Arrays (FEA) are multiple field emitting tips oriented or organized in a

pattern to scale up the emission derived from a single tip (Nation, et al. 1999) (Fursey

2005) (Fisher and Walker 2002). The TFE converter design employs the idea of the field

array through commonly orientated nanowires. Fig. 5.21 and Fig. 5.22 show Spindt type

field emitter arrays.
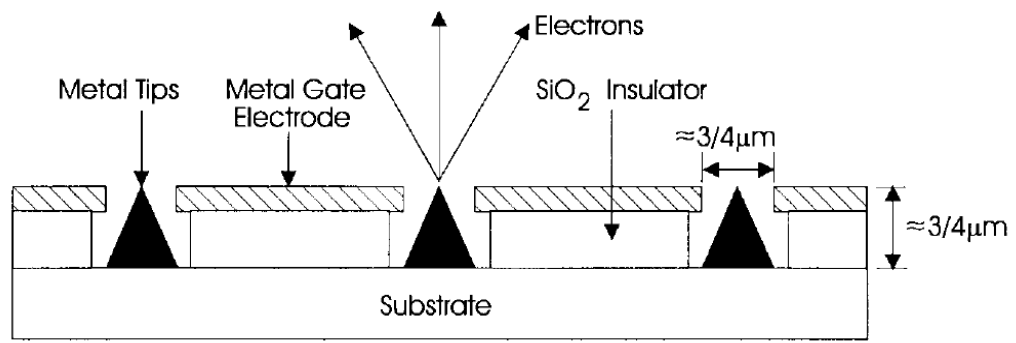
Fig. 5.21   Illustration gated field emitter array (Nation, et al. 1999)
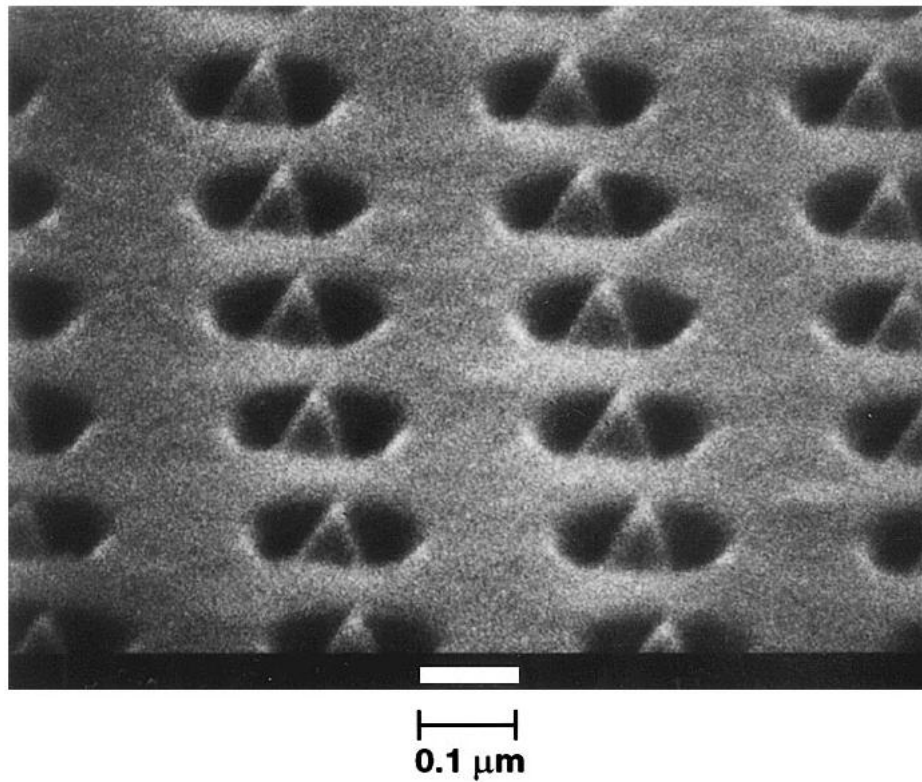
Fig. 5.22   SEM of gated field emitter array (Nation, et al. 1999)

The Spindt type field emitter arrays are similar to proposed nanowire field

emitter array except that the pyramid tip emitters are replaced by oriented nanowires.

Nanowires offer larger aspect ratios which improve the field enhancement factor and

115

nanowires can be grown in greater densities than pyramids tip emitters. The larger

aspect ratios offer better field enhancement and Fig. 5.23 shows the experimental

setup used to evaluate field emission properties of SiC nanowires in a study performed

by (Z. Pan, et al. n.d.).
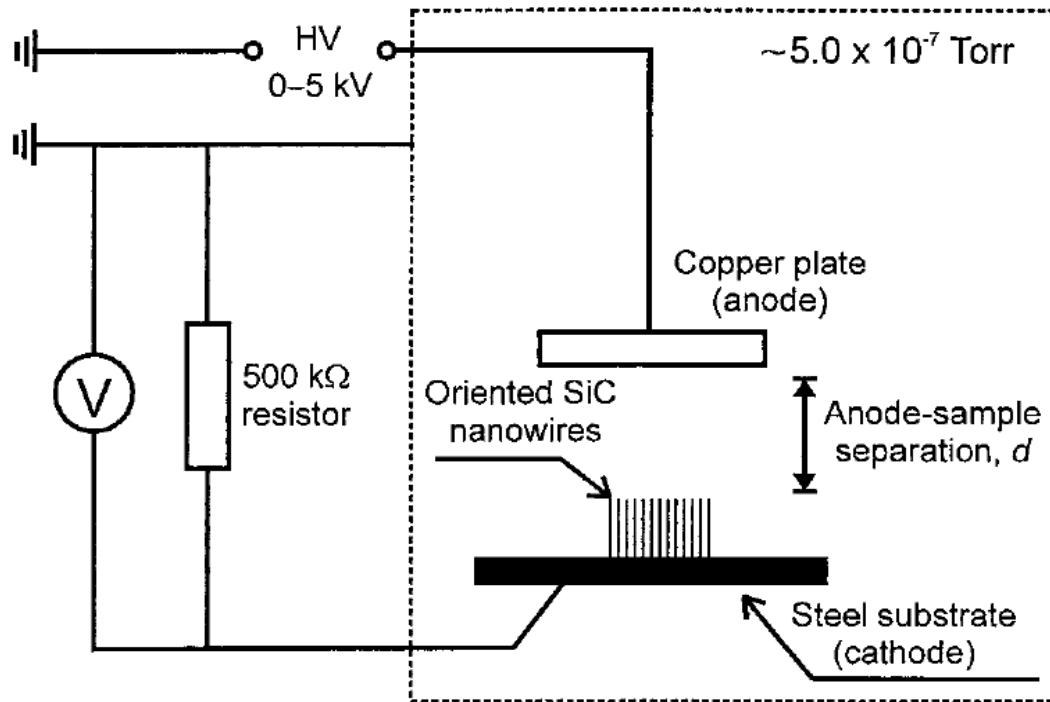
Fig. 5.23   Illustration of the experimental setup used to evaluate SiC nanowire field
                emission (Z. Pan, et al. n.d.)

Table 5.2 shows measured cold cathode emission currents from various tip

emission FEAs. The applied electric fields in these cases are much lower than those

suggested for TFE which occurs more readily at electric fields of around 1000 V/μm or

10^7 V/cm (Dolan & Dyke, 1954)(Fursey, 2005)(Murphy & Good Jr., 1956). The emission

116

models used in this thesis predict negligible emission currents at the electric fields levels

in these studies. This suggests that the emission modeling and assumptions in this

thesis are fairly conservative. The discrepancy between the modeling and experimental

results may be due to a number of factors. The studies don't report an emitter work

function so the modeling was performed with assumed values for the work function

based on the material. Also, the studies don't indicate whether the current density is

based on a projected emitter area or the actual profile area of the 3-D emitter surface.

Table 5.2   Tabulated empirical results for arrays of field emitters with nanoscale tip
                 emitters (Nation, et al., 1999)(Pan, et al., 2000)(Teo, et al., 2002)

Study	Nation et al	Pan et al	Teo et al
Emitter Description	Si FEA Pyramids	Oriented SiC Nanowires	Carbon Nanofibers
Tip Radius [nm]	5	10-40	5
Electric Field [V/μm]	Not Reported	2.5-3.5	7
Tip Density [per cm^2]	3×10^6	10^9-10^{10}	10^6-10^9
Current Density [A/cm^2]	2.1	1.0×10^{-2}	1.0×10^{-3}

c. SERVER WASTE HEAT APPLICATION

The TFE convertor design is not limited to a specific heat source application, but can

be optimized per application. In the following example the TFE convertor is used to

scavenge server component waste heat. Modeling was performed for a 150 W

component with an operating temperature limit of 400 K. The collector and shunt heat

sinks, as shown in Fig. 5.24, are assumed to dissipate their heat into a 300 K ambient.

The shunt heat sink thermal resistance was sized such that the operating temperature is

maintained at a constant 400 K. A constant component temperature can be achieved

117

with closed-loop feedback control between the component temperature and the air

mover.
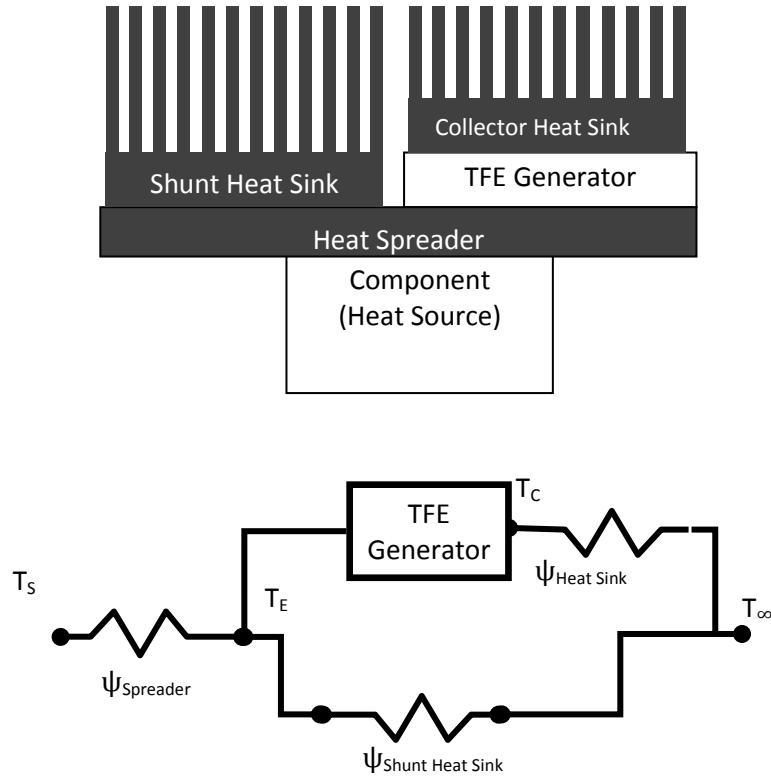
Fig. 5.24   Proposed server implementation the TFE convertor

The generator area should be maximized to increase the amount of converted waste

heat. The area is assumed to be 200 cm^2 based on the footprint for a large

microprocessor heat sink. However the power is normalized over the area to better

understand the generator performance independent of implemented area.

Using the TFE model provided in equations 3.30 and 3.36 through 3.45 and the

energy balances in equations 4.9 - 4.10, a parametric study of component temperature

and gate voltage effect on the generated power density was performed and shown in

Fig. 5.25 and Fig. 5.26. The plots show that there is a stronger dependence on applied

gate voltage than component operating temperature. Fig. 5.26, also shows that better

generation can be achieved at lower tip radii. From a device feasibility perspective the

power density results from this model are promising and would mean in significant

power savings in current server hardware.
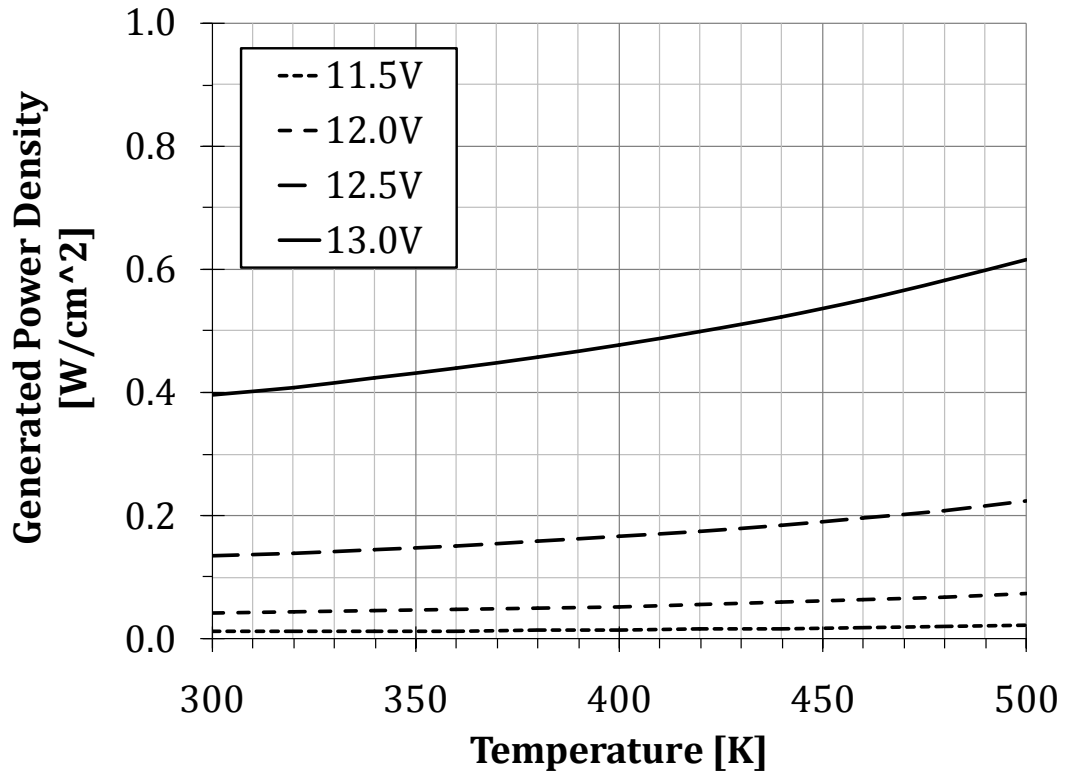
Fig. 5.25   TFE generated power density for a range of applied gate voltages (11.5V -
                 13.0 V) and component temperatures with a 10nm tip radius, 3 eV
                 emitter work function, 1.6 eV collector work function, and ambient
                 temperature of 300 K
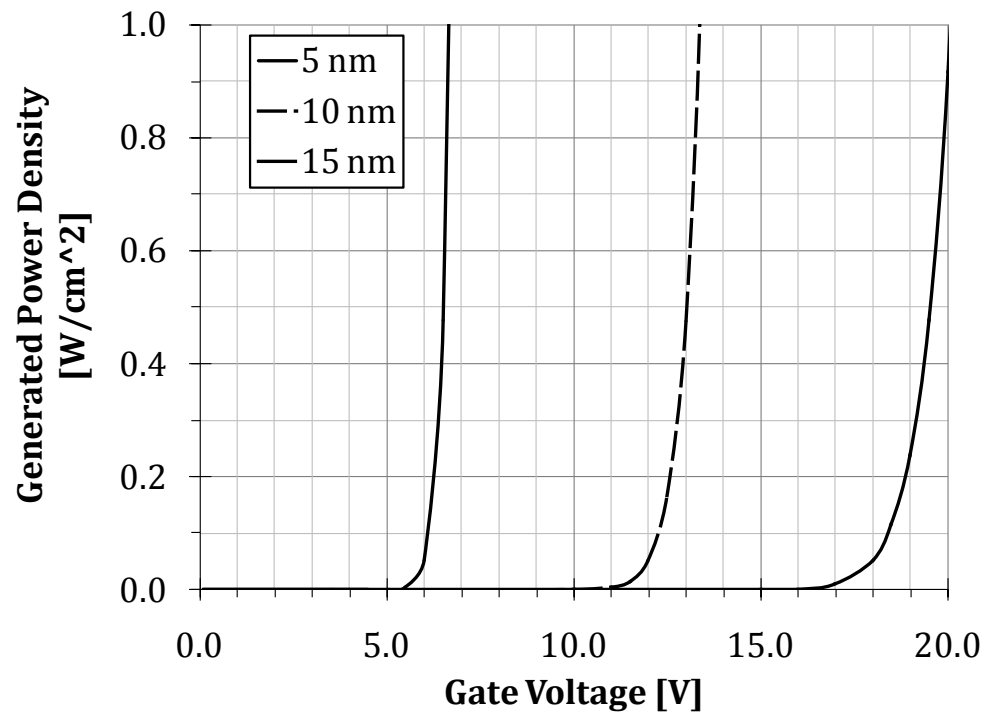
Fig. 5.26   TFE generated power density from a 150 W device for a range on nanowire radii (5 nm – 15 nm) and applied gate voltages with a 400 K component temperature, 300 K ambient temperature, 3 eV emitter work function, and 1.6 eV collector work function

Based on the current the electrical load should be sized such that the voltage is equal to the difference in work function. The operating potential can only be as high as the difference in work function. If the load is too high then the current will be restricted. Conversely, if the load is too low then the voltage will be less than the potential difference in electrodes and result in a reduction in power generation. Fig. 5.27 (A) illustrates that there is an optimal load resistance to maximize power generation and as expected the optimum efficiency of the device occurs at the optimum load resistance as shown in Fig. 5.27 (B).
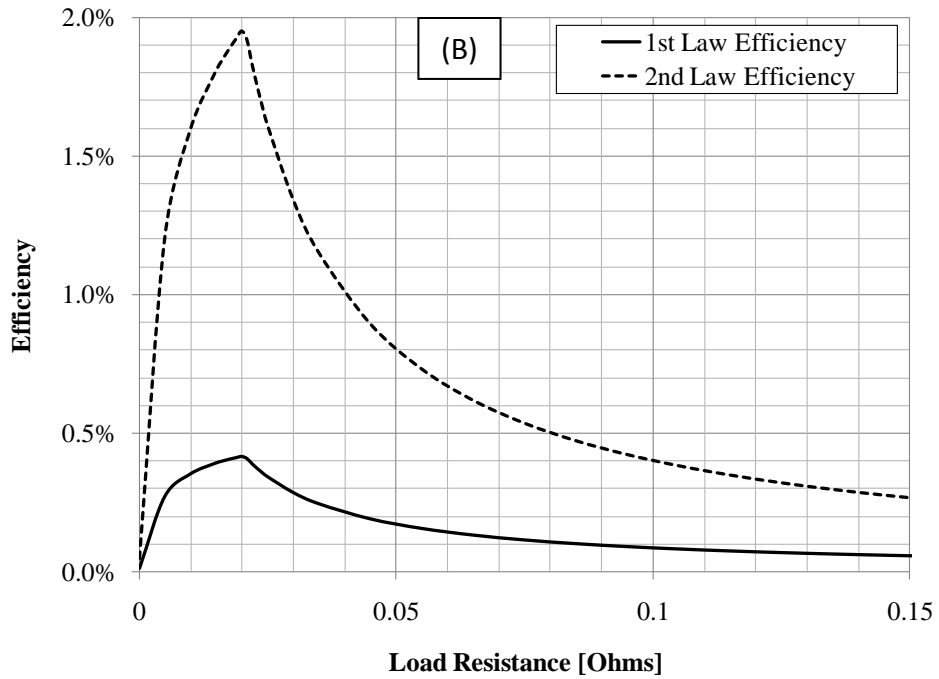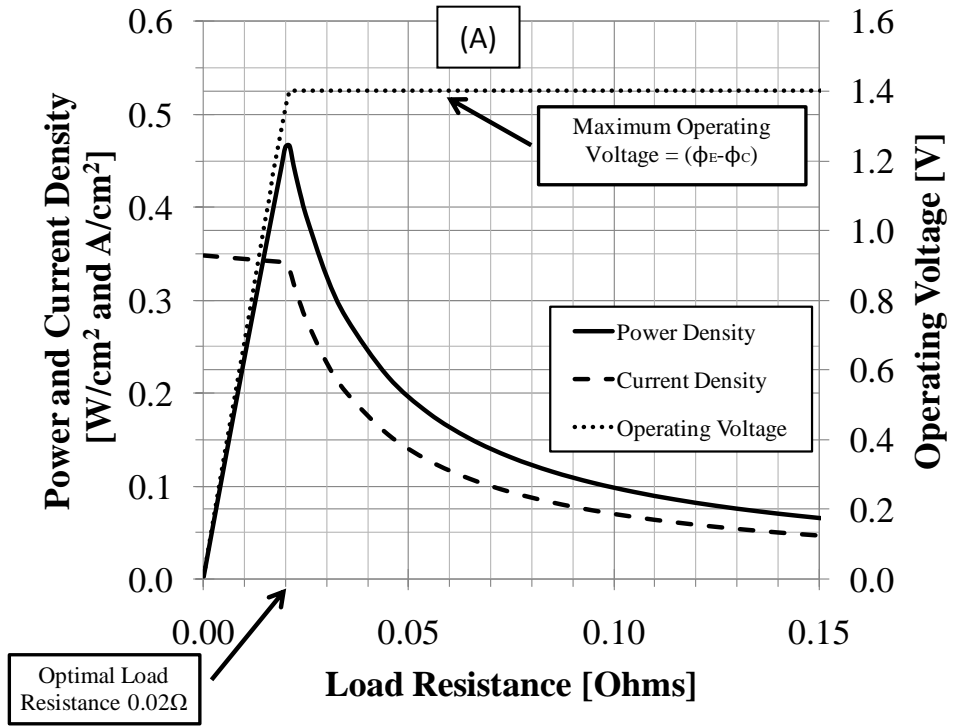
Fig. 5.27   Plot of (a) power density, current density, operating voltage, and (b) efficiencies as function of load resistance

6. PROPOSED FABRICATION OF NANOWIRE BASED STRUCTURE

In parallel to this study, Silicon nanowires have been fabricated by Jeff Scott as part of his undergraduate honors project and Dr. Hao Li of the University of Missouri-Columbia Mechanical Engineering department (Scott and Solbrekken n.d.). The following fabrication process and resulting nanowires are the sole achievement of Jeff Scott and Hao Li. This chapter provides documentation of their process and success in growing Si nanowires as well as a proposal for an experimental apparatus to test TFE nanowire device performance.

The nanowires were fabricated using the Vapor-Liquid-Solid (VLS) growth mechanism (Law et al., 2004 and (Wang, et al. 2000)), in a hot-wall Chemical Vapor Deposition (CVD) chamber as illustrated in Fig. 6.1. Creation of oriented nanowires starts with the fabrication of a substrate. A (111) oriented silicon substrate is chosen to help promote oriented nanowire growth. Patterned gold is used as nucleation cites for nanowire growth. Layers of organized sub micron polystyrene spheres are spun on the surface (Fig. 6.2) of the substrate to create a mask for the gold pattern deposition as shown in Fig. 6.3. The number of layers of spheres alters the size and density of patterned gold nucleation sites.

122
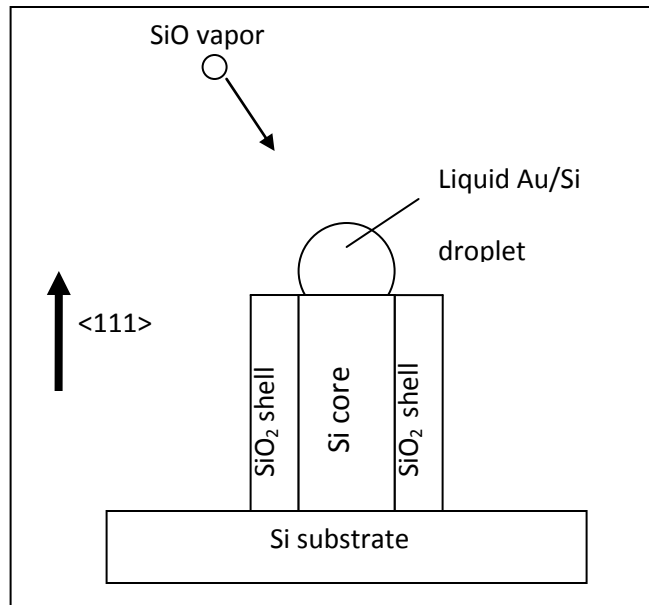
Fig. 6.1   Sketch of the theoretical Si nanowire that results from SiO vapor and VLS
               mechanism. Adapted from (Kolb, et al. 2004) by (Scott and Solbrekken
               n.d.)

The VLS process starts with the condensation of the vapor into liquid nucleating at a

metal catalyst particle. The liquid then cools to form a solid. One dimensional growth

occurs to form a nanowire or nanorod due to thermal conduction from the substrate

solidifying the liquid. Condensation continues at the tip which is still in the liquid phase.

Properly controlling this growth mechanism can yield nanowires and nanorods of

varying dimension, as shown in Fig. 6.4. The diameter of the nanowire is controlled by

changing the size of catalyst particle and length of the nanowire is controlled by altering

growth time. Other deposition parameters such as temperature and pressure are also

of importance.
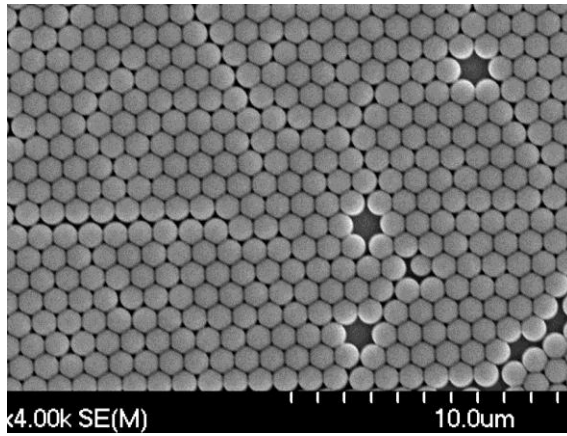
Fig. 6.2   SEM images of a single layer of polystyrene spheres (Scott and Solbrekken n.d.)
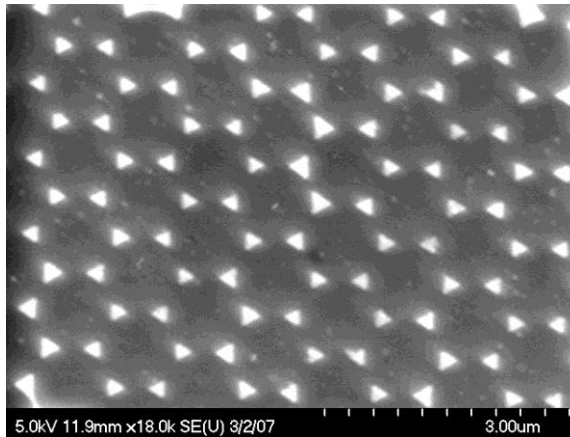
Fig. 6.3   SEM images of patterned gold film resulting from a single layer of polystyrene spheres (Scott and Solbrekken n.d.)
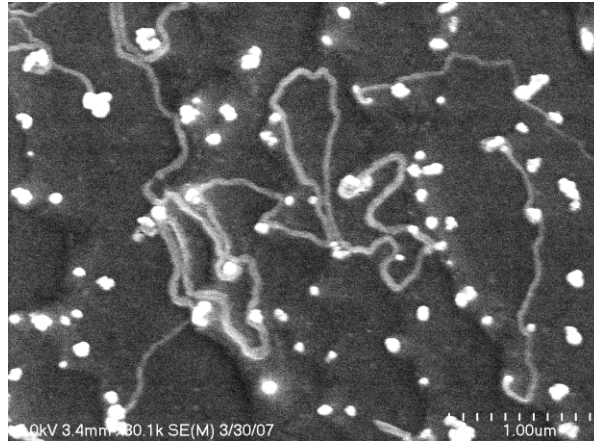
Fig. 6.4   SEM images of Si nanowire growth (gray lines), as well as a large number of SiO_2 deposits (white dots) (Scott and Solbrekken n.d.)

CVD Si nanowires grown with VLS or VS mechanism usually have an intrinsic thin

SiO_2 or graphite layer depending on experimental conditions. The SiO_2 layers can be

easily etched off by Hydrogen Fluoride and the graphite layer can be burned off. In

addition, the Si nanowires can also be oxidized at elevated temperatures to form SiO_2

layers. Therefore, Si nanowire diameter could be controlled by post-oxidization and

chemical etching.

The Vapor-Solid (VS) growth mechanism can also be used where phase change from

vapor directly into solid occurs. Nanowires can also be formed using carbon nanotubes

as both a precursor and template. The nanowires shown in Fig. 6.5 were fabricated

using this method in the lab of Co-PI Hao.

125
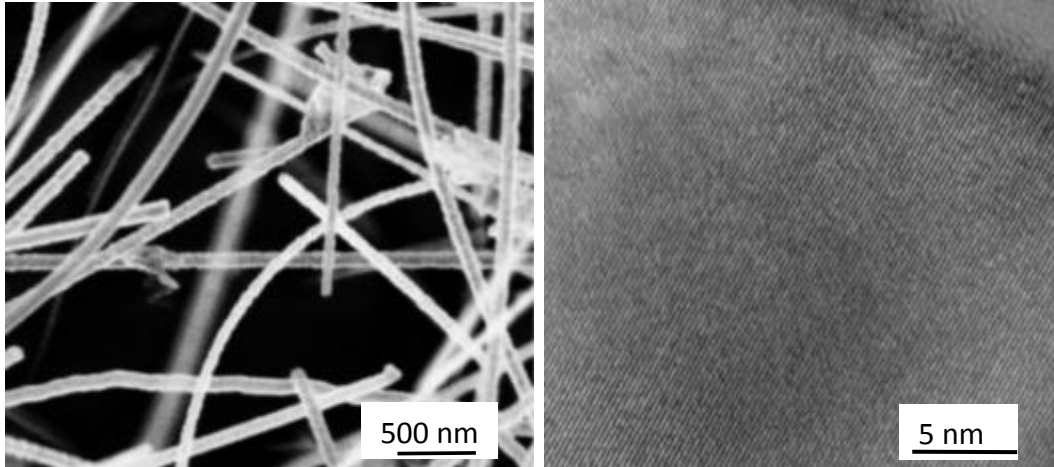
Fig. 6.5   Free standing SiC nanowires made from graphite particles and carbon
                nanotubes (Photos courtesy of Dr. Hao Li)

It is necessary to build an experimental prototype to validate the analytic models

developed for the TFE nanowire convertor. The proposed experimental apparatus is

shown in Fig. 6.6.
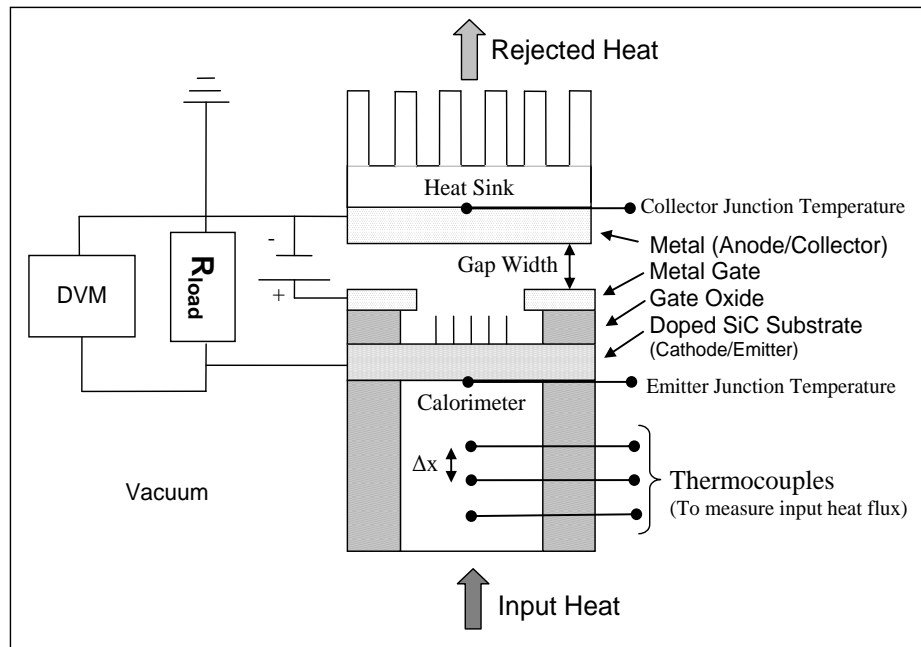
Fig. 6.6   Proposed experiment for TFE convertor prototype

The envisioned device will have a separate anode and gate. The electric field for field emission is generated between the nanowire tips and the gate. The gate is electrically isolated from the substrate by an oxide material which can be patterned using photolithography. The oxide layer can be grown and a metal layer will be deposited to form the gate. Photoresist is intended to protect the region where nanowires are to be located and be removed prior to nanowire growth. Nanowire growth will be performed using the hot-wall CVD and the VLS growth mechanism discussed earlier. Metal catalyst particles on the Si substrate surface are used to initiate the growth and control the diameter of the nanowires.

Leakage current through the gate is a major concern due to the higher gate voltage. The gate surface area will be substantially smaller than that of the collector to help minimize those losses. One of the goals for the experimental measurements is to understand the losses caused by leakage current and to develop ways for reducing those parasitic losses. Gate geometry, orientation and structure can be altered to understand their effect on leakage current.

The physical dimensions of the nanowires, the packing density of the nanowires, and the proximity to the metal gate can be characterized by scanning the cathode assembly using a scanning electron microsope. It is expected that the experiments will need to be conducted within a vacuum environment, although initial experiments can be attempted in an ambient pressure environment.

7. CONCLUSIONS AND FUTURE STUDIES

Although there is a significant environmental push to reduce energy consumption via waste heat recovery it is important to look at the bigger picture. For significant adoption of such technologies to occur I believe the energy saved by the device must be greater than the amount consumed to produce the device. Unless this is true, the net effect will be a drain on the environment.

Energy costs are rising due to both increased consumption and/or reduced supply. Adoption of solid state waste heat recovery has been cost prohibitive, but there will be an inflection point where the cost savings due to energy reductions outweighs the device/implementation costs of solid state recovery. Reduced manufacturing costs and increased device efficiencies will help drive this inflection.

The converter designs proposed in this thesis show promise of increasing energy conversion efficiency for solid state convertors, but are a long way from high volume manufacturing. The Magnetic Diode and TFE Convertor both combine known technologies and methods in a novel way.   The materials and manufacturing methods are available today to develop both proposed devices. Further material development, specifically with regards to a material's work function, will only improve the predicted results for these devices. Further design and optimization is required to minimize efficiency losses, and develop and refine manufacturing methods.

This thesis has presented unique substance including the invention of new and novel solid state energy conversion devices combined with the unique application of system level modeling approach and the novel application of waste heat recovery from a server. Some modeling assumptions and approximations where made to allow for estimating device efficiencies. These estimates provided an understanding of device feasibility. With a first order feasibility of these devices understood now there is an opportunity to add more modeling detail with less risk of the work being wasted on an infeasible device. However, the system level thermal modeling performed in this thesis is more detailed and provides for significantly improved results over the standard approach of modeling emission with constant temperature boundary conditions.

i.   MAGNETIC DIODE

The idea for the Magnetic Diode device was conceived with the intention to reduce the parasitic thermal radiation losses suffered in a traditional face to face TI diode. Thermal modeling illustrates that plate orientation provides a means to reduce the net thermal radiation transfer from the emitter electrode(s) to the collector electrode(s). Radiation from the electrodes is recovered using a like temperature plate facing the respective electrode. Use of the magnetic field to alter the trajectory of the electrons is a proven technique allowing for the unusual plate orientations. The modeling performed for the Magnetic Diode illustrates that a 2nd law efficiency of roughly 65%

129

could in theory be achieved. This is a marked improvement over many of the competing

devices (namely TE or conventional TI conversion).

The conclusion must be drawn that with existing material work functions at roughly

1.8 eV, low temperature operation (~1000 K) may be efficient but power densities will

be very low (~ 0.01 W/cm^2). This device may achieve higher output power by increasing

the source temperature; however there is a minor loss in efficiency. This device

illustrates a unique way to minimize thermal radiation losses by careful orientation of

the electrodes. Enhanced efficiencies are theoretically possible, however low

temperature TI emission is impractical with current state of the art materials.

Despite all of the proven technologies employed in this device there are still

significant hurdles to overcome even for high temperature operation. The challenges

facing the Magnetic Diode that would serve as next steps include: validation of the

electron scattering effect, magnetic field design and application.

ii.   TFE NANOWIRE CONVERTOR

Unlike TI emission, TFE can provide significant current densities at low temperatures.

The modeling shows that power densities on the order of 0.5 W/cm^2 can theoretically

be achieved with this device with an applied voltage of 5-10V depending upon the

diameter of the nanowire radius.   If this level of generation can be achieved in practice

then there would be opportunity to recover significant quantities of waste energy from

server components.

The next steps for the TFE nanowire convertor research would be to develop a more accurate model as well as experimentation to fully understand the magnitude and nature of leakage currents into the gate electrode. First steps in the fabrication of this device have been taken. Silicon nanowires have been produced per the VLS method. The next step in fabrication is to develop the ability to develop a method that incorporates the gate structure with the oriented nanowires.

8. APPENDIX

i. GENERIC THERMIONIC MODEL

The following is an example of Matlab code used to iteratively solve a parametric study of emitter temperature on device efficiency of a thermionic diode:

```
%   Dominick Lovicott
%   Thermionic Research
%   Example Thermal Resistance Model

clear
clc

    %   Constants
    KB = 1.381*10^-23;              % Boltzmann's Constant[J/K]
    Eo = 8.854*10^-12;              % Permittivity of a Vacuum[F/m]
    m = 9.109*10^-31;               % Mass of an Electron[kg]
    e = 1.602*10^-19;               % Charge of an electron [C]
    sigma = 5.67*10^-8;             % Stefan-Boltzmann Constant[W/m^2*K^4]
    pi = 3.14159265359;
    A1 = 1200000;                   % Emission Constant[Amps/m^2]

    %   Temperature Variables
    T8E = 1500;                     % Hot side Temperature[K]
    T8Emin = 500;                   % Hot side minimum temperature[K]
    T8C = 300;                      % Cold side Temperature[K]

    %   Misc
    L = 1*10^-2;  % Thickness of emitter and collector plates[m]
    A = 1;      % Crossectional area of emitter and collector plates[m^2]

    KE = 150; % Thermal conductivity of emitter plate[W/mK]
    KC = 150; % Thermal conductivity of collector plate[W/mK]

    EWF= 3;    % Emitter work function[eV]
    CWF = 2;   % Collector work function[eV]

    RE = .02;  % Thermal Resistance of emitter surface[K/W]
    RC = .02;  % Thermal Resistnace of collector surface[K/W]

    EE = .5;  % Emissivity of Emitter surface
    EC = 1;   % Emissivity of Collector surface

    %   View Factors

    % Radiation view factor for the emission from the emitter as seen by
    % the collector
    fE = .5;
    % Radiation view factor for the emission from the collector as seen by
    % the emitter
```

```matlab
    fC = .5;

    %   Iteration Variables

    O = 2;          % Number of k loop iterations (effieciency dependance)

    delta_k = (T8E-T8Emin)/O;        % k loop scaling constant

    tol = 10^-9;                     % tolerance of convergence
for k=1:O                      % Iteration loop for efficiency dependance

    M = 100;                         % Number of i loop iterations
    delta_i = 1/M;                   % i loop scaling constant
    % Calculation of emitter side source temperature[K]
    T8E = delta_k*k + T8Emin;
    % tracking of the emitter source temperature for plotting[K]
    T8Et(k) = delta_k*k + T8Emin;


    for i=1:M % Iteration loop for temperature calculations
    if i==1

        TET = T8E-100; % Temperature at the top of the emitter plate[K]
        TCT = T8C+100; % Temperature at the top of the collector plate[K]

        TEB = T8E-100; % Initial temperature of the bottom of the emitter[K]

      % Initial temperature of the bottom of the collector[K]
        TCB = T8C+100;

    else
        iteration(i)= i-1;% Keeps track of iterations for plotting purposes
        % Current density emitted by the emitter[Amps/m^2]
        JE(k) = (A1*TET(i-1)^2)*exp(-e*EWF/(KB*TET(i-1)));
        % Current density emitted by collector (AKA back emission)
        % [Amps/m^2]
        JC(k) = (A1*TCT(i-1)^2)*exp(-e*CWF/(KB*TCT(i-1)));
        % Radiation emitted from the emitter[W]
        qRE(i) = EE*A*sigma*TET(i-1)^4;
         % Radiation emitted from the collector[W]
        qRC(i) = EC*A*sigma*TCT(i-1)^4;
        % Heat rejected from the emitter due to emission [W]
        qE(i) = JE(k)*(EWF+(2*KB*TET(i-1)/e));
         % Heat rejected from the collector due to emission[W]
        qBE(i) = JC(k)*(EWF+(2*KB*TCT(i-1)/e))-(EWF-CWF)*(JE(k)-JC(k));


        % Heat supplied to the emitter plate [W]
        qs(k) = qRE(i)-fE*qRC(i)+qE(i)-qBE(i);
        % Heat rejected by the collector plate[W]
        qo(k) = fE*qRE(i)-qRC(i)+qE(i)-qBE(i);
        % Temperature of the bottom of the emitter plate [K]
        TEB(i) = -(qs(k))*RE+T8E;
        % Temperature of the bottom of the collector plate[K]
        TCB(i) = (qo(k))*RC+T8C;
        % Temperature of the top of the emitter plate[K]
        TET(i) = TEB(i)-qs(k)*(L/(KE*A));
        % Temperature of the top of the collector plate [K]
        TCT(i) = TCB(i)+qo(k)*(L/(KC*A));
        % Difference in temperature for the top of the emitter between the
```

```matlab
        % previous and current iteration        [K]
        delta_TET = abs(TET(i) - TET(i-1));
        % Difference in temperature for the top of the collector between
        % the previous and current iteration     [K]
        delta_TCT = abs(TCT(i) - TCT(i-1));

    if (delta_TET >= tol)
            M=M+1;
        elseif  (delta_TCT >= tol)
            M=M+1;
        end
    end
    end


    %   Efficiencies
    efficiency_1(k) = (EWF-CWF)*(JE(k)-JC(k))/(qs(k)); % 1st law efficiency
    efficiency_C(k) = 1-(T8C/T8E);                     % Carnot efficiency
    efficiency_2(k) = efficiency_1(k)/efficiency_C(k); % 2nd law efficiency

end

    %   Plots
    figure(1)
    plot(iteration,TET,iteration,TEB,':')
    title('Emitter Plate Temperatures')
    xlabel('Iteration')
    ylabel('Temperature [K]')

    figure(2)
    plot(iteration,TCT,iteration,TCB,':')
    title('Collector Plate Temperature')
    xlabel('Iteration')
    ylabel('Temperature [K]')

    figure(3)
    plot(T8Et,efficiency_1,T8Et,efficiency_2,':')
    title('Efficiency vs Temperature')
    xlabel('Temperature [K]')
    ylabel('Efficiency')
```

ii.   MAGNETIC DIODE MODEL

The following is an example of the Matlab code used to estimate Thermionic

emission current and efficiency as a function of temperature for various plate

separation angles of the Magnetic Diode:

```matlab
% Constants

KB = 1.381*10^-23; % Boltzmann's constant
e = 1.602*10^-19; % charge of an electron
sigma = 5.67*10^-8; % Stefan-Boltzmann Constant
pi = 3.14159265359;
A1 = 120; % Thermionic emission constant

% Variables

Ee = 1; % emitter emissivity
Ec = 1; % collector emissivity

Te_max = 2000; % Max Emitter temperature
Te_min = 400; % Min Emitter temperature
Tc = 273+100; % Collector temperature
EWF = 3; % Emitter Work Function
CWF = 1; % Collector Work Function
a_max = pi; % Maximum angle of plate separation



Na = 5; % Number of iterations for plate separtion angle
NT = 100; % Number of iterations for temperature

deltaa = a_max/Na; % Iteration size for separation angle
deltaT = (Te_max-Te_min)/NT; % Iteration size for temperature

for i=1:Na % Separation angle of 0

        if (i==1)
        a(i)=0;
        JC(i) =A1*Tc^2*exp(-e*CWF/(KB*Tc));

    elseif (i==2) % Separation angle of Pi/2
        a(i)=pi/2;
        JC(i) = 0;
    elseif (i==3) % Separation angle of Pi/1.1
        a(i) = pi/1.1;
        JC(i) = 0;
     elseif (i==4) % Separation angle of Pi/4
        a(i) = pi/1.01;
        JC(i) = 0;
     elseif (i==5) % Separation angle of Pi
        a(i) = pi;
        JC(i) = 0;
    end

      a_d(i) = a(i)*180/(pi);

    for j=1:NT % iteration loop for emitter temperature
```

```matlab
    Te(i,j) = deltaT*j+Te_min; % Emitter temperature calculation


        %Emitter current
        JE(i,j) = A1*Te(i,j)^2*exp(-e*EWF/(KB*Te(i,j)));

        % Thermal Radiation exchange
        Qr(i,j) = (1-sin(a(i)/2))*Ai*sigma*(Te(i,j)^4-Tc^4)/(1/Ee+1/Ec-
1);

        % 1st law efficiency
        NI(i,j) = ((JE(i,j)-JC(i))*(EWF-CWF))/
        (Qr(i,j)+JE(i,j)*(EWF+(2*KB*Te(i,j))/e)-JC(i)*(EWF+2*KB*Tc/e));

        % Carnot Efficiency
        NC(i,j) = 1 - (Tc/Te(i,j));

        % 2nd Law Efficiency
        NII(i,j) = NI(i,j)/NC(i,j);
    end

end

figure(1)
plot(Te,NI(1,:),'-',Te,NI(2,:),'--',Te,NI(3,:),':',Te,NI(4,:),':',
Te,NI(5,:),':',Te,NC(1,:))
xlabel('Temperature, [K]')
ylabel('Efficiency')
```

REFERENCES

Angrist, S. W. (1976). *Direct Energy Conversion.* Boston, MA.

Bejan, A. (1997). *Advanced Engineering Thermodynamics* (Second Edition ed.). New York.

Belady, C. L. (2007). *In the data center, power and cooling costs more than the IT equipment it supports*. Retrieved February 3, 2008, from http://electronics-cooling.com/articles/2007/feb/a3/

Brodie, I., & Schwoebel, P. R. (1994). Vacuum Microelectronic Devices. *Proceedings of the IEEE* , 1007-1034.

Caswell, W. (2007, January). *DELL H2C TECHNOLOGY:HYBRID COOLING FOR OVERCLOCKED CPUS.* Retrieved Februaury 20, 2010, from www.dell.com: http://www.dell.com/downloads/global/vectors/h2c.pdf

Cengel, Y. A., & Boles, M. A. (2002). *Thermodynamics: An Engineering Approach.* New York: McGraw-Hill.

Child, C. D. (1911). Discharge from Hot Cao. *Physical Review , 32*, 492-511.

CRC Press, Inc. (1983-1984). *CRC Handbook of Chemistry and Physics: 64th Edition.* Boca Raton: CRC Press, Inc.

Dolan, W. W., & Dyke, W. P. (1954). Temperature-and-Field Emission of Electrons form Metals. *Physical Review , 95*, 339-348.

Dushman, S. (1923). Electron Emission from Metals as a Function of Temperature. *Physical Review , 21* (6), 623-636.

Energy Information Administration. (2006). *Annual Energy Review.* DOE.

Energy Information Administration. (2007). *International Energy Outlook.* U.S. Department of Energy.

ENERGY STAR program. (2007). *Report to Congress on Server and Data Center Energy Efficiency.* U.S Environmental Protection Agency.

EPA Office of Air and Radiation. (2003). *ENERGY STAR: The Power to Protect the Environment Through Energy Efficiency.* US EPA.

EPA. (2007). *Report to Congress on Server and Datacenter Energy Efficiency.*

Fairbanks, J. W. (2006). Thermoelectric Developments for Vehicular Applications. *Diesel Engine-Efficiency and Emissions Research (DEER) Conference*, (p. 81). Detroit, MI.

Fisher, T. S., & Walker, D. G. (2002). Thermal and Electrical Energy Transport and Conversion in Nanoscale Electron Field Emission Processes. *Journal of Heat Transfer , 124* (5), 944-961.

Fowler, R. H., & Nordheim, L. (1928). Electron Emission in Intense Electric Fields. *Proceedings of the Royal Society of London , Series A*, 173-181.

Fursey, G. (2005). *Field Emission in Vacuum Microelectronics.* New York: Kluwer Academic/Plenum Publishers.

Gaertner, G., Geittner, P., Lydtin, H., & Ritz, A. (1997). Emission properties of top-layer scandate cathodes prepared by LAD. *Applied Surface Science* , 11-17.

Guth, E., & Mullin, C. J. (1942). Electron Emission of Metals in Electric Fields. *Physical Review , 61*, 339-348.

Hatsopolous, G. N. (1956, May). The Thermo-Electron Engine. *Thesis* .

Hatsopoulos, G. N., & Gyftopoulos, E. P. (1973). *Thermionic Energy Conversion: Volume I: Processes and Devices.* Cambridge, MA.

Hishinuma, Y., Geballe, T. H., & Moyzhes, B. Y. (2001). Refrigeration by combined tenneling and thermionic emission in vacuum: Use of nanometer scale design. *Applied Physics Letters* , 2572-2574.

Inropera, F. P., & Dewitt, D. P. (2002). *Introduction to Heat Transfer.* New York: John Wiley & Sons.

Jensen, K. L., O'Shea, P. G., & Feldman, D. W. (2002). Generalized electron emission model for field, thermal, and photoemission. *Applied Physics Letters , 20* (81), 3867-3869.

Kolb, F. M., Hofmeister, H., Scholz, M., Zacharias, M., Gosele, U., Ma, D. D., et al. (2004). Analysis of silicon nanowure growth by combining SiO evaporation with the VLS mechanism. *J. Electroncem. Soc.* (151), G472-G475.

Langmuir, I. (1923). The Effect of Space Charge and Initial Velocities on the Potential Distribution and Thermionic Current Between Parallel Plane Electrodes. *Physical Review , 21* (4), 419-435.

Langmuir, I. (1913). The Effect of Space Charge and Residual Gases on Thermionic Currents in High Vacuum. *Physical Review , 2* (6), 450-486.

Langmuir, I. (1929). The Interaction of Electron and Positive Ion Space Charges in Cathode Sheaths. *Physical Review , 33* (6), 954-989.

Liu, B. D., Bando, Y., Tang, C. C., Xu, F. F., & Golberg, D. (2005). Exellent Field-Emission Properties of P-Doped GaN Nanowires. *J. Phys. Chem. B* , 21521-21524.

Mackie, W. A., Hinricks, C. H., & Davis, P. R. (1990). Effective Work Function Measurements of Advanced Cathode Materials via a Thermionic Projection Micrscope System. *IEEE Transactions on Electron Devices , 37*, 2568-2574.

Mahan, G. D., & Woods, L. M. (1998). Multilayer Thermionic Refrigeration. *Physical Review Letters , 80* (18), 4016-4019.

Murphy, E. L., & Good Jr., R. H. (1956). Thermionic Emission, Field Emission, and the Transition Region. *Physical Review , 102* (6), 1464-1474.

Nation, J. A., Schachter, L., Mako, F. M., Len, L. K., Peter, W., Tang, C., et al. (1999). Advances in Cold Cathode Physics and Technology. *Proceedings of the IEEE , 87* (5), 865-889.

Office of Integrated Analysis and Forecasting. (1999). *Federal Financial Interventions amd Subsides in Energy Markets 1999: Primary Energy.* Washington DC: U.S. Department of Energy: Energy Information Administration.

Onsager, L. (1931). Reciprocal Relations in Irreversible Processes. I. *Physical Review* , 405-426.

Onsager, L. (1931). Reciprocal Relations in Irreversible Processes. II. *Physical Review* , 2265-2279.

Pan, Z., Lai, H.-L., Au, F. C., Duan, X., Zhou, W., Shi, W., et al. (2000). Oriented Silicon Carbide Nanowires: Synthesis and Field Emission Properties. *Advanced Materials* , 1186-1190.

Richardson, O. W. (1921). *The Emission of Electricity form Hot Bodies* (2nd Edition ed.). New York.

Scott, J., & Solbrekken, G. *Fabrication of Vertically-Aligned Silicon Nanowires for use in Enhanced Emission Devices.* MSGC Report.

Serway, R. A., & Beichner, R. J. (2000). *Physics: For Scientists and Engineers.* New York: Saunders College Publishing.

Shakouri, A., & Bowers, J. E. (1997). Heterostucture Integrated Thermionic Coolers. *Applied Physics Letters* , 1234-1236.

Solbrekken, G. L., Kazuaki, Y., & Bar-Cohen, A. (2004). Thermal Management of Portable Electronic Equipment using Thermoelectric Energy Conversion. *IEEE Inter Society Conference on Thermal Phenomenon* .

Solbrekken, G., Kazuaki, Y., & Bar-Cohen, A. (2004). Experimental Demonstration of Thermal Management using Thermoelectric Generation. *IEEE Inter Society Conference on Thermal Phenomenon* .

Soo, S. L. (1962). *Analytical Thermodynamics.* New Jersey: Prentice-Hall.

Tanner, P. G., Fraser, D. A., & Irving, A. D. (2005). Developments in thermionic engery converters. *IEE Proc.-Sci Meas. Technol. , 152* (1).

Teo, K. B., Chhowalla, M., Amaratunga, G. A., Milne, W. I., Pirio, G., Legagneux, P., et al. (2002). Field emission from dense, sparse, and patterned arrays of carbon nanofibers. *Applied Physics Letters* , 2011-2013.

Tolman, R. C. (1920). The Entropy of Gases. *J. Am. Chem.* , 1185-1193.

Wang, Z. L., Dai, Z. R., Gao, R. P., Bai, Z. G., & Gole, J. L. (2000). Side-by-side Silicon Carbide - Silica Biaxial Nanowires: Synthesis, Structure, and Mechanical Properties. *Applied Physics Letters* , 3349-3351.

Waterman, A. T. (1924). The Variation of Thermionic Emission with Temperature and the Concentration of Free Electrons within Conductors. *Physical Review , 24*, 366-376.

Weisbart, R. A., & Coker, D. R. (2001, May 17). *SEAT SURFACE TEMPERATURE IS THE LATEST MEASUREMENT OF CONSUMER COMFORT.* Retrieved February 20, 2010, from www.amerigon.com: http://www.amerigon.com/pdfs/AUTOMOTIVE-INTERIORS-PAPER-5-15-01.pdf

Westover, T. L., & Fischer, T. S. (2006). Analysis and Simulation of Refrigeration by Electron Emission. *IEEE* , 1177-1184.

Westover, T. L., & Fisher, T. S. (2006). Analysis and Simulation of Refrigeration by Electron Emission. *Thermal and Thermomechanical Phenomenon in Electronics Systems* (pp. 1177-1184). Itherm.

Wu, Z. S., Deng, N. S., Chen, J., Zhou, J., & Chen, J. (2002). Needle-shaped silican carbide nanowires: Synthesis and field electron emission properties. *Applied Physics Letters , 80* (20), 3829-3831.

Zhu, W., Bower, C., Zhou, O., Kochanski, G., & Jin, S. (1999). Large Current Density from Carbon Nanotube Field Emitters. *Applied Physics Letters* , 873-875.

Zuber, J. D., Jensen, K. L., & Sullivan, T. E. (2002). An analytical solution for mircotip field emission current and effective emission area. *Journal of Applied Physics* , 9379-9384.